

Computational analyses of the role of hippocampal oscillations in familiar and novel environments.

Ali Asgher Jeewajee

Thesis Submitted to University College London for the Degree
Doctor of Philosophy in Neuroscience



UMI Number: U591584

All rights reserved

INFORMATION TO ALL USERS

The quality of this reproduction is dependent upon the quality of the copy submitted.

In the unlikely event that the author did not send a complete manuscript and there are missing pages, these will be noted. Also, if material had to be removed, a note will indicate the deletion.



UMI U591584

Published by ProQuest LLC 2013. Copyright in the Dissertation held by the Author.
Microform Edition © ProQuest LLC.

All rights reserved. This work is protected against
unauthorized copying under Title 17, United States Code.



ProQuest LLC
789 East Eisenhower Parkway
P.O. Box 1346
Ann Arbor, MI 48106-1346

I, Ali Asgher Jeewajee, confirm that the work presented in this thesis is my own. Where information has been derived from other sources, I confirm this has been indicated in the thesis.

Acknowledgements

The work presented herein was conducted whilst I was funded by an MRC studentship granted by the Centre for Mathematics & Physics in the Life Sciences and Experimental Biology and I am indebted to both organisations for providing me with the opportunity to make this small contribution academia. I would also like to thank the ICN and its staff for creating such a fantastically enjoyable workplace.

I offer my warmest and sincerest thanks to my supervisors, John O'Keefe and Neil Burgess, whose patience, dedication and support have been so instrumental in the achievements made. I am especially grateful to my collaborators, Colin Lever, Stephen Burton, Caswell Barry, Francesca Cacucci, Robin Hayman and Tom Wills, without whose hard work collecting the data, the work done here would not have been possible. To my many colleagues, Alex Ioannides, Tom, John, Christian, Jack, Armelle, Chris, Lili, and Dmitry, thank you for your part in making this journey so much more pleasant.

I would also like to thank my friends, Zain, Shamim, Jew, Ramla, Khuzema, Sabina, Batool, The Vamans and Fuad for simply being there.

And most importantly to my family, my Mum, Dad and Zainab, who have supported me in every way for so long, I hope that this accomplishment brings you some of fulfilment it has brought me.

Abstract

The hippocampal formation is known to support several different types of spatial representation, and to play an important role in detecting environmental novelty. A striking aspect of hippocampal physiology is the theta rhythm, recorded in the electroencephalogram (EEG). This thesis investigates the role of the theta rhythm as an organising principle of the hippocampal formation, and in particular its role in the detection of novelty.

In the first experimental chapter, the behavioural correlates of principal cells across several regions of the hippocampal formation – head direction and conjunctive place by direction cells in the presubiculum, place cells in CA1 and grid cells in the MEC – are studied, with an emphasis on the contribution of running speed. Subpopulations of cells, both positively and a minority which are negatively modulated by speed are found in each region.

The second experimental chapter investigates the predictions of a recent model of entorhinal cortical grid cells. The model, based on the interference between somatic and dendritic oscillators, predicts that intrinsic firing frequency should exceed EEG theta frequency by a greater amount for small grids than for large grids and by a greater amount during fast running compared to slow. These relationships are confirmed in electrophysiological recordings in freely-moving rats.

The third experimental chapter reports the results of a detailed examination of the rodent EEG under conditions of novelty and familiarity. The oscillatory interference model predicts a reduction in the theta frequency in a novel environmental context. This is substantiated by the data and reveals a new mechanism for signalling novelty in the brain.

The fourth experimental chapter probes the specific roles played by the subiculum and CA1. There is debate as to whether the subiculum is an input as well as, traditionally considered, an output of the HF. I propose that subiculum is capable of informing CA1 and data is presented to show that subicular firing occurs earlier in the theta cycle and anticipates position further ahead than firing in CA1 does, and that this difference is modulated by familiarity with the environment.

Publications Arising

The following publications were generated from work conducted as part of this thesis:

Jeewajee, A. Lever, C. Burton, S. O'Keefe, J & Burgess, N. (2008). Environmental novelty is signalled by a drop in the hippocampal theta frequency. *Hippocampus*, **18**, 340-348.

Table of Contents

Acknowledgements	3
Abstract	4
Publications Arising	5
Table of Contents	6
Index of Figures.....	9
Index of Tables	11
1 Introduction.....	12
1.1 Preamble.....	12
1.2 Nomenclature	15
1.3 Structure and morphology of the hippocampal formation	16
1.3.1 Overview	16
1.3.2 Entorhinal cortex	20
1.3.3 Dentate gyrus.....	23
1.3.4 Hippocampus.....	26
1.3.5 Subiculum.....	29
1.3.6 Presubiculum and parasubiculum	31
1.3.7 Summary	32
1.4 Behavioural correlates of hippocampal cells.....	34
1.4.1 Functional properties of hippocampal cells.....	34
1.4.2 Sensory control of place cell firing	37
1.4.3 Remapping	39
1.5 Oscillatory properties of the hippocampal formation.....	43
1.5.1 Hippocampal electroencephalogram.....	43
1.5.2 Phase Precession.....	47
1.6 Models of hippocampal function	50
1.6.1 A brief review of computational modelling in the hippocampal formation.....	50
1.6.2 Interference models.....	53
1.6.3 Network models of grid cells.....	65
1.6.4 Other models involving the theta rhythm	66
2 General Methods.....	69
2.1 Animals.....	70

2.2	Surgery and electrodes	71
2.3	Single unit recording	73
2.4	Spike sorting & binning.....	74
2.5	Histology	75
3	Deciphering multiple functional correlates of firing across sub-regions of the HF	76
3.1	Introduction	76
3.2	Methods.....	79
3.2.1	Subjects	79
3.2.2	Behavioural training	79
3.2.3	Firing-rate maps	79
3.2.4	Criteria for data inclusion	80
3.2.5	Maximum likelihood method	80
3.3	Results.....	84
3.4	Discussion	90
4	The oscillatory interference model predicts a relationship between grid cell firing patterns and theta activity at different running speeds	92
4.1	Introduction	92
4.2	Methods.....	98
4.2.1	Animals.....	98
4.2.2	Behavioural training	98
4.2.3	Data analysis	99
4.3	Results.....	104
4.4	Discussion	111
5	Environmental novelty is associated with reduction of the hippocampal theta frequency.....	114
5.1	Introduction	114
5.2	Materials and Methods.....	117
5.2.1	Subjects	117
5.2.2	Electrode implants and localisation.....	117
5.2.3	Screening and training procedures before the test trials.....	117
5.2.4	Test trial series	118
5.2.5	Analysis	120
5.3	Results.....	122
5.4	Discussion	130

6	Functional organisation of the HF: is the subiculum an input or an output stage?	133
6.1	Introduction	133
6.2	Materials and Methods.....	135
6.2.1	Subjects	135
6.2.2	Data Analysis	135
6.3	Results.....	138
6.4	Discussion	152
7	General Discussion	157
7.1	Grid cell firing in the oscillatory interference model	158
7.2	Novelty and the theta rhythm	160
7.3	Organisation of hippocampal activity.....	162
7.4	Conclusions.....	163

Index of Figures

Figure 1.1 Depiction of the hippocampal axes	16
Figure 1.2 Gross anatomy of the rat hippocampus shown in horizontal and coronal section ...	17
Figure 1.3 Horizontal section through the rat hippocampal formation.....	19
Figure 1.4 Position and connectivity of the entorhinal cortex.....	20
Figure 1.5 Laminar and topographical organization of the entorhinal projection to the dentate gyrus, the hippocampus, and the subiculum	23
Figure 1.6 Overview of connectivity in the hippocampal formation	25
Figure 1.7 Summary of the transverse organization of the connections through the hippocampal formation.....	29
Figure 1.8 Example of the spatially constrained firing typical of a CA1 place cell	34
Figure 1.9 Example of the spatial firing of an entorhinal grid cell	37
Figure 1.10 Remapping in CA1 place cells induced by olfactory and visual changes, a complex interplay of several different forms of remapping is evident	40
Figure 1.11 Theta rhythm during movement and pharmacological intervention.....	46
Figure 1.12 Theta phase precession in CA1 cell recorded on the linear track as the rat runs from left to right.....	49
Figure 1.13 Basic 1D interference model and the effect of speed.....	55
Figure 1.14 Directional interference patterns	60
Figure 1.15 Schematic of the association of grid to environment via phase reset of grid cells by place cells.....	62
Figure 1.16 Moiré interference between two theta micro-grids.....	65
Figure 2.1 Design of the 'poor-lady' microdrive.....	72
Figure 2.2 Example screen shots from Tint spike sorting software.....	74
Figure 2.3 Histological photomicrograph of cresyl violet stained coronal section of a rat hippocampus	75
Figure 3.1 Example comparisons between ML and standard ratemaps.....	85
Figure 3.2 Distribution of R-values of linear fits to ML speed ratemaps.....	88
Figure 3.3 Normalised firing rate across a) Grid cells, b) TPD cells, c) HD cells, and d) Place cells.....	89
Figure 4.1 The 2D oscillatory interference model	96
Figure 4.2 Robustness of frequency estimates to variations in smoothing characteristics.....	101

Figure 4.3 The temporal characteristics of grid cell firing	105
Figure 4.4 Differences between intrinsic and EEG frequencies and the effect of running speed across cells	107
Figure 4.5 Instantaneous intrinsic and EEG frequencies as a function of speed	108
Figure 4.6 Difference between intrinsic and EEG frequencies and the relationship to grid scale	109
Figure 4.7 Directional modulation of frequencies with respect to the moiré interference model.	110
Figure 5.1 Experimental paradigm for collection of data used in chapter 5 and 6.....	119
Figure 5.2 EEG frequencies and speeds for individual rats and trials	123
Figure 5.3 Effect of novelty on theta frequency.....	124
Figure 5.4 Average over rats of baseline-adjusted theta frequency for each trial in the experiment.....	125
Figure 5.5 Effect over days on baseline-adjusted theta frequency.....	126
Figure 5.6 Effects over days on baseline-adjusted theta frequency in data sub-sampled to maintain constant median running speed	129
Figure 6.1 Cross-correlogram between subicular and CA1 spike trains, averaged over 52 trials, each contributing at least 3 cells to respective spike trains from each region (black line)	139
Figure 6.2 An example of spatial anticipatory differences in a simultaneously recorded CA1 and subicular ensemble of cells from day 2.....	141
Figure 6.3 Distribution of spatial anticipatory differences between subiculum and CA1	142
Figure 6.4 Differences in ensemble mean spatial anticipation between subicular and CA1 ensembles	144
Figure 6.5 Results from theta phase analysis.....	148
Figure 6.6 Speculative model of the organisation hippocampal activity during familiarity and novelty	155

Index of Tables

Table 3.1 Proportions of cells in each region positively and negatively modulated by speed...	87
Table 5.1 Correlation between median running speed and theta frequency per trial per rat. .	128
Table 6.1 Number of putative pyramidal cells recorded from each region at key stages of the test trial series	138
Table 6.2 Means and s.e.m. for relative spatial anticipation between CA1 and Subiculum for all data and simultaneous recorded data only, measured in days 1-3 and divided by cells, ensembles or rats	143
Table 6.3 Means and s.e.m. for relative spatial anticipation between CA1 and Subiculum for all data and simultaneous recorded data only, measured on only the first two day 1* (environment 'a') only and divided by cells, ensembles or rats	145
Table 6.4 Means and s.e.m. for relative spatial anticipation between CA1 and Subiculum for all data and simultaneous recorded data only, measured on measured on only the 3 rd and 4 th trial of day 1* (environment 'b') only and divided by cells, ensembles or rats	146
Table 6.5 Regressing ensemble optimal timeshift with the either behavioural or experimental variables did not explain difference in optimal timeshifts between CA1 and subiculum.	147

1 Introduction

1.1 Preamble

It has been in the study of the hippocampus that many of the general principles of modern neuroscience have been established. The intricacies of neurotransmission, long-term potentiation (LTP) – a form of plasticity thought to underlie learning, and the discovery of the neurogenesis of dentate granule cells throughout adulthood are but a few examples. Its unique anatomy – with all principal cells in a single layer and synaptic inputs to well-defined laminae, the capacity of the hippocampal slice to survive *in vitro* for long periods of time and the ability to isolate single cells, *in vivo*, in behaving animals have all contributed to making the hippocampus the most widely studied structure in the brain. These features, together with its specific role in declarative memory, its relatively well understood and distinct architecture and its established locus of pathology for epileptiform activity and neurodegenerative disorders such as Alzheimer's disease have made it a model structure for the systems approach to studying neuroscience.

One of the emerging hypotheses has been that the involvement of oscillations in hippocampal function is of paramount importance (Paulsen & Sejnowski, 2006; Sejnowski & Paulsen, 2006). There are many different oscillations of different frequencies in the hippocampus but a particularly important one is the theta oscillation. A 6-12 Hz oscillation, it is the largest measurable signal in extracellular local field potential recordings and execution of hippocampal mnemonic functions is critically dependent on its presence (Winson, 1978). Theta has been implicated in a number of roles, including organizing and synchronising activity across related structures and providing control over induction of LTP, and by inference, the storage and retrieval of information from the hippocampus. Another possible function would be providing a clock mechanism by which individual cell spikes may be timed. Indeed one of the key discoveries in hippocampal pyramidal cells and one of the most robust examples of temporal coding in the brain is the phenomenon of phase precession (see section 1.5.2), where the phase of each spike with respect to the concurrent theta rhythm reliably precesses from one cycle to next, increasing the resolution of spatial coding of hippocampal place cells (O'Keefe & Recce, 1993).

These ideas regarding timing and oscillations, and their specific contributions to the function of the hippocampal formation (HF) will be probed in this thesis. To this end, a large collection of single unit and local field potential data, from multiple sub-regions of the HF in behaving rats, will be analysed. In chapter 3, the results from an investigation of the effects of speed on a collection of cells from medial entorhinal cortex, dorsal presubiculum and CA1 are presented. These results demonstrate that there exists a small population of cells in each region, which show a robust negative correlation with speed. In chapter 4, data on recently discovered grid cells in the entorhinal cortex is explored in order to test specific predictions of an oscillatory interference model of their origin. These data support and constrain this type of model, whose key features are based on the oscillatory properties of individual cells specifically in the theta band. The results provide evidence for the theta rhythm as a phenomenon directly involved in the formation and maintenance of principal cells of the entorhinal cortex and necessary for them to exhibit their particular firing patterns and environmental correlates. In chapter 5, the dynamics of the theta rhythm during the exploration of novel environments is examined. Surprisingly, the frequency of the theta oscillation is modulated by novelty, decreasing in novel environments. This decrease is even greater in environments that violate the rat's expectation of encountering a habituated context than that seen in simple novelty, when there has been no previous familiarisation with any particular context. The results of this chapter propose a physiological mechanism for signalling the cognitive concept of novelty in the hippocampus. In chapter 6 this study is extended to consider the relationships between populations of cells recorded simultaneously from the subiculum and the CA1 fields of the hippocampus. The findings here indicate that far from the traditional view that subiculum is the output of the hippocampal formation, it may be part of the input to the system, informing the hippocampus about context-invariant environmental features. This is based on evidence that the subiculum is found to fire earlier in the theta cycle than its major afferent region CA1 and prospectively codes the spatial domain further ahead of the rat than CA1, with both effects showing plasticity in the face of novelty. Finally, in the last chapter, these results are discussed in view of the ideas stated above and with respect to theoretical models of hippocampal functions involving theta oscillations and our wider understanding of the hippocampal formation.

However, before discussing these results, a brief overview of the relevant literature is presented next.

1.2 Nomenclature

Throughout this document the *hippocampal formation*, following Amaral & Witter (1995), is considered to include six distinct regions: dentate gyrus (DG); the Cornu Ammonis (CA) fields CA1, CA2 and CA3; subiculum; presubiculum; parasubiculum; and entorhinal cortex (EC). '*Hippocampus*', where used, is considered to apply only to CA1, CA2 and CA3. Note, this nomenclature is predicated on the largely unidirectional connections that link these six areas and which distinguish them from neo-cortical structures (Amaral & Witter, 1995). As such it departs from the scheme applied elsewhere, for example by Scharfman *et al.* (2000), in which the hippocampal formation is considered to consist exclusively of allocortex; being the DG, CA fields, and subiculum; three layered structures consisting of a single cell layer between plexiform layers. The term '*place cell*' (O'Keefe & Recce, 1993) is used exclusively to apply to pyramidal cells of the CA1 and CA3 regions that exhibit spatially constrained firing. Similarly '*grid cell*' (Hafting, Fyhn, Molden, Moser, & Moser, 2005) describes dLMEC cells that exhibit spatially stable firing arranged in a periodic, triangular grid that spans the environment. This definition likely includes stellate cells from layer II and pyramidal cells from layers III, V and VI. Other cell types will be defined as is necessary but in general will simply be referred to by region (e.g. 'cells in the subiculum that exhibit spatial firing').

1.3 Structure and morphology of the hippocampal formation

1.3.1 Overview

In the rat, the hippocampal formation represents a significant component of the central nervous system, occupying half the cortical volume and presenting a combined surface area nearly equivalent to the entire neocortex (1.2cm^2 vs. 1.5cm^2) (Swanson, 1983; Amaral & Witter, 1995). In gross outline, the hippocampal formation resembles a pair of 'C's with the open face of the 'C' being most rostral, the entire structure being buried below the neocortical sheet (see Figure 1.1 & Figure 1.2). The long axis is referred to as the septo-temporal axis, with the septal pole being both rostral and dorsal to the temporal pole. For this reason septo-temporal is often used synonymously with dorso-ventral. A further axis, the transverse axis, is defined running medial to lateral, such that regions closest to the DG are considered to be proximal; those closest to the rhinal sulcus and postrhinal cortices are considered to be distal. Finally, the radial axis is defined orthogonally to both of these, such that surfaces close to the ventricle are considered to be deep, and those closer to the hippocampal fissure, superficial.

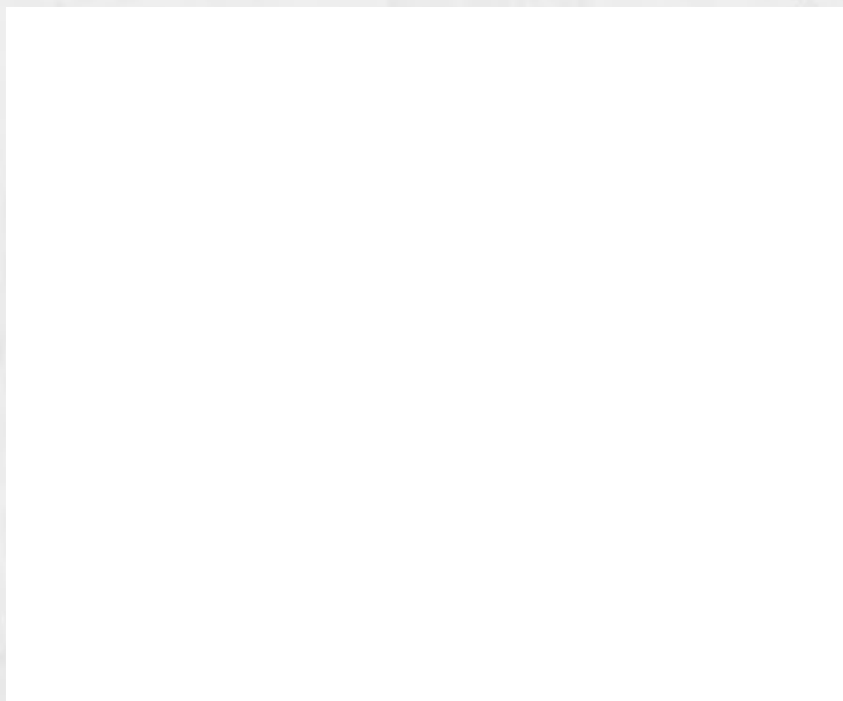


Figure 1.1 Depiction of the hippocampal axes. Longitudinal – from septal to temporal, transverse – the expanded cross-section, proximal regions are closer to the DG, while distal is towards the entorhinal cortex (beyond CA1). Finally radial, is perpendicular to both of these (perpendicular to the cell layer in the expanded cross-section), where superficial is towards the hippocampal fissure (line above DG) and deep is in a direction away from it. From (Amaral & Witter, 1989), expanded cross-section originally illustrated in (Andersen, Bliss, & Skrede, 1971).



Figure 1.2 Gross anatomy of the rat hippocampus shown in horizontal and coronal section. **A)** The hippocampi are shown in position below the neocortical sheet. Left hippocampus is coloured red. The fornix (f) is indicated descending to its subcortical targets. **B)** Horizontal sections taken at three dorso-lateral levels along the hippocampus reveal its differing composition; EC is only evident at ventral levels. **C)** Coronal sections taken at three rostro-caudal levels. CA1 and CA3, principal fields of hippocampus. CPu, caudate and putamen. DG, dentate gyrus. Fi, fimbria. S, subiculum. Adapted from (Amaral & Witter, 1995).

The constituents of the hippocampal formation change considerably at various positions along the septo-temporal axis (Figure 1.2B&C). At the septal pole, for example, only the DG and CA fields are present, these are easily identified in slices by the distinctive interlocking 'C' shape formed by the cell layers in each (Figure 1.1 & Figure 1.3A). The subiculum appears about a third of the way along the axis with the presubiculum and parasubiculum located even more temporally. Finally, the EC is located ventrally, at the most caudal portion of the cortex. There are two main fibre systems serving the hippocampal formation. The major fibre bundle of the hippocampal formation is the fimbria-fornix pathway. The surface of the hippocampus is covered by a thin sheet of myelinated fibres called the alveus, which contains extrinsic efferent and afferent fibres and fibres forming part of the intrahippocampal network. At temporal levels, subcortically directed fibres extend obliquely and collect at the lateral edge of the hippocampus to form the fibre bundle known as the fimbria (Figure 1.3B). It increases in thickness towards the septal pole as more fibres are added. The fimbria departs the hippocampal formation at its septal extreme and descends to the basal forebrain; from this point it is referred to as the fornix. Immediately prior to the fornix, a large number of fimbria fibres give rise to the ventral hippocampal commissure; the majority of these fibres project to hippocampal fields in the other hemisphere with a smaller number joining the contralateral fornix. The fornix itself branches several times, ultimately innervating multiple subcortical targets such as the septal nuclei, anterior thalamic nuclei, mammillary bodies and hypothalamic areas (Gloor, 1997). The other fibre system is the angular bundle which carries entorhinal as well as para and presubicular fibres and is located between the entorhinal cortex and para and presubiculum and is the primary route via which neocortical inputs reach the dentate gyrus and hippocampus. The angular bundle gives rise to the dorsal hippocampal commissure and this is the main route by which fibres travel from the entorhinal cortex to other hippocampal fields and also whereby the presubiculum contributes a major projection to the contralateral entorhinal cortex.

The emphasis of the following subsections is on relevance. Anatomical detail is omitted where it is not considered relevant to the models and data that are the focus of this work. A complete review of hippocampal anatomy is provided by

Amaral and Witter (1995) in their excellent chapter in the Rat Nervous System and by Amaral and Lavenex's work in The Hippocampus Book (Amaral & Lavenex, 2007).



Figure 1.3 Horizontal section through the rat hippocampal formation. A. Nissl-stained section. B. Line drawing shows the various regions, layers, and fibre pathways. C. Timm's sulphide silver-stained section. Note the three bands of the molecular layer of the dentate gyrus in C. The outer band corresponds to the terminal zone of the lateral perforant pathway; the middle unstained region corresponds to the terminal zone of the medial perforant pathway; the inner band corresponds to the zone of termination of the associational and commissural pathways of the dentate gyrus. ab, angular bundle; al, alveus; CA1, CA1 field of the hippocampus; CA2, CA2 field of the hippocampus; CA3, CA3 field of the hippocampus; DG, dentate gyrus; EC, entorhinal cortex; fi, fimbria; gel, granule cell layer of the dentate gyrus; hf, hippocampal fissure; ml, molecular layer of the dentate gyrus; Para, parasubiculum; pd, pyramidal cell layer of the hippocampus; pl, polymorphic layer of the dentate gyrus; Pre, presubiculum; sl, stratum lucidum of CA3; sr, stratum radiatum of the hippocampus; sl-m, stratum lacunosum moleculare of the hippocampus. Roman numerals: cortical layers. Bar in A = 500 μ m and applies to all panels. Adapted from (Amaral & Lavenex, 2007).

1.3.2 Entorhinal cortex

The rodent entorhinal cortex (EC) is a six layered structure located at the ventro-posterior extremity of the cerebral hemisphere. It is bordered laterally by the rhinal sulcus and medially by the presubiculum (Figure 1.4a&b). On the basis of morphology and connectivity, the region can be subdivided into two fields, lateral and medial entorhinal cortex (LEC and MEC), often referred to as the lateral and medial entorhinal areas (LEA and MEA). Despite their names the MEC is, largely speaking, caudal to the LEC, with the two triangularly shaped regions being placed so as to form a trapezoid structure.

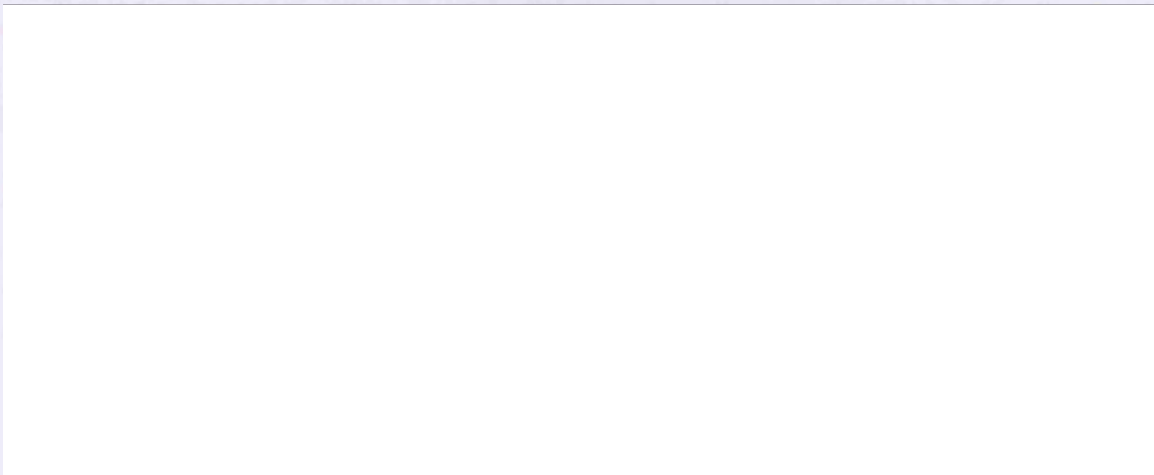


Figure 1.4 Position and connectivity of the entorhinal cortex. a) Left hemisphere of rat brain, the triangularly shaped LEC (green) and MEC (red) can be made out on the posterior surface bordered by perirhinal (PER) and postrhinal (POR) cortices. The hippocampal formation (HF) is indicated in purple. b) Horizontal section through the hippocampal formation's subfields; scale bar indicates 100µm. The postrhinal cortex, LEC and MEC are indicated as before with the parasubiculum (PAS) and presubiculum (PRS) proximal to those structures. Below the cortical sheet, the interlocking 'C's of the CA fields and dentate gyrus (DG) are clearly visible. The less dense pyramidal cell layer of the subiculum (S) is also very clear. Image adapted from (Witter & Moser, 2006).

In both the LEC and MEC, layers II, III, V and VI are the principal cell layers, leaving two plexiform layers, layers I and IV; layer IV, the lamina dissecans is less distinct in the LEC. Stellate cells comprise the majority of layer II and are the principal origin of the perforant path to the dentate gyrus and CA3. Pyramidal, multipolar, and horizontal cells are also found in layer II, though in lesser numbers (Figure 1.3B). In common with other cell layers in the EC, layer II produces multiple collaterals, which in this case innervate only superficial layers (Kohler, 1986; Kohler, 1988), and in the case of the MEC are known to provide excitatory connections between stellate cells (Kumar, Jin, Buckmaster, & Huguenard, 2007). Pyramidal cells, the principal cell type of layer III, originate

projections to CA1 and the subiculum and like layer II send collaterals to superficial layers, though mainly I and III (Figure 1.3C). These cells also send apical dendrites up to layer I where they likely synapse with the sparse inhabitants of that layer: GABA-ergic neurons, as well as horizontal and stellate cells (Witter, Groenewegen, Lopes da Silva, & Lohman, 1989). The organisation of layers V and VI is more complex and less well understood, relying to an extent on Golgi work conducted during the 1930s (e.g. (Lorente de No, 1933)). Superficial layer V is dominated by large pyramidal cells that send axons to the deep white matter and thus out to other cortical regions. The same cells also dispatch collaterals to all layers of the EC, though predominantly to layers V and VI. However, in deep layer V and layer VI, various cell types send highly collateralised axons to influence a column of cells in layers I, II and III and also project out of the EC via white matter. Putative GABA-ergic interneurons are found in all layers though in increased concentration in superficial layers (Swanson, Kohler, & Bjorklund, 1987).

The superficial layers of the EC receive much of their extrinsic cortical input via the postrhinal and perirhinal cortices which in turn receive input from unimodal and poly-modal association areas. In particular, the perirhinal cortex receives strong olfactory projection from the piriform cortex, while the postrhinal cortex receives a greater proportion of visual and visuo-spatial inputs from the retrosplenial, posterior parietal and cingulate cortices (Burwell, Witter, & Amaral, 1995; Burwell & Amaral, 1998b; Burwell & Amaral, 1998a). This distinction is maintained within the EC, with perirhinal cortex primarily projecting to the LEC, and postrhinal cortex to the MEC. In addition, the superficial EC receives direct neocortical projections from unimodal, notably olfactory, and poly-modal association areas, and these too follow a similar scheme, such that the MEC receives predominantly visuo-spatial inputs (Burwell & Amaral, 1998b). The deep layers of the EC also receive cortical afferents from a variety of areas including the medial prefrontal region and agranular insular cortex (Insausti, Herrero, & Witter, 1997). These deep inputs are generally viewed as modulatory, influencing the flow of information out of the hippocampal formation, and stand in contrast with superficial afferents which are assumed to convey information destined for the hippocampus. The EC also receives a number of subcortical inputs from structures as diverse as the

amygdaloid complex, the septum, thalamic nuclei and various structures in the hypothalamus.

The perforant path, so called because it passes through, or perforates the hippocampal fissure, represents the primary entorhinal input to the hippocampus. Originating mainly but not exclusively from layer II stellate cells and layer III pyramidal cells, it projects to all fields of the hippocampus (Germroth, Schwerdtfeger, & Buhl, 1989; Kohler, 1985; Kohler, 1986; Kohler, 1988). Based on topographical considerations, it is possible to distinguish at least three axes that relate to the organisation of the perforant path. Firstly layer II cells project primarily to the DG and CA3, while layer III projects largely to CA1 and the subiculum (Figure 1.6). A further distinction can be made based on whether projections originate in the MEC, LEC, or an intermediate zone around the division between them. At the level of the DG and CA3 this second axis is reflected in the radial termination site of perforant path fibres: projections from the LEC terminate in the outer third of the molecular layer and in similar superficial sites in the stratum lacunosum-moleculare; fibres originating in the MEC, on the other hand, terminate in the middle third of the DG and at more superficial sites in CA3. Electrophysiological investigations support the intuitive conclusion that individual cells within these areas are likely to be influenced by projections from both the LEC and MEC (McNaughton & Barnes, 1977). In contrast, at the level of CA1 and the subiculum, the lateral and medial components of the perforant path terminate at different transverse positions. For example, the medial perforant path reaches proximal CA1 and distal subiculum, whereas lateral fibres terminate in distal CA1 and the adjacent, proximal section of the subiculum (see Figure 1.7). A third axis lies across the MEC – LEC division such that cells located medially in the EC, project to temporal positions within the hippocampus and those located laterally project to the septal levels. To clarify, medial and lateral bands drawn across the EC as a whole actually cut across both areas (Figure 1.5). A final, important consideration is that both the septo-temporal and proximo-distal arrangements described above, are reciprocated by projections back from CA1 and the subiculum to deep layers of the EC. These projections are point-to-point so for example, proximo-temporal CA1 which receives perforant input from the medial extent of the MEC, the

region in which grid cells are found, will project back to that same section of the MEC.



Figure 1.5 Laminar and topographical organization of the entorhinal projection to the dentate gyrus, the hippocampus, and the subiculum. The surface of the entorhinal cortex is represented on the left (the rhinal sulcus is to the left). Layer II entorhinal cortex projections to the dentate gyrus and the CA3 and CA2 fields of the hippocampus terminate in a laminar fashion; the LEA projects superficially in the molecular layer and the stratum lacunosum moleculare, and the MEA projects deeper. In contrast in CA1 and subiculum, layer III entorhinal cortex projections are organized topographically; the LEA projects to the distal CA1 and proximal subiculum (i.e., at the CA1/subiculum border), and the MEA projects to the proximal CA1 and distal subiculum. Laterally situated portions of the entorhinal cortex project to septal levels of the hippocampal formation, whereas progressively more medial portions of the entorhinal cortex project to more temporal levels of the hippocampal formation. Adapted from (Amaral & Lavenex, 2007).

1.3.3 Dentate gyrus

The dentate gyrus (DG), the simplest and therefore the best studied of the hippocampal fields, is comprised of three layers. The most superficial is the



Granule cells themselves are the principal cell type of the DG, generating efferents to CA3. Estimates of the number of these cells vary, though typically fall above 1×10^6 for a single hemisphere, making them one of the most numerous cell types in the hippocampal formation (West, Slomianka, & Gundersen, 1991). The subgranular zone of the DG is one of only two regions in the adult where new neurons are constantly being produced well into adulthood. Although the dentate volume doesn't increase in adulthood, once matured, neonate cells are preferentially recruited into spatial memory networks (Bayer, Yackel, & Puri, 1982; Kee, Teixeira, Wang, & Frankland, 2007). Intimately associated with granule cells are the inhibitory pyramidal basket cells, found along the deep surface of the granule cell layer, they form synapses with, and peri-cellular plexuses around the cell bodies of granule cells. The most prominent cell type of the polymorphic layer is the mossy cell.

The primary extrinsic input to the DG contacts the molecular layer via the perforant path from layer II of the EC (Figure 1.6). Minor projections to this layer also arise in the pre and parasubiculum (Kohler, 1985). The DG also receives limited input from subcortical structures, the most notable being septal projections from the medial septal nucleus and the nucleus of the diagonal band of Broca. Septal fibres mainly terminate in the polymorphic layer, the majority being cholinergic with a smaller proportion being GABA-ergic. The DG also receives afferents from the brainstem, for example from the locus coeruleus and raphe nuclei, as well as from the hypothalamus.

In addition to intrinsic inhibitory inputs provided by a variety of basket cell types, the DG also exhibits two types of intrinsic excitatory connection. Granule cells give rise to distinctive, unmyelinated axons, called mossy fibres bound for CA3, which also form thinner collaterals that innervate the polymorphic layer forming synapses with glutamatergic (excitatory) mossy cells, pyramidal basket cells as well as other GABA-ergic cell types. In turn, mossy cells, and possibly other cell types from the polymorphic layer, project back to the molecular layer forming excitatory synapses with granule cells and basket cells. Mossy cells have an extraordinarily extensive axonal plexus ramifying throughout the polymorphic layer at considerable distances from the soma, innervating as much as 75% of the long axis of the hippocampus. Curiously, their effects on

granule cells are weakest at the level of origin and stronger at more distal levels along the septo-temporal axis (Amaral & Witter, 1989). Mossy cells are the recipients of massive granule cell innervation. Thus, it appears they pass on the collective output of granule cells at one septo-temporal level, to those of another distant level. This is combined with the associational connections of mossy cells to inhibitory basket cells, which in turn innervate granule cells locally, providing both feedforward excitatory connections to distant granule cells and feedforward disynaptic inhibition at more local levels.



Figure 1.6 Overview of connectivity in the hippocampal formation. A. Neurons in layer II of the entorhinal cortex project to the dentate gyrus and the CA3 field of the hippocampus proper via the perforant pathway. Neurons in layer III of the entorhinal cortex project to the CA1 field of the hippocampus and the subiculum via the perforant and alvear pathways. The granule cells of the dentate gyrus project to the CA3 field of the hippocampus via mossy fibre projections. Pyramidal neurons in the CA3 field of the hippocampus project to CA1 via Schaffer collaterals. Pyramidal cells in CA1 project to the subiculum. Both CA1 and the subiculum project back to the deep layers of the entorhinal cortex. B. Projections along the transverse axis of the hippocampal formation; the dentate gyrus is located proximally and the entorhinal cortex distally. In both A & B not shown are the extensive recurrent collaterals between CA3 pyramidal cells. Adapted from (Amaral & Lavenex, 2007).

The ultimate and main target of the mossy fibres is the CA3 field. In CA3 they pass just above the pyramidal cell layer in the stratum lucidum; in proximal regions of CA3 mossy fibres also terminate within and below the pyramidal cell layer. Connections between the mossy fibres and proximal dendrites of CA3 pyramidal cells are unusual; comprising complex en passant presynaptic terminals known as mossy fibre expansions, coupled with postsynaptic branched spines called thorny excrescences. Not only are these terminals extremely large, up to 8µm, but each mossy fibre might make as many as 37 contacts with a single pyramidal cell (Chicurel & Harris, 1992). Together with their size, the location of these synapses, close to the cell body may imply that mossy fibres exert a powerful influence over CA3 pyramidal cells. Conversely each mossy fibre contacts relatively few, about 15, pyramidal cells which indicates that each pyramidal cell receives input from around 70 granule cells.

1.3.4 Hippocampus

All of the Cornu Ammonis¹ fields (CA1, CA2 and CA3) share a similar laminar structure. The principal cell layer is the densely packed pyramidal layer sandwiched between the deep, relatively cell free stratum oriens and superficial stratum radiatum. Both of these contain the extensive CA3 to CA3 associational synapses and CA3 to CA1 Schaffer collateral synapses. In CA3 only, an additional layer, the stratum lucidum is interposed between the pyramidal cell layers and stratum radiatum. Finally, in all fields the perforant path terminates in the most superficial layer, the stratum lacunosum-moleculare. In the following description CA2 is largely ignored, this reflects both a historical uncertainty about its relationship to CA1 and CA3 (it can be seen as a terminal section of CA3) as well as its relatively small size compared to the other CA fields.

Pyramidal cells are the principal cell type of CA1 and CA3, comprising most of the cells in the pyramidal cell layer. From each cell, basal dendrites descend into the stratum oriens while apical dendrites reach up into the stratum radiatum and stratum lacunosum-moleculare. CA1 pyramidal cells tend to be smaller

¹ *Cornu Ammonis* refers to the horn of Amun. Amun, a god, initially depicted by the Egyptian civilisation, later became associated with the ram. Though originally used to depict the hippocampus as a whole, Cornu Ammonis now refer to the single layered fields of the hippocampus, which can be seen in stained cross sections Figure 1.3 to share a similar curved form to the horn of a ram.

than those from CA3 both in terms of somata and dendritic arborisation. Along with the principal pyramidal cells, two types of interneuron, pyramidal basket cells and axo-axonic cells, have their cell bodies in or adjacent to the pyramidal cell layer. In both cases their dendrites span all levels of the field, with the axons of the basket cells innervating the soma and proximal dendrites of pyramidal cells, whereas axo-axonic cells form synapses onto the axons of pyramidal cells. Several other non-pyramidal cell types are found throughout CA1 and CA3, the majority being immunoreactive for GABA, and as such are presumed to be inhibitory interneurons. Indeed, a recent count identified nearly 20 different types of interneuron distinguished on the basis of morphology and histology (Somogyi & Klausberger, 2005).

CA3 and CA1 both receive extrinsic input from the EC via the temporoammonic path while CA3 is also driven by mossy fibres from the DG. The EC input represents the major cortical input to these fields; CA3 in particular has no other known connection with the neocortex. However, the main source of input for both fields comes from within the hippocampus; CA3 generates highly collateralised axons that innervate all levels of the ipsilateral and contralateral CA fields. This is its defining characteristic, CA1 cells on the other hand show little associational connectivity. This results in an abrupt end in the CA3 layer in Timm's sulphide stained sections, (Figure 1.3C). The CA3 to CA1 connections, known as Schaffer collaterals are highly divergent and a single CA3 cell can project to as much as 65% of the septo-temporal extent of CA1 (Li, Somogyi, Ylinen, & Buzsaki, 1994). Connection density is not uniform though and a complex topography relates the septo-temporal and proximo-distal position of cells in CA3 to their termination site in CA1 (for complete details see Ishizuka, Weber, & Amaral (1990)). One feature of note is that proximal CA3 cells project most heavily to distal CA1, while distal CA3 projects most heavily to proximal CA1. The CA3 to CA3 (associational) connections are similarly divergent and also exhibit a topographic organisation such that projection targets of cells in proximal portion of CA3 are less widely spread than those located more distally (Ishizuka, Weber, & Amaral, 1990). Additionally, in the rat but not in primates, CA3 cells produce commissures that innervate homologous fields in the contralateral hemisphere (Blackstad, 1956). Indeed, a single CA3 cell can

generate collaterals destined for both the ipsilateral and contralateral hemispheres (Swanson, Sawchenko, & Cowan, 1980).

Aside from the dense associational connections and Schaffer collaterals, the only other major target of CA3 is the lateral septal nucleus, to which it is reciprocally connected. In addition to the connectivity described in the previous paragraph, CA1 provides major input to the subiculum and EC. In the case of the latter structure the topography of these connections reciprocates the topography of direct EC to CA1 connections (described above). Subicular afferents are also topographically organised such that proximally positioned CA1 cells project to the distant, distal portion of the subiculum, whereas distal CA1 cells project to the proximal subiculum. CA1 axons exit CA1 at the level of the stratum oriens and terminate in the pyramidal cell layer and deep molecular layer of the subiculum.

Both CA3 and CA1 also receive projections from the amygdala, though in the case of CA3 these are mainly limited to the temporal region. CA1 alone receives additional cortical input from perirhinal and postrhinal cortices, and sends return projections back to the former structure as well as to retrosplenial cortex. Similar to the DG, CA3 and to a lesser extent CA1 receives and returns subcortical input from the septum, specifically the medial septal nucleus and diagonal band of Broca. CA3 also receives some afferents from hypothalamic regions, whereas CA1 is targeted by thalamic afferents from regions such as the nucleus reunions. Finally, both structures receive input from brain stem nuclei such as the raphe nuclei.



Figure 1.7 Summary of the transverse organization of the connections through the hippocampal formation. This figure highlights the possibility that information is segregated, or "channelled," through the hippocampal formation and ultimately reaches different recipients of hippocampal output. Adapted from (Amaral & Lavenex, 2007).

1.3.5 Subiculum

In addition to CA1, the subiculum originates the other major projection back to the EC. It is also the source of the chief output from the hippocampal formation to subcortical structures and the major origin of the fibres of the fornix. As such, the subiculum is thought to be the final step in the hippocampal processing loop. For a recent review of the anatomy of the subiculum see (Witter, 2006) and (Amaral & Lavenex, 2007). The border between CA1 and the subiculum is marked by a loss of the stratum radiatum which is replaced by the subiculum molecular layer, and a concomitant widening of the pyramidal cell layer (Figure 1.3). The stratum oriens of CA1 is also lost at this point. The deep portion of the molecular layer is continuous with the stratum radiatum of CA1 and is the site at which CA1 afferents terminate. The most superficial section of the molecular layer, on the other hand, is continuous with the stratum lacunosum-moleculare of CA1 and receives afferents from the EC.

Similar to the hippocampus, the principal cell type of the subiculum is a large pyramidal cell that populates the pyramidal cell layer. Though morphologically similar, electrophysiological criteria distinguish at least two subpopulations: regular spiking cells and intrinsically bursting cells. Bursting cells are mainly

found deep in the pyramidal layer, whereas regular spiking cells are more numerous superficially (Greene & Mason, 1996). In addition bursting cells give rise to local axonal distributions that remain largely within the area circumscribed by their apical dendrites, while regular spiking cell axons have a more widespread distribution along the transverse axis, pointing to a rudimentary columnar and laminar organisation. Interestingly, it is believed that only the bursting cells project to the EC. Relatively little is known about subicular interneurons, though many smaller cell types are found in the pyramidal cell layer, some of which are immunoreactive for GABA.

The subiculum is the major target of CA1 efferents. It also exhibits internal associational connections such that subicular pyramidal cells project to more temporal regions of the subiculum but rarely, if ever, project more septally. Beyond this, commissural connections either to or from the subiculum have never been found. Subicular efferent targets include the presubiculum, terminating largely in layer I with some deeper termination sites in the dorsal presubiculum, while in the parasubiculum they also target layer I with some synapses in superficial layer II. Both sets of connections are topographically organised, such that the septal subiculum projects to dorsal and caudal regions of the para and presubiculum, while temporal subiculum targets ventral and rostral regions (Witter & Groenewegen, 1990). As with CA1, subicular projections to the EC reciprocate the topography of EC to subicular connections (point-to-point). Hence the proximal subiculum projects to the LEC whereas more distal areas reach the MEC. The principal termination site in EC is layer V; though afferents also reach layer VI, as well as the more superficial layer III. This topographical organisation of subicular efferent projections is preserved to all of its targets; in principle maintaining the transverse topography of the CA1 to subiculum connections (see Figure 1.5 and Figure 1.7). This is coupled with a marked septo-temporal topography. Thus, different septo-temporal levels of the subiculum project to progressively different portions of EC (as described previously in CA1, see Figure 1.5), lateral septal nucleus, medial mammillary nucleus and nucleus accumbens, the amygdala and a number of other subcortical targets. While the topography is graduated in this axis, the transverse organisation of subicular efferents is discrete. Along the entire septo-temporal axis, though clearer septally than temporally, two non-overlapping

populations of cells give rise to projections to specific brain structures. These include, among others, the infralimbic, prelimbic and perirhinal cortices, which receive proximal subicular projections, and retrosplenial cortex, which receives input from distal subiculum. The subiculum also generates input to the medial and ventral orbitofrontal cortices.

1.3.6 Presubiculum and parasubiculum

The pre and parasubiculum do not fit quite so nicely into the notion of a 'hippocampal processing loop' as do the other structures of the hippocampal formation. Indeed, it remains unclear whether they should be considered as an input or an output. Amaral & Witter (1995) conclude that these two structures are most akin to an input as they project to superficial layers of the EC. However, they also concede that strong reciprocal connectivity with the anterior thalamic nuclei marks them out as a conduit for thalamic control over the hippocampal formation.

The presubiculum, placed distally to the subiculum, is sometimes subdivided into the presubiculum and postsubiculum, the latter structure being synonymous with 'dorsal presubiculum'. Together with the adjacent parasubiculum, the presubiculum is distinct from the allocortical hippocampus in that it is multi-laminate like the EC, and as such six layers can be distinguished. In both structures, layers II and III are densely populated by pyramidal cells, while deeper layers, which are continuous with the deep layers of the EC, are populated by a variety of different cell types.

The pre and parasubiculum both generate internal associational connections, as well as commissures to homotopic regions of the contralateral hemisphere. However, most striking is their dense interconnectivity with anterior thalamic nuclei, which is unique to these portions of the HF. Thalamic connectivity is best described in the presubiculum, in that dorsal regions are known to receive input primarily from laterodorsal and anterodorsal nuclei, while more ventral regions are reached by projections from laterodorsal and anteroventral nuclei. In turn the presubiculum sends a massive return projection back to the anterior thalamic nuclei. In addition to the subicular input mentioned previously, other cortical inputs arrive from the retrosplenial cortex and to a lesser extent visual

area 18b. Interestingly, the pre and para-subiculum both project bilaterally to each other. Subcortical inputs are received from the medial septal nuclei, the diagonal band of Broca, mammillary nuclei and the brain stem.

Aside from the reciprocal thalamic connectivity the two major outputs of the pre and parasubiculum are to structures within the hippocampal formation. Both send substantial afferents to superficial layers of the EC; the presubiculum primarily to layer III of the MEC while the parasubiculum innervates layer II of the MEC and to a lesser extent the LEC. The location of the pre and parasubicular terminal field in the entorhinal cortex is determined by the proximo-distal and dorsoventral location of the cells of origin. In addition, the presubiculum generates input to the DG, CA fields and subiculum. However the parasubicular input to the DG is much more developed. Interestingly, Amaral and Lavenex (2007) suggest that these final two points may indicate a route by which thalamic input can influence the early stages of information processing in the hippocampal formation.

1.3.7 Summary

In synopsis, a simple view is that hippocampal connectivity describes a processing loop, albeit a loop with several sub-loops. Highly processed sensory information reaching the superficial layers of the EC is then routed into the hippocampus proper, either via the dentate-CA3 fields or directly to CA1. Back projections from CA1 to the deep layers of the EC as well as similar projections from the subiculum close the loop. Finally, projections from the deep layers of the EC either return the output to other cortical regions or redirect it to superficial layers of the EC, presumably from where it re-enters the loop or modulates the entrance of novel information.

In addition to the largely unidirectional connectivity, the HF is characterised by massively convergent and divergent connections such that small areas of one region can influence large areas of the next, while a single neuron might receive wide-ranging afferent projections. Given the septo-temporal topography of the hippocampus and the segregation of exteroceptive and interoceptive inputs via the lateral to medial parts of the entorhinal cortex respectively (Figure 1.5), it may be speculated that different parts of the hippocampus specialise in subtle

ways. The proximo-distal topography of connections in the hippocampus, also respected by a segregation of input from LEC and MEC, implies the possibility of multiple partially independent channels of information flow. Finally despite unidirectional connectivity, information flow is far from serial. Projections from EC to DG, CA3, CA1 and subiculum imply many parallel processing streams, consistent with the finding that CA1 place cells are apparently normal after surgical destruction of CA3 connections to CA1 (Brun, Otnass, Molden, Steffenach, Witter, Moser, & Moser, 2002).

1.4 Behavioural correlates of hippocampal cells

Place cells, hippocampal pyramidal cells that exhibit spatially localised activity, were first identified by O'Keefe & Dostrovsky (1971). Since the initial discovery, cells with spatially modulated firing have been found in almost all areas of the hippocampus and in some surrounding areas e.g. dentate gyrus (Jung & McNaughton, 1993), entorhinal cortex (Quirk, Muller, Kubie, & Ranck, Jr., 1992; Hafting et al., 2005), and subiculum (Sharp & Green, 1994)). Although early work was conducted on rats, similar cells have subsequently been found in other species of rodent (Tonegawa, Tsien, McHugh, Huerta, Blum, & Wilson, 1996), including bats (Ulanovsky & Moss, 2007), pigeons (Bingman, Siegel, Gagliardo, & Erichsen, 2006), monkeys (Rolls, Miyashita, Cahusac, Kesner, Niki, Feigenbaum, & Bach, 1989; Ono, Nakamura, Fukuda, & Tamura, 1991; Hori, Tabuchi, Matsumura, Tamura, Eifuku, Endo, Nishijo, & Ono, 2003; Ludvig, Tang, Gohil, & Botero, 2004) and even humans (Ekstrom, Kahana, Caplan, Fields, Isham, Newman, & Fried, 2003).

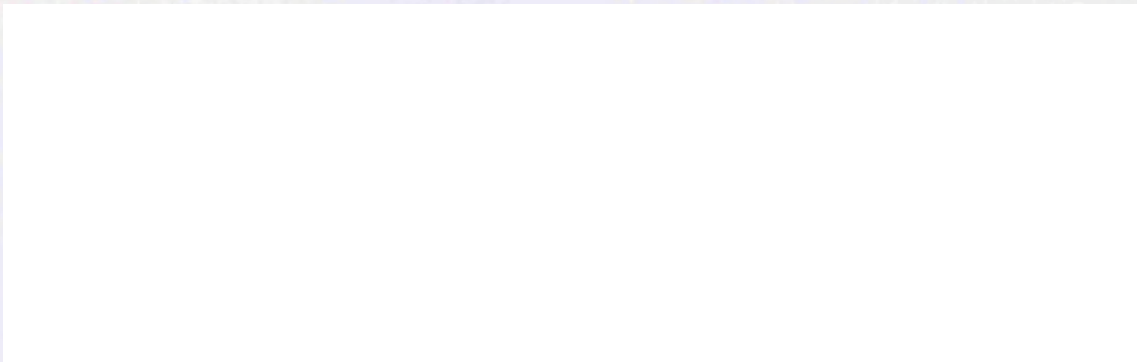


Figure 1.8 Example of the spatially constrained firing typical of a CA1 place cell. Four minute recording made in a 70cm square enclosure. From left to right: Left) Rat's path is denoted by the continuous black line with action potentials indicated by the superimposed red dots; each dot indicates the animal's position when an action potential was fired. Middle) Rate map constructed from raw data shown to the left. The firing rate of the place cell was calculated for each bin - in this case the environment was divided into approximately 30 by 30 bins. Peak rate is indicated above the map and warmer colours represent higher firing rates. White indicates unvisited bins. Right) Collectively, several place fields, of the type shown in the left panel, each indicated by a different colour may provide a spatial representation of the entire environment. Adapted from (Barry, 2008).

1.4.1 Functional properties of hippocampal cells

The striking quality of place cells is that they seem to provide a precise representation of an animal's position in its environment. At the time of discovery, this was one of few examples if any, of a robust correlation between firing rate and behaviour. The background firing rate of place cells is very low,

effectively being zero. When an animal enters the receptive field (place field) of a cell, its firing rate rapidly increases, typically to a maximum between 5Hz and 15Hz (Figure 1.8). In addition to this rate code, place cells also exhibit a temporal code, called phase precession, introduced in more detail in 1.5.2. Interestingly, in a given environment, the majority of place cells are silent with only about a third of CA3 and CA1 cells being active (Thompson & Best, 1989; Guzowski, McNaughton, Barnes, & Worley, 1999; Leutgeb, Leutgeb, Treves, Moser, & Moser, 2004). In an open environment, activity is independent of the animal's orientation (O'Keefe, 1976). In essence, firing is best correlated with the position of an animal's head (Muller & Kubie, 1989), and can be used to infer it (Wilson & McNaughton, 1993). Conversely, environments or tasks that constrain an animal's path often result in place fields developing a strong directional component to their firing (McNaughton, Barnes, & O'Keefe, 1983; Markus, Qin, Leonard, Skaggs, McNaughton, & Barnes, 1995). Speed of movement is also known to influence the firing of place cells, such that on average, faster running results in higher rates of spike discharge (McNaughton et al., 1983).

Place fields seem to be randomly distributed across an environment, with perhaps a tendency to be smaller and more numerous near to the environmental boundaries (Hetherington & Shapiro, 1997). Place cell firing can be detected within the first few minutes of an animal's entrance into a novel environment, although it is initially unstable and less robust than in a familiar space (Wilson & McNaughton, 1993). In invariant conditions, place fields are extremely stable, in some cases persisting for months (Best & Thompson, 1984). During a single exposure to an environment, a place cell will continue to fire each time an animal moves through its field; although the cell's firing rate can be somewhat variable between runs (Muller, Kubie, & Ranck, Jr., 1987).

Complementary representation of orientation, independent of location, is found in the 'head-direction' cells of the lateral mammillary bodies, anterior thalamus and presubiculum (Taube, Muller, & Ranck, Jr., 1990a; Taube, Muller, & Ranck, Jr., 1990b; Taube & Muller, 1998) and even the retrosplenial and medial prestriate cortices (Chen, Lin, Green, Barnes, & McNaughton, 1994; Chen, Lin, Barnes, & McNaughton, 1994). These cells fire whenever the animal's head is

pointing in a given direction (Taube et al., 1990a; Burgess, Cacucci, Lever, & O'Keefe, 2005), independent of the animal's location and the geomagnetic field (Sharp, Blair, & Cho, 2001). Head direction cells in some regions tend to be anticipatory, i.e. they code for future head directions by as much as 90 ms (Blair, Cho, & Sharp, 1998; Blair & Sharp, 1995). Spatial anticipation in place cells is something that will be investigated in more detail in chapter 6. More recently, cells which code for position and head direction conjunctively have been found in the dorsal presubiculum; theta-modulated place by direction cells (TPDs) exhibit spatially constrained firing that is dependent on orientation (Cacucci, Lever, Wills, Burgess, & O'Keefe, 2004). Cells sensitive to head angular velocity, which presumably play a role in integrating head-direction, and are required by neural network models of the head direction system, have been found in dorsal tegmental nucleus (Bassett & Taube, 2001).

More recently an interesting, spatially modulated cell has been discovered in the rat medial entorhinal cortex (Hafting et al., 2005). These cells, called grid cells, have a remarkable firing pattern where the receptive field forms patches of firing at points which lie at the vertices of a triangular grid (Figure 1.9). Grid cells were originally found in the dorsal area of the lateral band of the MEC in layer II. Subsequently, deeper layers III, V and VI have also been shown to have grid cells but while those of layer II are independent of head direction, sub-populations of cells in deeper layers have been found to be modulated by head direction as well (Sargolini, Fyhn, Hafting, McNaughton, Witter, Moser, & Moser, 2006). However, the directional tuning of these cells tends to be much broader than that of pure head direction cells.

In most cases grids are incredibly regular, and can be described in terms of three variables: orientation – the angle of the grid relative to an arbitrary axis, spacing or grid scale – the distance between adjacent peaks, and offset – the position of the grid in two dimensional space (Figure 1.9B). It is striking that grids from the same animal, or more accurately the same hemisphere, seem to share the same orientation (Sargolini et al., 2006). Grid scale, however, is topographically organised such that grids recorded from dorsal positions have a smaller spacing than those found more ventrally (Hafting et al., 2005). This is complementary to a similar dorso-ventral increase in place field size found by (Maurer, Van

Rhoads, Sutherland, Lipa, & McNaughton, 2005). Finally, offset is apparently randomly distributed, even for cells recorded from the same tetrode. Thus, a relatively small population of grids from the same dorso-ventral position will effectively tile the environment. Note, under the assumption that peaks are indistinguishable, a population of same scale grids has limited ability to uniquely encode an animal's position. Consideration of additional grid sets from different dorso-ventral positions increasingly mitigates this problem (O'Keefe & Burgess, 2005; Blair, Welday, & Zhang, 2007).

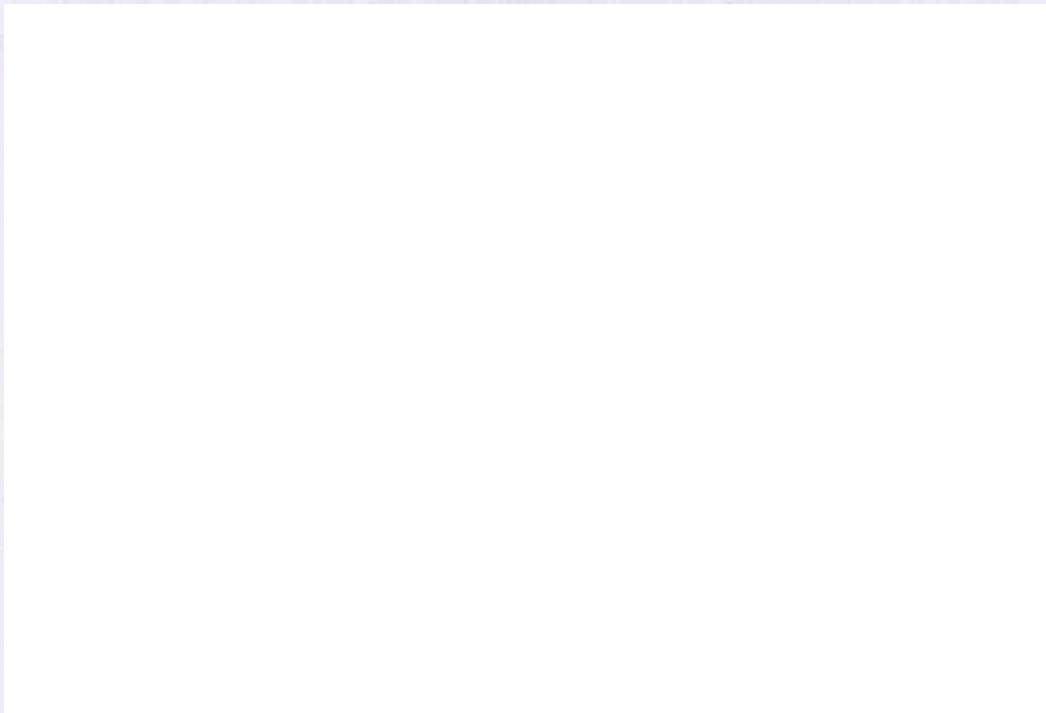


Figure 1.9 Example of the spatial firing of an entorhinal grid cell. a) Left, firing recorded from a 1m by 1m enclosure, 20 minutes worth of data shown. Rat's path is depicted by the continuous black line, action potentials (light blue) are superimposed. Right, rate map constructed from raw data to left. Peak rate is shown above the map, colour code as before. b) Three descriptive measures can be extracted from a regular grid: orientation, how the entire grid is rotated relative to an arbitrary horizontal axis; offset, and displacement of the grid relative to an arbitrary point; and spacing, and the distance between adjacent grid peaks. Adapted from (Barry, Hayman, Burgess, & Jeffery, 2007).

1.4.2 Sensory control of place cell firing

Consistent with the anatomical detail indicating highly processed multimodal input to the HF from higher order association areas, early studies showed that place fields are not defined by a single modality of sensory information, but will make use of whichever are available, including visual, tactile, olfactory and auditory inputs (Best & Thompson, 1989; Save, Nerad, & Poucet, 2000). This is also true of head direction cells and both persist under removal of subsets of

cues (O'Keefe & Nadel, 1978; Nakazawa, Quirk, Chitwood, Watanabe, Yeckel, Sun, Kato, Carr, Johnston, Wilson, & Tonegawa, 2002). The absence of spatial cues from one modality tends to be compensated for by cues from other modalities (Save et al., 2000). For example, congenitally blind rats exhibit normal place fields (Save, Cressant, Thinus-Blanc, & Poucet, 1998) and head direction cells, place cells and grid cells still fire normally in complete darkness, likely being maintained by a combination of path integration (dead-reckoning) and non-visual cues. In the temporary absence of other cues, path integration (Etienne & Jeffery, 2004), can also support a place cell representation (O'Keefe, 1976; Quirk, Muller, & Kubie, 1990; Etienne, Maurer, & Seguinot, 1996). However, in the absence of external sensory information, the path integration process rapidly succumbs to cumulative error (Etienne et al., 1996). In terms of the hierarchy of influence of these various inputs, it seems that stable visual cues at or beyond the edge of the reachable environment exert a powerful control over the orientation of the place cell (O'Keefe & Nadel, 1978; Jeffery & O'Keefe, 1999) head-direction cell (Taube et al., 1990b) and grid-cell representations (Hafting et al., 2005). This representation is synchronised so that rotation of a single polarising cue in a cylindrical environment causes a complementary rotation in both the entire place cell and head direction cell ensemble (Muller & Kubie, 1987; Knierim, Kudrimoti, & McNaughton, 1998).

Physical boundaries or impediments also have a powerful effect on place cell and grid-cell firing. Changes to the shape or topography of an environment have also been used to investigate the nature of the inputs driving place cell activity. Comparing recordings from the same cells made in rectangular environments whose dimensions were systematically varied, O'Keefe and Burgess (1996) noted that the location of peak firing typically maintained a constant position relative to the nearest walls. In addition to this, several fields were stretched along the axes of the environment, with some becoming bimodal in the larger environments. Similar parametric responses have been recorded across a variety of different shaped environments (Lever, Cacucci, Burgess, & O'Keefe, 1999). Recently, a similar paradigm has been used to show that grid cells are also affected by the environment's shape. Barry *et al.* (2007) showed that grid cells deform parametrically with change in the length of either dimension of a rectangular box. Extension or contraction of the box in one dimension

resulted in extension or contraction of the grid spacing in that dimension alone. On average grid spacing was found to change by around 50% of the change in the length of the box. O'Keefe and Burgess (1996), see also Burgess & O'Keefe (1996), proposed that place cells received inputs that are tuned to respond to the presence of a barrier at a given distance along a given allocentric direction, with sharper tuning at shorter distances (for a recent review of this model see Barry & Burgess (2007)). Related, but more localised effects have also been observed by Muller *et al* (1987). He showed that bisecting a place field with a barrier would often cause the cell to stop firing, while those with more distant fields remained unchanged. In short, it seems that impediments to movement, be they the walls of the environment, a free standing barrier or even a sheer drop at the edge of a platform, play a key role in defining place cell firing. In contrast to the influence of extended barriers, Cressant *et al.* (1997), showed that isolated objects within the environment failed to affect place cell firing. However, the same objects did influence place fields when moved to the edge of the environment, where they acted as orientation cues. Similarly, when placed in a line they functioned as an extended barrier.

1.4.3 Remapping

Remapping is not a well defined concept in spatial studies of hippocampal cells (Knierim, 2003) and is often used to refer to a range of related phenomena (Knierim, 2003). Typically, a perturbation of an animal's surroundings or motivational state can cause some or even all of the cells in a representation to radically change their behaviour (O'Keefe & Nadel, 1978; O'Keefe & Speakman, 1987; Muller & Kubie, 1987; Markus *et al.*, 1995). Subtle modifications however, can also elicit small but reliable changes in the behaviour of cells.

Historically, the concept of remapping has been shaped by Marr's ideas about pattern completion and separation (Marr, 1971), and O'Keefe and Nadel's restatement of Tolman's cognitive map (O'Keefe & Nadel, 1978; Tolman, 1948). As such, there has been a tendency to see remapping purely as the process by which a unique hippocampal code is generated for a new environment (Muller, 1996). In fact many studies do provide evidence that the pattern of activities of place cells may represent a memory trace at the neuronal ensemble level (Moser & Paulsen, 2001). This view is supported by work which demonstrates a

complete reorganisation of place cell activity after changes were made to an animal's enclosure (Bostock, Muller, & Kubie, 1991) and by functional considerations which saw the DG as being well placed to orthogonalise activity in the recurrent CA3 network (Marr, 1971; Rolls et al., 1989). Further evidence for this view has been provided by Wills, Lever, Cacucci, Burgess, & O'Keefe (2005), who show abrupt changes in the place cell representation of trained animals, when their environment is changed parametrically between two shapes.



Figure 1.10 Remapping in CA1 place cells induced by olfactory and visual changes, a complex interplay of several different forms of remapping is evident. Three simultaneously recorded cells are shown (a-c). Trials were run in a 70cm enclosure that allowed independent manipulation of colour and odour. Four configurations were possible: white-vanilla (top left), white-lemon (top right), black-vanilla (bottom left), black-lemon (bottom right). A further trial was run with all the lab lights turned out; thus the rat was introduced into the enclosure (configured as white-lemon) without being able to perceive its colour. All cells show clear remapping between the black and white environments; two distinct representations were apparent after the animal's first exposure to the enclosures, as such this seems to be an example of complex or complete remapping. Two of the cells (b&c) also show a configural response; they respond differently in the black-vanilla and black-lemon enclosures (Anderson, Hayman, Chakraborty, & Jeffery, 2003). This effect developed slowly over the course of several recording session and might be thought of as slow rate remapping. Finally in the dark at least two of the cells (a&b) exhibit place fields different to any of those seen in the light trials. Again this effect developed slowly, early trials were always the same as the black-lemon trial or white-lemon trial. Hence this might be thought of as slow position remapping. Adapted from (Barry, 2008).

Classically, exposure to a sufficiently novel environment will cause most cells to abruptly fire in a different location relative to the environment boundaries or not fire at all. At the same time, cells which were previously silent may now begin to fire (Bostock et al., 1991). Many other types of changes have been characterised under different experimental conditions that have variously been called: 'rate remapping' (Hayman, Chakraborty, Anderson, & Jeffery, 2003; Leutgeb et al., 2004), where cells change their firing rate while maintaining their position in an environment; 'slow remapping' (Lever, Wills, Cacucci, Burgess, & O'Keefe, 2002; Barry, Lever, Hayman, Hartley, Burton, O'Keefe, Jeffery, & Burgess, 2006), where initially cells fire in the same location but slowly change their location after sufficient exposure; 'local remapping' (Knierim & Rao, 2003; Rivard, Li, Lenck-Santini, Poucet, & Muller, 2004; Lenck-Santini, Rivard, Muller, & Poucet, 2005), where some cells follow translations of objects placed within the environment and 'partial remapping' (Skaggs & McNaughton, 1998; Knierim et al., 1998; Yoganarasimha, Yu, & Knierim, 2006). Grid cells have been shown to alter their orientation and also exhibit a small increase in grid scale in novel environments (Fyhn, Hafting, Treves, Moser, & Moser, 2007). Novel environments will usually cause head direction cells to change their absolute preferred orientation. Interestingly however, the preferred directions of an ensemble of head direction cells will maintain a fixed relationship to each other (Ranck, Jr., 1984; Taube et al., 1990b; Knierim et al., 1998; Taube & Burton, 1995). In short, different types of novelty have varying effects on place cells and grid cells and may indicate the complexity of their representation.

Unfortunately the mechanisms that mediate remapping are not understood. We do know that NMDA (N-Methyl-D-Aspartate) receptors (Kentros, Hargreaves, Hawkins, Kandel, Shapiro, & Muller, 1998) and protein synthesis are necessary for a remapped representation to stabilise. However, the locus of the receptors and protein synthesis machinery targeted in these studies is unknown and it is difficult to interpret the results (Agnihotri, Hawkins, Kandel, & Kentros, 2004) though see Nakazawa *et al.* (2002). Based on our current understanding, a tentative conclusion might be that 'remapping' actually represents several different processes that can occur independently or in tandem. At least one of these processes being a form of rapid pattern separation, while one or more of the others, is characterised by a slow discrimination between partially

conflicting representations. In the former case, the results from chapter 5 shed some light on part of this story.

1.5 Oscillatory properties of the hippocampal formation

1.5.1 Hippocampal electroencephalogram

An electrode placed in the hippocampus will record distinct patterns of activity in the 0-200 Hz range that correlate to an array of behavioural, attentional and sensory stimulation. The EEG reflects the activity of large numbers of neurons and likely includes contributions from action potentials of all cell types, excitatory and inhibitory post-synaptic potentials and dendritic and glial slow potentials (O'Keefe, 2007).

In the hippocampus of the freely moving rat, six prominent EEG patterns have been identified: four rhythmical; theta (6-12 Hz), beta (12-30 Hz), gamma (30-100 Hz) and ripple (100-200 Hz) waves and two non-rhythmical; large-amplitude irregular activity (LIA) and small-amplitude irregular activity. Some patterns can co-occur (e.g. theta and gamma) whereas others tend to be mutually exclusive (e.g. theta, LIA and SIA).

Relatively little is known about beta, gamma and SIA activity. Both beta and gamma waves have been reported in widespread brain regions of humans and animals. In the hippocampal formation they are most strongly represented in the entorhinal cortex and dentate gyrus. The physiological properties and behavioural correlates vary between animals but have been found to be involved in olfaction. Dentate gamma waves occur during sniffing only in the presence of odours (Vanderwolf, 2001). This activity is dependent on the perforant path input from the entorhinal cortex, whose lesions abolish gamma in the dentate while enhancing them in CA1/CA3. Dentate beta waves, on the other hand, appear to occur in response to olfactory stimuli that signal or mimic the presence of predators, eliciting a fear response or behavioural avoidance (Vanderwolf, 2001). SIA tends to occur primarily at transitionary phases between different types of behaviour in the rat e.g. being awakened from sleep or when abruptly halting voluntary movement (Whishaw & Vanderwolf, 1971; Jarosiewicz, McNaughton, & Skaggs, 2002).

LIA (or sharp waves) tends to occur during behaviours that do not change the animal's location such as sitting quietly, eating, drinking, grooming and during slow wave sleep (SWS). They are synchronised throughout large parts of the

hippocampus and have been proposed to originate in CA3 (Buzsaki, Horvath, Urioste, Hetke, & Wise, 1992; Chrobak & Buzsaki, 1996; Csicsvari, Hirase, Mamiya, & Buzsaki, 2000). Often around the negative peak of a sharp wave, there is a high-frequency 120-200 Hz oscillation (ripple). In general these occur during periods of low arousal and may represent an idling state of the hippocampus or the absence of some aspect of hippocampal function such as theta activity. Consistent with this idea, pharmacological suppression of the medial septum and DBB has no effect on LIA while eliminating theta (Bland, Trepel, Oddie, & Kirk, 1996). In addition, recordings of medial septal cells show reduced firing rates during LIA and lesions of the fornix decrease neither frequency nor amplitude of ripples or sharp waves.

An alternative hypothesis is that LIA is an active state whose function is to strengthen synaptic modifications that have occurred during immediately prior periods. Buzsaki (1989) conjectured that synchronous volleys of CA3 afferent activity impinging on CA1 dendrites are similar to the type of tetanic stimulation known to promote LTP. A related idea is that LIA is involved in the transfer of information from the hippocampus to the neocortex.

The theta rhythm has been the most extensively studied pattern of the EEG spectrum, since its discovery in the rabbit hippocampus by (Jung & Kornmuller, 1938). In the rat hippocampus it is the largest signal, whose peak in the EEG power spectrum overshadows all others. Although not uniformly distributed in phase or amplitude across the hippocampus, a consistent frequency is maintained. And whereas synchronous large amplitude theta is prominent in CA1 and dentate gyrus it is usually absent in CA3. Despite this CA3 pyramidal cells show excellent correlation with theta phase recorded elsewhere (see Buzsaki (2002) for a recent review of the cellular basis of theta and section 1.5.2 below for a discussion of phase precession).

Careful experiments by Vanderwolf (1969) found that theta activity tended to be best correlated with voluntary movements. In fact we know that there are two types of theta, termed attentional or a-theta and translational or t-theta. a-theta is found to be approximately 2 Hz lower than t-theta (see Figure 1.11). Both types are dependent on input from the medial septum and diagonal band of

Broca – the major cholinergic input to the hippocampal formation. Lesions of the medial septum or inactivation by intraseptal injection of the anaesthetic procaine or muscimol (an agonist of the inhibitory neurotransmitter GABA_A), eliminate all theta in the HF (Lawson & Bland, 1993) and Figure 1.11 (lower panel). Intraseptal injection of the cholinergic antagonist atropine selectively eliminates a-theta (Figure 1.11 (lower middle)), while cholinergic agonists (e.g. carbachol) produce a perpetual theta state regardless of the animal's locomotive state (Figure 1.11 (upper and upper middle)). An expected increase in theta frequency in (Figure 1.11 (lower middle)) is not always observed, this may be due to the different locations of injection and recording and differential effects of GABAergic and cholinergic projections from the septum. Lesions of the entorhinal cortex selectively remove t-theta, the remaining a-theta is abolished when followed by injections of atropine (Kramis, Vanderwolf, & Bland, 1975). There is some evidence that t-theta is dependent on serotonin and glutamate.

The first type, a-theta correlates best with arousal or attention occurring naturally in response to a noxious stimulus or when an animal is immobile but preparing to move. Sainsbury and colleagues have shown it to be dependent on the level of pre-existing arousal (Sainsbury, Heynen, & Montoya, 1987; Sainsbury, Harris, & Rowland, 1987). Thus, a neutral stimulus such as a tone, which ordinarily has little effect, readily elicits a-theta if the animal has been previously sensitised with an arousing stimulus such as the sound of an owl or the sight of a predator. One possibility is that a-theta represents sub-threshold activity of the motor system or the activation of movement programs in the absence of movement itself. Evidence for this comes from two studies (Sinnamon, 2000; Sinnamon, Jassen, & Ilch, 2000), where recorded theta activity in anaesthetised rats before, during and after hind-limb stepping movements elicited by electrical stimulation or pharmacological block of the mid-brain raphe nucleus. Both manipulations elicited the lower frequency pre-movement a-theta with t-theta accompanying the hind-limb stepping movements.



Figure 1.11 Theta rhythm during movement and pharmacological intervention. Raw trace (left) and power spectrum (right) of the EEG in rat hippocampus following movement after an intraseptal injection of the cholinomimetic carbachol (**Top**). **Upper middle**: Immobility under the same conditions results in a lower frequency referred to as a-theta. **Lower middle**: Intraseptal injection of the anti-cholinergic atropine, does not abolish theta (known as t-theta). The expected higher frequency is not always seen, perhaps due to the separate locations of injection and recording (septal and hippocampal respectively, see main text). However, theta is not present at all under atropine and immobility (**Bottom**). *Source*: (Lawson & Bland, 1993).

Translational or t-theta is associated with movement. It occurs most readily with walking, running, swimming and jumping – the common factor being translation through space. It also occurs during exploratory head-movements such as sniffing, indicating that it is translation of the head which is the critical element or more specifically generation of motor outputs that would normally result in the translation of the head through space. The frequency of theta is correlated slightly with speed of movement or the rapidity with which a movement is initiated, differing reliably by perhaps as much as 0.5 Hz between the fastest and slowest movements (Rivas, Gaztelu, & Garcia-Austt, 1996; Slawinska & Kasicki, 1998; Whishaw & Vanderwolf, 1973). Both types of theta also occur during sleep. Pharmacological studies show that theta recorded

during the actual eye movements of the REM phase of sleep are unaffected by cholinergic drugs and therefore resemble θ -theta, and that outside of these episodes is α -theta.

One obvious function of the theta rhythm is as a synchronising mechanism, locking the entire hippocampal formation into one global processing mode and organising activity in each region with respect to the others. Simultaneous recordings confirm this by showing that EEG activity across say the CA1 pyramidal layer is in synchrony throughout the hippocampus (Mitchell & Ranck, Jr., 1980; Fox, Wolfson, & Ranck, Jr., 1986; Bullock, Buzsaki, & McClune, 1990). This organisation may even extend at some level to regions beyond the hippocampal formation. Another function of theta may be to coordinate control over long-term potentiation and thus the storage and recall of information. LTP is dependent on precise timing relationships between presynaptic and postsynaptic activity, patterns which rarely occur naturally, but could easily be supported by the theta rhythm (Paulsen & Sejnowski, 2000). Theta burst electrical stimulation of hippocampal afferents is an effective way to induce LTP. Furthermore, there is some evidence that volleys arriving at different phases of the ongoing theta are differentially effective. Inputs arriving at the positive phase of CA1 theta result in synaptic potentiation, whereas those arriving at the negative phase result in depotentiation (Pavlides, Greenstein, Grudman, & Winson, 1988; Huerta & Lisman, 1995; Orr, Rao, Houston, McNaughton, & Barnes, 2001). Thus, in their model, Hasselmo, Bodelon, & Wyble (2002) proposed that various phases of theta represent different modes of operation. Specifically, the peak of CA1 theta is the period during which encoding of new information from the entorhinal cortex takes place, and the trough is the period during which retrieval of information from the hippocampus to the entorhinal cortex occurs.

1.5.2 Phase Precession

Principal cells of the dentate gyrus, hippocampal CA1, CA3 and grid cells in layer II of the entorhinal cortex do not fire in a continuous pattern when the rat runs through a place field. Instead they burst with a frequency a little higher than that of the theta rhythm. Many experiments on running wheels found that place cells preferred to fire at the positive peak of dentate gyrus theta. O'Keefe

and Recce however, first noted, in experiments where rats were made to run through place fields on a linear track, that the phase of spike firing with respect to the theta rhythm actually changed in a systematic way (O'Keefe & Recce, 1993). When the rat entered the place field the cell began to fire at a particular (late) phase of theta. As the animal progressed through the field the bursts of unit firing occurred at a successively earlier phase of each subsequent theta cycle. In most cases the firing phase will precess through an entire 360° but usually no more (Figure 1.12 see also (Maurer, Cowen, Burke, Barnes, & McNaughton, 2006)). Dentate granule cells precess by a lesser amount and usually start firing at an earlier phase. This phenomenon is partly explained by cells firing rhythmically at a frequency higher than that of theta.

While firing rate may code for a number of factors in addition to location, for example speed, the phase of firing is correlated with the animal's position in a place field and this correlation is higher than for time after entry into the field or instantaneous firing rate. Jensen & Lisman (2000) show that with certain assumptions, the decoding accuracy of a rat's location on a linear track can be improved by more than 40% over firing rate alone by including the phase of firing.

More specifically, Huxter, Burgess, & O'Keefe (2003) showed that phase coded for the proportion of the field traversed, independently of rate within the field, which varied as a function of rat's speed. In particular, when the distance between the ends of a linear track were changed, the size of the field changed in proportion but also the rate at which the each cell precessed adapted to maintain the correlation between phase and a fixed proportion of total field size. There is some evidence to support the idea that phase can represent non-locational variables such as the orientation of a running wheel in running wheel experiments (Hirase, Czurko, Csicsvari, & Buzsaki, 1999) and in REM sleep (Harris, Henze, Hirase, Leinekugel, Dragoi, Czurko, & Buzsaki, 2002).

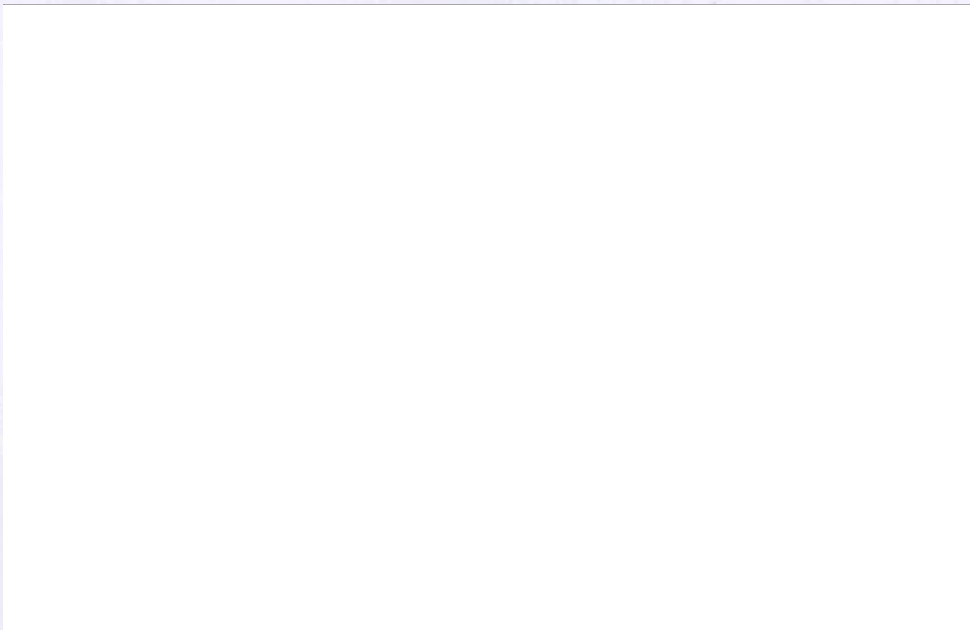


Figure 1.12 Theta phase precession in CA1 cell recorded on the linear track as the rat runs from left to right. The phase of each spike is plotted on the ordinate axis against track position on the abscissa. Phase correlates best with position on track *Source:* (Huxter, Burgess, & O'Keefe, 2003).

Although more difficult to see, phase precession is also present in place fields in the open environment (Burgess, Recce, & O'Keefe, 1994; Skaggs, McNaughton, Wilson, & Barnes, 1996). In this case the effect is independent of the direction from which the rat enters the field. In other words phase precesses from late to early whether the rat enters from the north and exits from the south or enters from the east and exits from the west etc. There is some evidence that grid cells also display phase precession in a similar manner to place cells (Hafting, Fyhn, Moser, & Moser, 2006).



1.6 Models of hippocampal function

Few regions of the brain have received such focussed interest from computational theorists as the hippocampus. These models have allowed the relationship between cognitive behaviour and neural and metabolic activity to be probed quantitatively in context of the wealth of available experimental literature. Models specified in the explicit language of mathematics provide an unambiguous and precise definition of a theory or hypothesis. Furthermore, computer simulations can test these models to compare their performance against experiments. In this sense, computational models leave less space for misunderstanding and reinterpretation. Thus, compared to verbal explanations, a mathematical model accompanied by simulations provides a greater certainty that an idea is actually practicable, and provides specific, testable hypotheses. A well constructed and relevant model can suggest important experiments and manipulations to resolve outstanding theoretical questions. These investigations should further inform and evolve existing models *et cetera*, thereby playing a fundamental role in the progress of our scientific understanding of brain and behaviour.

The hippocampus is an excellent microcosm for computational modelling at all levels of complexity by virtue of its simple architecture, well understood anatomy, oscillatory properties, presence of LTP, influence of neuromodulators and relatively well defined role in behaviour. It provides an accessible arena in which to test mathematical tools, which maybe of great significance beyond its boundaries, across many regions of the brain. Most models of the hippocampus have concentrated on either its spatial or mnemonic functions, usually appealing to either its feedforward or recurrent neural connectivity or its oscillatory properties. The following sections review models for which the data presented are of most relevance. First let us briefly review the major contributions to the history of place cell firing. For a more complete treatment see Burgess N. (2007).

1.6.1 A brief review of computational modelling in the hippocampal formation

Place field models

The earliest computational model of place cell firing was developed by Zipser (1985). In his basic feed forward model, Zipser described place fields as the

thresholded sum of a set of landmark detectors. In turn, each landmark detector responded maximally when the retinal area subtended by specific distal landmarks matched a pre-stored state. Depending on the number of landmarks available and on the number of landmark detectors employed, place fields produced by the model produced a good match to experimental data. Fields were resistant to cue removal and responded appropriately to cue manipulation. Zipser's approach, relating multiple egocentric views to a single allocentric position, is typical of a local view model and has been used widely. However, like other models that describe place cell firing purely in terms of visual input it makes no predictions about the maintenance of place fields in the dark (Quirk et al., 1990).

Sharp (1991) is one of the first studies to present a simulation incorporating learning and the notion of egocentric bearing to environmental landmarks. Sharp described a three layer network such that sensory inputs drove putative entorhinal cells that fed forwards to drive place cells. The sensory inputs took two forms, one type being sensitive to the distance of a cue from the rat and the other being jointly sensitive to distance and egocentric angle to the cue. Being a local view model, rats were only assumed to perceive cues within their current field of view. At each level of the network, simple competitive learning mediated by basic Hebbian plasticity followed by weight normalisation, served to bind specific 'views' to the firing of specific place cells. The model learnt to produce well defined place fields that were omni-directional in the open field but which remained directional if exploration was confined to certain orientations. Crucially though, the model saw all place fields as initially being directional, becoming omni-directional only after exploration; experimental data seems to suggest that the opposite effect occurs (Frank, Stanley, & Brown, 2004). At about the same time O'Keefe's 'centroid' model (O'Keefe, 1991) employed a similar approach to sensory input but did not utilise learning; the position of multiple landmarks were encoded in terms of egocentric position and distance from the rat.

Based on their observation that the position and size of place fields can be controlled by manipulation of environmental boundaries, O'Keefe & Burgess (1996) proposed a rudimentary model of place cell activity. The model

suggested that place fields might be described as the summed threshold of two or more Gaussian tuning curves, peaked a specific distance from certain environmental boundaries. These were putative boundary vector cell (BVC) inputs. There are three key points here: firstly, the Gaussians were defined in allocentric coordinates; they responded to objects that were treated as continuous surfaces; and finally that their width was proportional to their tuning distance (i.e. distance between the Gaussian's peak and the wall it responded to). Note that the model implicitly assumes that sensory information is transformed from egocentric to allocentric coordinates prior to reaching the hippocampus. This model was subsequently simulated (Burgess, Jackson, Hartley, & O'Keefe, 2000), to show that it could match the experimental results of O'Keefe & Burgess (1996). It was updated to account for firing in different shaped environments once connections to place cells were established in a particular environment (Hartley, Burgess, Lever, Cacucci, & O'Keefe, 2000). Finally, it was further evolved to explain the observation by Fenton, Csizmadia, & Muller (2000) that inconsistent cue rotation produced inhomogeneous parametric variations in place field position and incorporate learning and development of place fields in static environments, which were subsequently modified with additional intra-arena boundaries and objects (Barry et al., 2006; Barry & Burgess, 2007).

Recurrent network models

Marr's seminal paper (Marr, 1971) laid out a mathematical formulation that may be implemented in hippocampal structures to perform the function of a content-addressable memory. These models were further refined using biologically plausible constraints by others (Hopfield, 1982; Amit, 1989; Rolls & Treves, 1997; Redish, 1999; Hasselmo & McClelland, 1999; McClelland, McNaughton, & O'Reilly, 1995) and stressed the recurrent connectivity of the CA3 subfield as being particularly well-adapted for this purpose. They are based on attractor dynamics, where connections between cells are arranged with short-range excitation and long-range inhibition such that learned memories form wells in the energy surface of the space of states that the cell population can be in. Inputs to the cells that are sufficiently close to an attractor will eventually evolve to it. Thus, a partial or corrupted input of a pre-learned memory should evolve to an actual, accurate memory.

Recurrent network models have also been used to model spatial behaviour and sensory control of place cells. The first of these was published by Wan, Touretzky, & Redish (1994), where each place cell was driven by egocentric, allocentric and path integrative inputs. Later, Samsonovich & McNaughton (1997) provided their 'chart' model of path integration, which proved to be more influential, by simulating an actual mechanism for path integration. They envisaged path integration being conducted by a continuous attractor manifest in the recurrent CA3 network. These ideas were further developed by Brunel & Trullier (1998) and in particular by Kali & Dayan (2000), whose model learnt to associate prominent cues with places and could subsequently respond to a novelty signal to relearn new associations and provide a new representation of an environment. In the absence of sufficient novelty, geometric changes in the environment, modelled as variations in the learned parameters, allowed place cells to be modified in a manner consistent with that found in experiments such as O'Keefe & Burgess (1996). Angular path integration in the head direction system is much easier to implement since the relationship between the preferred directions of head direction cells are invariant under novelty. Thus, Zhang (1996) produced a linear attractor model of the head direction system (see also Skaggs, Knierim, Kudrimoti, & McNaughton (1995)). To function, these models have two main requirements: that the strength of connections between CA3 place cells or head direction cells decreases proportionate to the distance between their place fields (as with models of content addressable memory); and that there exists a population of appropriately connected 'shifter cells' with spatially constrained firing that is also modulated by speed and heading (e.g. similar to the TPD cells of Cacucci *et al.* (2004), see also chapter 3). The first of these requirements, in conjunction with appropriate feedback inhibition, can lead to the creation of a stable 'bump' of activity in CA3 neurons, which moves to track the rat's position given the appropriate inputs from the "shifter" cells.

1.6.2 Interference models

One of the fundamental questions of systems neuroscience concerns the functional role of the temporal characteristics of neuronal firing. As mentioned earlier phase precession represents one of the strongest examples of temporal coding in brain. When first discovered by O'Keefe & Recce (1993), they proposed a mechanism – the dual oscillator model, by which phase precession

might be explained. The idea was that the cell's membrane potential was the sum of two oscillators of slightly differing frequencies, the lower of which represented the ongoing theta rhythm. The resulting interference pattern would have a low frequency envelope corresponding to the place field and a carrier frequency at the mean of the two. Firing would occur at the peaks of the carrier frequency, and being slightly higher than the theta frequency, successive peaks would occur at successively earlier phases of the theta oscillation, thereby producing phase precession. This simple model had a number of problems. Firstly it produced a periodic pattern of firing, whereas place cell firing tends to be localised, so a mechanism was required to extinguish extra-field firing. It also required a mechanism to reset the phase on entry to a place field so that precession showed the late-to-early pattern correlated with position. In addition, in order to maintain a stable field and the phase precession effect required the difference in frequency between the two oscillators to be proportional to speed (see Figure 1.13).

This model was elaborated upon by Lengyel, Szatmary, & Erdi (2003), who specified explicit, biologically plausible bases for the oscillators. They described the first as being a somatic, hyperpolarising, sub-threshold, membrane potential oscillation, mediated by subcortical inputs and synchronised with the theta rhythm. The second oscillator was a dendritic membrane potential oscillator. A study by Kamondi, Acsady, Wang, & Buzsaki (1998) has shown the membrane potential of proximal dendrites to oscillate at theta frequency and in antiphase with the somatic membrane potential. Dendrites were shown to be able to sustain intrinsic membrane potential oscillations, which were frequency modulated by the level of depolarisation. In this way speed modulated inputs could affect the level of depolarisation in a speed-dependent manner, adjusting the frequency of the dendritic oscillator so as to maintain a place field of fixed size. The speed dependent effect is exemplified in Figure 1.13. This figure shows an example of a rat running through a place field at two different constant speeds. At each speed, two oscillators are shown to interfere in such a way as to produce a typical place cell ratemap overall but also produce phase precession on each run through the field, as found in experiments. The model describes the size of the place field as the half period of the envelope of the interference pattern. The frequency difference between the interfering oscillators is adjusted

by speed so that the half period always corresponds to the time taken to traverse the place field at that speed. The model presented in Lengyel *et al.* (2003), demonstrated both a rate and spiking neuron model, which could reproduce many of the firing characteristics of experimentally recorded place cells (see also Figure 4.1).

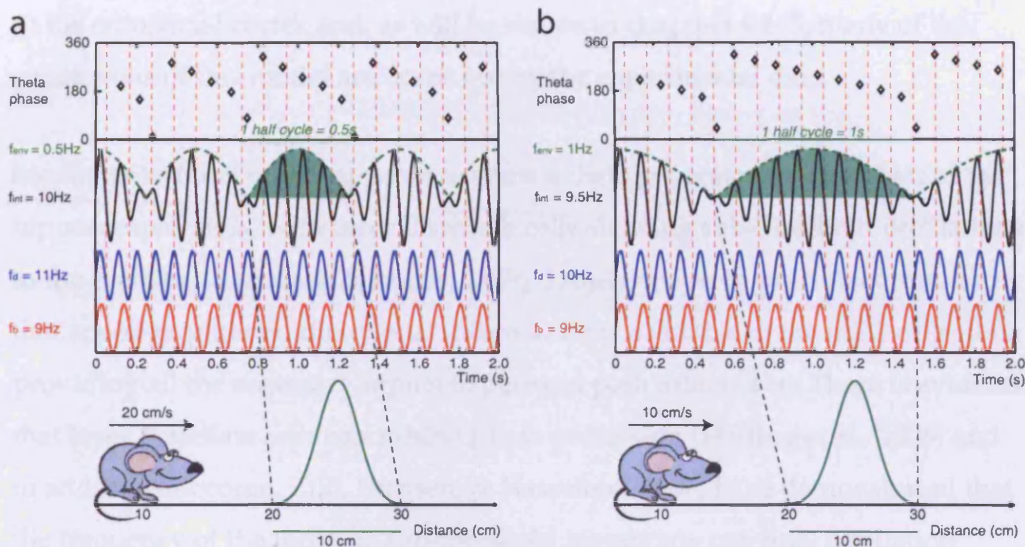


Figure 1.13 Basic 1D interference model and the effect of speed. Red and blue sinusoids represent two oscillators at differing frequencies, where the red oscillator represents a baseline oscillator with constant frequency and the blue oscillator, a dendritic oscillator, whose frequency is modulated by speed. Superposition creates an interference pattern (black), representing the cell's somatic membrane potential, the peaks of which precess with respect to the lower frequency, baseline oscillation. Compare positions of black diamonds (spikes, occurring at the peaks of the interference pattern) with those of the red, vertical, dashed lines, which represent the peaks of the baseline oscillator. The green line is the envelope of the interference pattern, where one lobe (half a cycle, shaded in green) represents a place field. a) shows a rat running at 20 cm/s (fast) and b) a rat running at 10 cm/s (slow). At the constant faster speed the rat will traverse a place field, (10 cm in width, green bell shaped curve below, facing the rat) in half a second. The dendritic frequency increases above the baseline frequency, such the half-period of the envelope matches this. At half this speed (b) the rat will take 1 sec to traverse the field. The frequency of the dendritic oscillator adjusts so that once again the half-period of the envelope matches this. In this way the size and position of the place field is maintained.

The discovery of grid cells (Hafting *et al.*, 2005) in the rodent MEC renewed interest in the dual oscillator model since the regular, repeating, triangular grid-like firing resembled the periodic firing pattern naturally generated by the model and overcame the need to suppress extra-field firing (O'Keefe & Burgess, 2005). This led to two interference models of grid cells: the oscillatory interference model (Burgess, Barry, & O'Keefe, 2007) and the moiré interference model (Blair *et al.*, 2007).

Oscillatory interference model

The oscillatory interference model starts from the basic one-dimensional dual oscillator model (Figure 1.13) and extends it to two dimensions to account for grid cell firing. The need for phase-resetting and speed dependent changes in frequency still exist and an additional directional dependence is required by the oscillators but as noted earlier, speed and directional information are available to the entorhinal cortex and, as will be shown in chapters 4 & 5, many of the predictions of this model are borne out by the experimental data.

Medial entorhinal cortex appears to show a theta generator independent of the hippocampal theta, with layer II stellate cells showing sub-threshold oscillations in the theta band (Alonso & Llinas, 1989). Projections from pre-subiculum imply that speed-modulated directional information is available to the mEC cells, thus providing all the necessary inputs to perform path integration. There is evidence that layer II stellate cells can exhibit phase precession (Hafting et al., 2006) and in addition Giocomo, Zilli, Fransen, & Hasselmo (2007) have demonstrated that the frequency of the intrinsic sub-threshold membrane potential oscillation covaries with dorso-ventral variation in grid scale, as predicted. Grid cells are thus an excellent candidate for this type of model

The dual oscillator model begins by proposing two oscillators. Following Lengyel *et al.* (2003) and Burgess *et al.* (2007), one of them is considered to be a “somatic” oscillator, at a baseline frequency f_b Hz and is common to many cells. The second is a dendritic oscillator with frequency f_d Hz, which is required to increase above the somatic oscillator in proportion to the speed of the rat's motion s . This may be modelled in two ways, additively or multiplicatively:

$$f_d = f_b + \beta s \quad (1.1)$$

$$f_d = f_b (1 + \beta s) \quad (1.2)$$

The type of speed dependence makes different predictions, and will be probed in later chapters. The constant β reflects intrinsic properties of the dendrite or cell and effectively sets the scale of the grid. Both inputs are summed, producing a beat interference pattern that reflects the somatic membrane potential, and at

the peaks of which the cell should exceed firing threshold. Thus, firing frequency should reflect a “carrier” wave at the mean,

$$f_i = \frac{(f_b + f_d)}{2} = f_b + \frac{\beta s}{2} \quad (1.3)$$

where f_i gives the intrinsic firing frequency of the cell, modulated by the “envelope” at $(f_d - f_b)$ Hz. Therefore, in general, when the two frequencies have differing amplitudes a_b and a_d and initial phase difference φ_d :

$$\begin{aligned} a_d \cos(f_d t + \varphi_d) + a_b \cos(f_b t) = \dots \\ 2a_s \cos\left(\frac{(f_d + f_b)t}{2} + \frac{\varphi_d}{2}\right) \cos\left(\frac{(f_d - f_b)t}{2} + \frac{\varphi_d}{2}\right) + (a_d - a_b) \cos(f_d t + \varphi_d) \end{aligned} \quad (1.4)$$

Since the carrier frequency, f_i exceeds theta in a speed dependent way (equation (1.3)), its phase precesses by a half cycle relative to theta. Imagine a somatic oscillator (theta) at 9 Hz and a dendritic oscillator at 11 Hz. The carrier would be at 10 Hz and the envelope at 2 Hz. In one lobe of the envelope – 0.5 s – the carrier would have completed 5 cycles, while the somatic oscillator will have completed 4.5 cycles, thus differing in phase by half a cycle (see for example Figure 1.13 and Figure 4.1a). Varying the relative amplitudes of the two inputs can result in phase precession by an entire cycle as seen in the data (Lengyel, Szatmary, & Erdi, 2003). The size of the place field, L , is given by

$$L = \frac{1}{\beta} \quad (1.5)$$

Indirect evidence for this model was reported by Maurer *et al.* (2005), who confirmed the result that place fields increase in size dorso-ventrally (Jung, Wiener, & McNaughton, 1994), but in addition reported a concurrent decrease in intrinsic frequency of firing. The intrinsic frequency was measured by the first peak in the spike train autocorrelogram, which measures the likelihood of firing a particular time after a given spike. Many interneuron autocorrelograms typically peak around 100ms, indicating theta-modulation of firing, however, phase precession implies that this peak should occur earlier in pyramidal cells (O'Keefe & Recce, 1993). They also found that intrinsic firing frequency was even higher in dorsal hippocampal cells with smaller fields than those in ventral

hippocampus. This implies that β decreases dorso-ventrally, decreasing the difference between the dendritic and somatic oscillators and increasing the size of the place field (by increasing the envelope).

This model can account for grid cell firing in two dimensions if two or more such interference patterns combine appropriately at the soma. The frequencies of dendritic oscillations are now modulated by speed *and* direction. Input to each dendritic oscillator, and hence the amount by which its intrinsic frequency f_d exceeds the baseline frequency f_b , is assumed to depend on the component of movement velocity in a preferred direction ϕ_i . Under the additive or multiplicative model, the frequency of each dendritic oscillator and the resulting distance between the peaks in the envelope now vary as:

$$f_d = f_b + \beta s \cos(\phi - \phi_i) \quad (1.6)$$

$$L = \frac{2}{\sqrt{3}\beta} \quad (1.7)$$

$$f_d = f_b (1 + \beta s \cos(\phi - \phi_i)) \quad (1.8)$$

$$L = \frac{2}{\sqrt{3}f_b\beta} \quad (1.9)$$

The manner in which dendritic frequency rises above the baseline frequency has interesting implications. For example, one observation on grid cell firing is the apparent increase in scale when rats are exposed to an environment sufficiently novel to cause global remapping in place cells. In the additive case, this would require a change in β , perhaps reflecting changes in afferent or intrinsic entorhinal connectivity. In the multiplicative model however, this may also be achieved by a global reduction in baseline frequency. As we shall see in chapter 5, the discovery that novelty is accompanied by a corresponding decrease in theta frequency lends weight to this version of the model. In the 2D case, phase precesses according to distance travelled along a specific running direction ϕ_i . The resulting interference pattern resembles parallel bands across a 2D environment (Figure 1.14A). A cross-section along ϕ_i would look like a 1D interference pattern (Figure 1.13). In order to achieve a triangular grid-like firing pattern, two or more such interference patterns with preferred directions

differing by multiples of 60° are required to multiply at the soma – i.e. each is required to provide a significantly depolarising input for the cell to exceed firing threshold. Thus grid cell firing is given by,

$$\begin{aligned}
 f(t) &= H \left\{ \prod_{i=1}^n [\cos(f_d t + \varphi_i) + \cos(f_b t)] \right\} \\
 &= H \left\{ \prod_{i=1}^n \cos\left(\frac{[f_d + f_b]t + \varphi_i}{2}\right) \cos\left(\frac{[f_d - f_b]t + \varphi_i}{2}\right) \right\}
 \end{aligned} \tag{1.10}$$

where H is a threshold linear function ($H(x) = x$ if $x > 0$ and $H(x) = 0$ otherwise), f_b is the theta frequency, s is running speed, β is a positive constant and f_d is given by equation (1.6) or (1.8). The resulting membrane potential oscillation is a linear interference pattern whose amplitude varies with distance travelled in the preferred direction because the phase difference between the dendritic and baseline oscillations is the time integral of their frequency difference, which is proportional to running speed in the preferred direction. In other words the phase difference between the dendritic and baseline oscillators effectively integrates speed in a particular direction, providing a path integration signal to the EC and possibly the hippocampus.

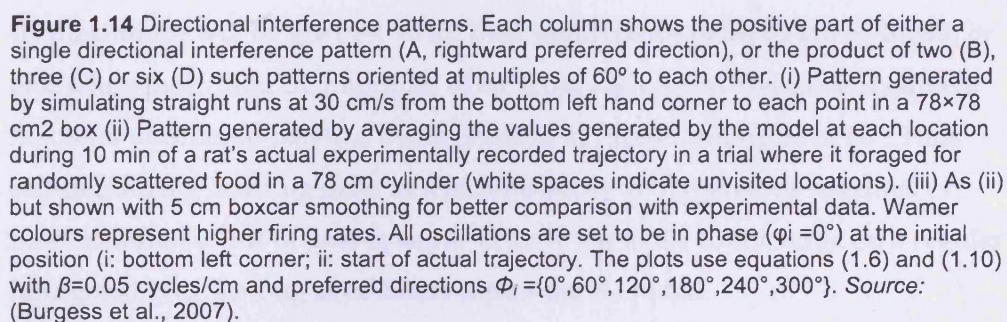


Figure 1.14 Directional interference patterns. Each column shows the positive part of either a single directional interference pattern (A, rightward preferred direction), or the product of two (B), three (C) or six (D) such patterns oriented at multiples of 60° to each other. (i) Pattern generated by simulating straight runs at 30 cm/s from the bottom left hand corner to each point in a 78×78 cm² box (ii) Pattern generated by averaging the values generated by the model at each location during 10 min of a rat's actual experimentally recorded trajectory in a trial where it foraged for randomly scattered food in a 78 cm cylinder (white spaces indicate unvisited locations). (iii) As (ii) but shown with 5 cm boxcar smoothing for better comparison with experimental data. Warmer colours represent higher firing rates. All oscillations are set to be in phase ($\phi_i = 0^\circ$) at the initial position (i: bottom left corner; ii: start of actual trajectory). The plots use equations (1.6) and (1.10) with $\beta = 0.05$ cycles/cm and preferred directions $\Phi_i = \{0^\circ, 60^\circ, 120^\circ, 180^\circ, 240^\circ, 300^\circ\}$. Source: (Burgess et al., 2007).

In this framework we can define two symmetrical models, one has 4 subunits separated by 60° and 120° and the other has 6 subunits each separated by 60° . These models are interesting for two reasons. First they create grid nodes which are circular, whereas those with fewer inputs are generally elliptical to some extent (Figure 1.14). The other is that this cell will not show phase precession, although each component subunit does. This is because each subunit is multiplied by one with an opposing preferred direction, whose dendritic frequency falls below theta by the same amount that the subunit in question rises above it. The opposing subunit thus shows reverse phase precession and its product (or sum) with its partner is phase locked to theta. This type of arrangement may account for layer III grid cells which are thought to not show phase precession but not layer II. For this we need to make a further

modification to equation (1.6) or (1.8). Dendritic subunits must now be paired and each pair is arranged at 60° to one another. Paired units are now tuned to preferred direction by rectified cosine and interfere with one another before multiplying at the soma. The caveat with this scheme is that it requires symmetrical models with $n=\{4, 6\}$ subunits to produce phase precession. See Figure 4.1c for further elaboration on this variant of the model.

$$f_d = f_b + \beta s \cos(\phi - \phi_i)^+ \quad (1.11)$$

$$f_d' = f_b + \beta s \cos(\phi - \phi_i + \pi)^+ \quad (1.12)$$

Anatomically, layer II stellate cells show 4-8 noticeably thick proximal dendrites, consistent with the range of dendritic subunits posited by the model. A rationale in favour of at least three (as opposed to only two) dendritic subunits can be put forward in terms of the organising principles of neural circuits. If directional inputs to the dendritic oscillators are chosen at random, the frequency with which all oscillators are simultaneously strongly active (i.e. their product is near its maximum) will be greatest when their interference patterns are co-linear, or else when they differ by multiples of 60° from each other. The same argument holds for additional patterns being oriented at further multiples of 60°. Thus self-organizing learning rules in which plasticity is triggered by maximal or near-maximal levels of post-synaptic activity are likely to converge on a regular hexagonal grid, so long as co-linear inputs are excluded.

In models with three or more dendritic subunits, the phase of the third has to be set relative to those of the other two such that the linear interference patterns correctly align. The overall n-tuplet of phases determines the grid's spatial phase with respect to the environment. Grid cells reliably fire with the same spatial phase from trial to trial in a familiar environment, which implies they rapidly become linked with environmental cues. Recent evidence (Barry et al., 2007), which shows that grids deform proportionally to parametric changes in each dimension of a rectangular environment, further implicates the primacy of the environmental boundaries in this association. However, the model assumes there is no error in the system's evaluation of running speed and heading direction. In general error in both would rapidly accumulate causing degradation of the grid cell's stability over time. This problem may be overcome

by periodically resetting all the dendritic oscillators to the same phase as that of the theta rhythm (or the common somatic input) at any of the grid nodes. This function could be performed by place cells (see Figure 1.15). Although there is no direct evidence that this occurs phase resetting of the theta rhythm by sensory stimuli has been observed e.g., (Buzsaki, Grastyan, Tveritskaya, & Czopf, 1979; Williams & Givens, 2003).

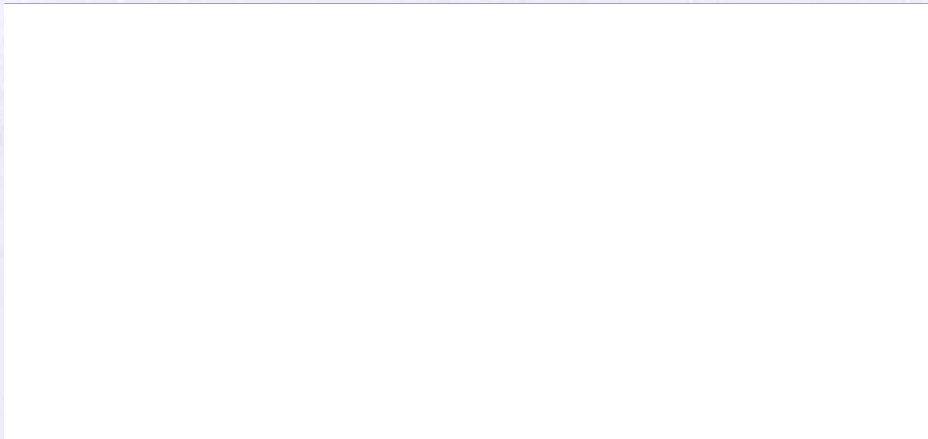


Figure 1.15 Schematic of the association of grid to environment via phase reset of grid cells by place cells. **a)** Left: Diagram showing anatomical connection from MEC grid cell (pale blue) with three dendritic subunits (green, blue, red) to hippocampal place cell (gold) and feedback from place cell onto the dendrites of the grid cell. Center: the maximal firing of the place cell occurs in phase with theta (above, dashed line), and resets dendritic membrane potentials to be in phase with theta (below), Right: the path of the rat in the open field and the place cell's firing field (gold, above). In a familiar environment connections from the place cell to the grid cell are developed due to their coincident firing fields (right: above and middle). These connections enable maximal firing of the place cell to reset the phases of the grid cell's dendritic membrane potential oscillations (MPOs) to be in phase with theta—forcing the grid to stay locked to the place field at that location, by ensuring that the envelopes of the three dendritic linear interference patterns coincide at the location of the place field (below right). Sensory input from the environment (especially boundaries), via lateral entorhinal cortex (IEC), keeps the place field locked to the environment. Only one place cell and one grid cell are shown—in practice one would expect multiple grid cells (with firing at the place field) to project to the place cell, and multiple place cells (with coincident place fields) to project to the grid cell. Simulations **b)** with no error are highly corrupted **c)** when error is introduced in the estimate of current direction (addition of random variable from Normal distribution $N(0, 108)$) and distance travelled (multiplication by $1+\delta$, where δ is drawn from $N(0, 0.1)$) for each time step (separated by $1/48$ s). **d)** shows how phase reset described by the mechanism above, at only a single location (indicated by arrow) in a 78 cm cylinder, can restore grid stability (phase of all dendritic oscillators set to 0° , 84 times in 10 mins). Adapted from (Burgess et al., 2007).

Place cells, well known to be controlled by environment specific sensory stimuli and boundaries in particular are well placed to mediate environmental control of grid cells. Consistent with the known anatomy of entorhinal-CA1 connectivity, place cells would form strong connections through coincident firing with grid cells whose nodes overlap their fields. As a consequence of phase precession in place cells, peak firing occurs at the peaks of the ongoing

theta rhythm, and the connections should be such as to allow the cell to reset the phase of dendritic input to that of the somatic input.

Is such a mechanism of phase reset biophysically plausible? Incident spikes will depolarise the dendritic membrane potential, a strong enough signal should cause sufficient depolarisation to force the oscillation to its peak amplitude and thus a fixed phase. With the correct wiring it should be possible to set the phase of each dendritic oscillator to the same phase. However, there is no direct experimental evidence that this happens; indeed we do not have a robust biophysical model for how intrinsic subthreshold oscillations are produced and maintained in CA1 and entorhinal cells. *In vitro* recordings in entorhinal cortical slices shows that a relatively wide band of frequencies exist (Nolan, Dudman, Dodson, & Santoro, 2007), yet somehow these translate to a relatively narrow band of frequencies in the theta range in both the EEG and the spike train autocorrelogram as shown in chapter 4. There is the additional problem of the electrotonic arrangement of separate dendritic and somatic compartments in such a way as to promote interference between the required compartments and not between others. Finally, the model takes no account of the possible effects of backpropagation along a dendrite of an action potential fired by a cell.

Moiré interference model

A second related model is that of Blair *et al.* (2007), the moiré interference model. The model is based on the interference of micro-grids, which are hypothesised to be the primary source of the theta rhythm. Micro-grids can be pictured (Figure 1.16) as cells (though they do not necessarily need to be), which have a finely spaced hexagonal grid. As the rat runs through the field, patches of high activity are encountered at a frequency around the theta frequency. Figure 1.16 illustrates how grid cell firing patterns are formed, two micro grids with slightly differing spatial frequencies, λ and $\lambda + \alpha\lambda$ can combine to form a grid like interference pattern on a larger scale. Here α is a fractional factor by which the second micro-grid is greater in scale than the first. The scale of the interference pattern can be changed by changing the relative scale of the micro-grids (i.e. α) and the offset of the interference pattern can be adjusted by changing the relative phase of the micro-grids. Thus, the interference pattern can be made to mimic the varying properties of a grid cell.

The scale of the grid cell is given by $S\lambda$, where scale factor S is given by $S = 1 + \alpha/|\alpha|$ and approaches infinity as the difference in spatial frequency between micro-grids approaches zero. Grids formed in this way exhibit normal phase precession, such that whatever angle a rat enters the field from phase precesses from late to early. A similar effect is produced when the micro-grids are rotated relative to each, but with important implications for phase precession. As with the oscillatory interference model the frequencies of the micro-grid need to change with speed so as to maintain a stable interference pattern with fixed scale and offset. This is achievable if λ and α vary as functions of speed V :

$$\lambda(V) = \frac{V}{f_1} \quad (1.13)$$

$$\alpha(V) = \frac{-1}{1 + \frac{f_1 \lambda_m}{V}} \quad (1.14)$$

where $\lambda_m = S\lambda(V)$, a constant moiré grid scale, as long as (1.14) is true. Micro-grids are formed as the sum of three gratings oriented at 60° to one another:

$$G(\underline{r}) = g\left(\sum_{k=1}^3 \cos(\underline{\omega} \cdot (\underline{r} - \underline{c}))\right) \quad (1.15)$$

Where g is a monotonically increasing gain function, $\underline{\omega}$ are three equal length vectors oriented along the directions of the three gratings, whose length determines the micro-grid scale and \underline{c} represents the offset or spatial phase. Moiré grids are formed by a thresholded, rectified and smoothed sum of two micro-grids:

$$M(\underline{r}) = [G(\underline{r}) + G((1 + \alpha)\underline{r}) - \mu]^+ * K \quad (1.16)$$

Where μ is the activation threshold and K is a smoothing kernel (see Blair *et al.* (2007) for details)



Figure 1.16 Moiré interference between two theta micro-grids. Two basis grids with identical angular orientation but different vertex spacings, λ (red) and $\lambda + \alpha\lambda$ (green), intersect to form a moiré grid shown in black to the right of the basis grids. The vertex spacing of the moiré grid is $S\lambda$, where S is a scaling factor that depends on α . In this example, $\alpha = 0.15$ and $S = 7.66$. b, Another example of a moiré grid formed by the length scaling rule, with $\alpha = 0.10$ and $S = 1.0$. Adapted from (Blair et al., 2007)

1.6.3 Network models of grid cells

Two further, similar theoretical models based on recurrent connectivity and attractor dynamics between clusters of grid cells have also been published (Fuhs & Touretzky, 2006; McNaughton, Battaglia, Jensen, Moser, & Moser, 2006).

Triangular lattice patterns emerge quite generically and robustly in networks whose nodes have local excitatory and longer-range local inhibitory connectivity that is symmetric and translation-invariant (Murray, 2003). As with the oscillatory models described above, both network models assume that grid cells are involved in path integration computations using trajectory information from speed and direction sensitive inputs to update position. However, in their current form they are purely rate based models, unable to exhibit temporal codes that are likely to be used by these cells. The model of Fuhs & Touretzky (2006) is designed with a topographical organisation of cells, where neighbouring grid cells have similar phases with recurrent connectivity between grid cells and extrinsic connectivity with directional and speed sensitive cells as

described. However, nearby grid cells do not show similar spatial phase, indeed cells recorded on a single tetrode display the entire range of possible phases. Additionally, there is contention within the literature as to the robustness of grid cells modelled by Fuhs & Touretzky (2006) under realistic rat trajectories. It has been shown by Burak & Fiete (2006) that while short 300 ms directional inputs correctly translate the collective activity of grid cells in a speed dependent way, longer trajectories with continuously varying speed and direction result in an incoherent firing pattern.

An alternative model (McNaughton et al., 2006), describes a non-topographical network with a toroidal connectivity matrix to account for the spatial periodicity of the firing pattern. In a similar scheme to the model of Samsonovich & McNaughton (1997), in order to displace the representations in accordance with the animal's trajectory, this model introduces an additional layer of cells whose firing is modulated by place, head direction and speed. This model is less affected by the inherent instabilities of the Fuhs & Touretzky (2006), because it uses periodic boundary conditions and a connectivity matrix that is not fully rotationally symmetric.

A simulation of this type of model shows that it is indeed capable of describing realistic grid cells with stable fields. Additional modelling of place cell and boundary vector inputs show that it can accommodate experimental findings of Barry *et al.* (2007) see (Laptev, 2008).

1.6.4 Other models involving the theta rhythm

The data presented in this thesis are of relevance to a number of other models which indicate a role for the theta rhythm and we turn to these briefly. Lisman & Idiart (1995) presented a model of working memory, in which phase advance was interpreted as a buffer for the serial recall of events. Specifically, a network of neurons exposed to a sequence of stimuli over natural time scales e.g. seconds, could compress this sequence in the firing of spikes at the peaks of high frequency (40 Hz) gamma oscillations riding on the theta oscillation. The gamma oscillation, whose period is of the order of 25 ms partitions the theta cycle into seven subcycles, within each subcycle the propensity of a particular cell to spike is determined by an after-depolarising potential (ADP), which

ensures that if a spike fired in one subcycle it fires again in the same subcycle in subsequent theta cycles. Inhibition is a critical element of this model and its removal results in loss of the gamma oscillation required to maintain the sequence from one theta cycle to the next (see Mann & Paulsen (2007) for a review of inhibitory mechanisms in oscillatory activity). It is unclear however, how this model squares with the abundant literature demonstrating the effective spatial correlates of phase precession. This model was elaborated upon to incorporate interactions with long term memory (Jensen & Lisman, 1996a), to perform storage and recall separately using NMDA receptors (Jensen & Lisman, 1996b; Jensen, Idiart, & Lisman, 1996). Other similar models that depend on the association of place cells firing earlier on a path to those later along it (i.e. where the sequence being recalled is a sequence of positions) have since been proposed (Touretzky & Redish, 1996; Wallenstein & Hasselmo, 1997).

Hasselmo *et al.* (2002) proposed a model of episodic storage and recall guiding spatial behaviour. In lesion studies of the fornix (Numan, 1978; M'Harzi, Palacios, Monmaur, Willig, Houcine, & Delacour, 1987; Whishaw & Tomie, 1997), rats are strongly impaired on a spatial task that reverses previously learned behaviour. Their claim is that the rat's inability to learn the reversal is due to interference from the memory of an existing learned association between a particular choice and reward. For example, the rat may have learnt to associate a left turn on a T-maze with reward, which was post-lesionally changed to a right turn. Their proposal is that memory encoding and retrieval is subserved by the theta oscillation. The theta rhythm provides windows of opportunity optimised for either, based on the phase of the theta oscillation (Paulsen & Moser, 1998). The model states that firing of entorhinal layer II perforant path inputs to the stratum lacunosum-moleculare are enhanced during the peak phase of theta (measured at the hippocampal fissure) concomitant with an increase in LTP and an increase of presynaptic inhibition of associational connections between neurons in CA3 and CA1. Thus the cholinergic projection from the medial septum is required to maintain the theta oscillation and GABA_B receptors are proposed to provide fast phasic modulation of synaptic transmissibility.

Evidence for this model arises from the observation that tetanic stimulation of the type proposed to induce LTP, does so more readily in the dentate gyrus of anaesthetised and freely moving rats when applied at the positive phases of theta (Pavrides et al., 1988; Orr et al., 2001). Similar effects are seen in slices and in anaesthetised animals, in the stratum radiatum of CA1, where application of the tetanic stimulus at negative phases also causes depotentiation (Huerta & Lisman, 1995; Holscher, Anwyl, & Rowan, 1997). In addition, current source density (CSD) analysis across layers in CA1 (Brankack, Stewart, & Fox, 1993), shows that current sinks in the stratum lacunosum moleculare (perforant path terminal layer) are in anti-phase with sinks in the stratum radiatum (associational connections terminal layer). Of course the model assumes that novel information to be encoded in CA3/CA1 arrives from the cortex via the perforant path, while information to be retrieved is stored in CA3 associational connections. Thus, in the encoding phase, associational transmission is to be damped while LTP is enhanced so that novel cortical inputs can be stored without interference from existing memories. In the retrieval phase, cortical inputs and learning are suppressed and associational transmissibility is restored so that memory recall may occur without interference from cortical inputs (see Hasselmo & Eichenbaum (2005) for a review).

2 General Methods

The methods in the following sections give an overview of the general experimental procedures employed to obtain single unit data. Some of the data appear in published work and the reader is referred to these studies for detailed methods (Cacucci et al., 2004; Barry et al., 2007; Lever et al., 2002).

All electrophysiological recording and animal handling was conducted by Francesca Cacucci and Tom Wills (Chapter 3), Caswell Barry and Robin Hayman (Chapter 4) and Colin Lever and Stephen Burton (Chapters 5 & 6).

The sections below outline the experimental methodology involved in conducting *in vivo* electrophysiological recording studies and are generic to obtaining the data used in the following chapters. Issues regarding chapter-specific analyses are treated within chapter-specific methods subsections.

2.1 Animals

Male Lister Hooded rats (250-400g and 3-6 months of age at implantation) were used in these studies. Prior to surgery animals were housed communally, four to a cage, with free access to water and food. After surgery the rats were transferred to individual Perspex cages with access to water and food sufficient to reduce their initial weight to ~85-90%, which was then to be increased by 5 g per week. All animals were maintained on a 12:12 light-dark cycle. All work was conducted within the terms of appropriate Home Office Project and Personal licences.

2.2 Surgery and electrodes

Anaesthesia was induced and maintained with an isoflurane-oxygen mix (1.5-4l/min). Intra and post-operative analgesia was provided by 0.1ml Vetergesic (buprenorphine - intramuscular injection) and for a further three days in the form of Vetergesic laced jelly (0.5ml buprenorphine twice a day). Prior to surgery animals received 0.1ml Baytril (enrofloxacin - subcutaneous injection) as a microbial prophylaxis and continued to receive Baytril in their water for seven days after surgery (4.0ml enrofloxacin/100ml water). During surgery Vaseline was used to cover the rats' eyes to prevent corneal damage and the animals' bodies were wrapped with bubble wrap to maintain body temperature.

Each animal received one or two 'poor-lady' microdrives (Figure 2.1) (Axona Ltd., St. Albans, UK) loaded with one, two or four variously spaced stereotrodes or tetrodes (Recce & O'Keefe, 1989) of twisted 17-25µm HM-L coated platinum-iridium wire (90% - 10%) (California Fine Wire, Grover Beach, CA, USA). The 'poor-lady' design allows tetrodes to be advanced through the brain in steps as small as 25µm, although tetrodes cannot be moved independently of one another. Prior to surgery tetrodes were cut level with one another and were sterilised by immersion in ethanol. The animal's head was fixed in a stereotaxic frame with lambda and bregma in the horizontal plane, and the skull was exposed. The dura was retracted and the tetrodes were implanted, perpendicular to the skull, at a depth of 1.3 - 1.5mm relative to the intact dura. Microdrives were secured to the skull using seven stainless steel bone screws and dental acrylic mixed 3:1 with Aureomycin (chlortetracycline hydrochloride) powder. The most anterior screw on the right side was used as a ground electrode.

Prior to recording, tetrodes were advanced in 50 - 200µm steps. In the case of the hippocampal rats, electrodes were advanced until ripples, high frequency (~200Hz) oscillations, were seen on the EEG. At this point electrodes were moved more cautiously until hippocampal complex spike cells were detected on the oscilloscope. Details of recording sites were reconstructed using records of electrode movement, physiological markers and post-mortem histology.

Electrophysiological markers for the MEC are less distinct and electrodes were advanced slowly (steps $\leq 100\mu\text{m}$) until multiple large-amplitude units were obtained. This process took place in the experimental room and animals remained in an elevated holding area. Animals were returned to their home cage for at least four hours between screening sessions.

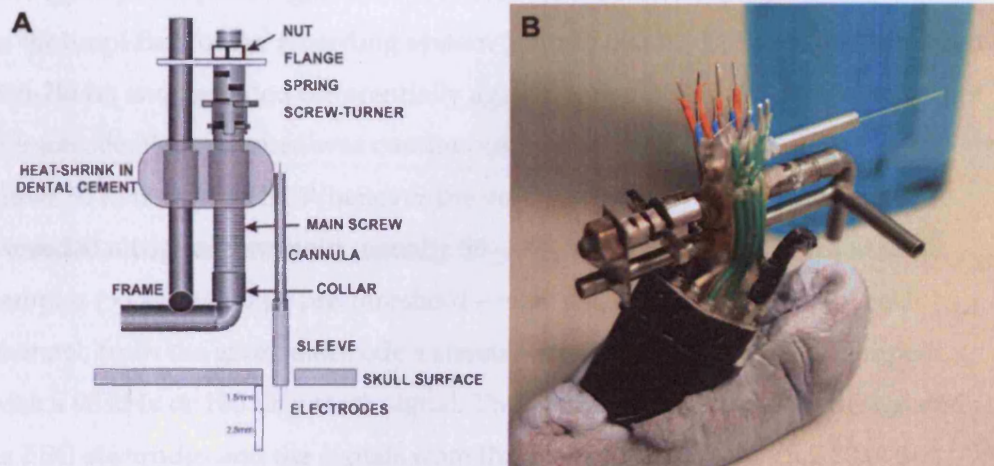


Figure 2.1 Design of the 'poor-lady' microdrive. During surgery the frame is attached to the animal's skull with bone screws and dental acrylic. A full turn of the screw advances the cannula and electrodes by $200\mu\text{m}$.

2.3 Single unit recording

After recovery from surgery, an Axona recording system (Axona Ltd., St. Albans, UK) was used to acquire the single unit and positional data. Local field potentials from each of the electrodes passed through an RC-coupled, unity-gain operational amplifier mounted on the animal's head and fed to the recording system using lightweight wires. In order to detect spikes, the signal was first fed through a preamplifier (gain 1,000), passed through a switching matrix, then on to the amplifiers of the recording system (gain 15,000-50,000) and finally filtered (0.5-7kHz) and recorded differentially against a channel on a separate tetrode or stereotrode. Each channel was continuously monitored at a sampling rate of either 50 kHz or 48 kHz. Whenever the voltage from any given electrode exceeded a trigger threshold (usually 50 – 90 μ V), a spike was recorded as 50 samples (~1 ms: ~200 μ s pre-threshold – ~800 μ s post-threshold) from each channel, from the given electrode's stereotrode or tetrode and time stamped with a 96 kHz or 100 kHz clock signal. Two of the microwires were designated as EEG electrodes and the signals from there were amplified with a 10,000-20,000, band-pass filtered at 0.34-125 Hz and sampled at 250 Hz.

The position and orientation of a rat in the apparatus was captured using an overhead video camera, which recorded the position of one or small infrared light emitting diodes (LEDs) on the animal's head-stage. The image was digitized and sampled at a rate of 50Hz to identify the rat's position. The animal's head direction was extracted using the relative position of the two LEDs, one large, one small, positioned 8cm apart at a known angle to the rat's head. In the case of the single LED head-stage, head direction was inferred from the animal's trajectory.

2.4 Spike sorting & binning

Spike sorting was performed offline using a data analysis suite (Tint, Axona Ltd., St. Albans, UK). Action potentials were assigned to putative principal cells based on differential amplitude, waveform and temporal autocorrelation (see Figure 2.2). Many interneurons are also recorded and can be distinguished on the basis of waveform properties. Only cells which could clearly be identified as fulfilling amplitude, waveform and temporal firing criteria corresponding to pyramidal/stellate cells were included in the analysis. The animal's position and concomitant spikes were binned into a 64 x 64 bin array covering the camera's field of view. Unsmoothed rate maps were calculated by dividing the number of spikes assigned to a bin by the cumulative occupancy of the bin. Smoothed rate maps were constructed as follows, the firing rate for bin i was the number of spikes in a 5 x 5 kernel centred on i divided by the cumulative occupancy of the same bins.

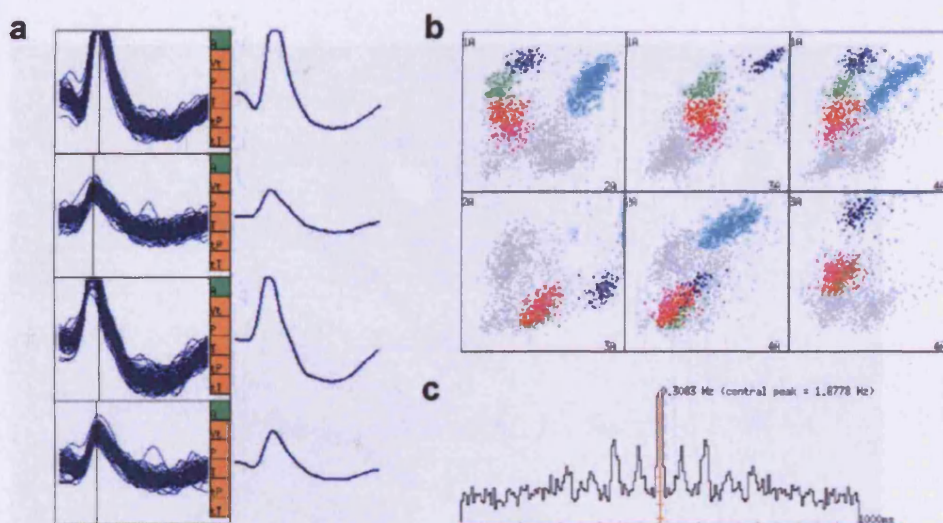


Figure 2.2 Example screen shots from Tint spike sorting software. a) Superimposed waveforms (left) corresponding to multiple action potentials captured on four spatially separated electrodes. Mean waveform for each channel is shown on the right. b) Peak to trough amplitude of each spike on each channel is plotted against its amplitude on each of the other channels. The dark blue 'cluster' corresponds to the waveforms in A. c) Temporal autocorrelation corresponding to the light blue cluster in B. The autocorrelation is calculated for each pair of spikes and indicates the probability of encountering spikes with a given lag, a range of -1000 to 1000ms is shown. Theta modulation of approximately 8Hz is clearly visible.

2.5 Histology

At the end of the experiment rats received an overdose of Euthatal (Sodium pentobarbital) and were transcardially perfused first with phosphate buffered saline and then with 4% paraformaldehyde (PFA) solution. The brains were removed and stored in 4% PFA for at least one week prior to sectioning. 40 μ m frozen sections were cut (sagittal sections for entorhinal implants, coronal for hippocampal), mounted on gelatine-coated glass slides and stained with cresyl violet for visualisation of the electrode tracks/tips. High resolution images were acquired using an Olympus microscope, Xli digital camera (XL Imaging Ltd) and Xli-Cap image capture software. Individual images were imported into Photoshop CS2 for PC (Adobe Systems) and assembled into composites. These were compared with the depth and layer at which cells were acquired by extrapolation with reference to the record of tetrode movements after taking account of brain shrinkage (see Figure 2.3).

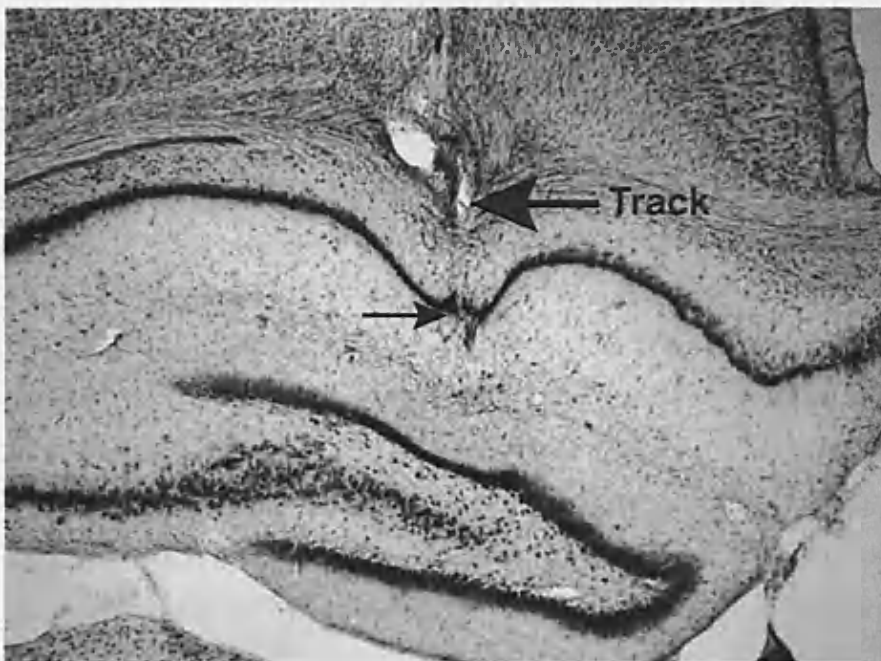


Figure 2.3 Histological photomicrograph of cresyl violet stained coronal section of a rat hippocampus. The large arrow labelled Track indicates tissue damage and other indicators of the track made by a given tetrode. The small arrow indicates location of the tetrode tips puncturing the CA1 field of the hippocampus.

3 Deciphering multiple functional correlates of firing across sub-regions of the HF

3.1 Introduction

Single-unit recording literature provides excellent examples of hippocampal cell responses purely to a single behavioural variable such as location or head-direction. Quite often however, cells will display selectivity to more than one spatial variable. For example place cell responses have been known to be correlated with speed of locomotion. A problem thus arises in single-unit recording studies of freely moving animals: many cells will erroneously display multi-variate selectivity as a result of heterogeneous sampling of behavioural states. This often occurs as an inherent limitation of the experimental conditions. How does one mitigate the effects of inhomogeneity of behavioural sampling? Furthermore, how does one assess the relative effects of multiple variables on the firing rate of a cell which may respond to two or more variables?

In standard analyses the experimenter collects the number of spikes fired in different intervals of the behavioural variable (e.g. the binning of an environment into $n \times n$ divisions) and divides by the time spent in each interval, thereby building up a firing rate map or histogram which is often smoothed for clarity. However, inhomogeneous sampling of behavioural states may lead to dependencies in the firing rate amongst them, leading to artefactual effects. Inhomogeneity in the sampling of orientations will cause place cell firing to show an apparent preferential response to those head-directions sampled most frequently when the animal is in the place field. Likewise, inhomogeneity in the sampling of places will cause head-direction cells to show an apparent preferential response to those places sampled most frequently with the preferred head-direction. As a concrete example, consider a place cell which fires when an animal enters the north side of a circular environment. If the receptive field is close to the boundary, the animal can only approach it from the south and will sample the field through a limited range of orientations. The cell firing distribution will incorrectly show a place cell which has a directional tuning to these orientations. Inhomogeneity of sampling is unavoidable in freely moving animals, and is often particularly acute at the boundaries of an environment but can occur anywhere.

Suppose we are interested in the independent, modulatory influences on firing rate of different spatial variables such as location x divided into N_x bins centred on the positions x_i and head-direction θ divided into N_d bins centered on directions θ_j . Our data consist of the number of spikes n_{ij} and the 'dwell time' t_{ij} corresponding to locations x_i and directions θ_j . The standard spatial and directional firing rate maps would be defined as $f(x_i) = n_i / t_i$ and $f(\theta_j) = n_j / t_j$. The presence of a directional effect beyond the artefactual effect of inhomogeneous behaviour interacting with a 'true' locational effect, can be detected using the 'distributive hypothesis' (Muller, Bostock, Taube, & Kubie, 1994). This idea posits a 'null' hypothesis – there is no influence of direction other than that caused by inhomogeneous sampling. In this case the effect of location is assumed to be 'true':

$$f'(\theta_j) = \frac{\sum_i t_{ij} (n_{ij} / t_i)}{\sum_i t_{ij}} \quad (3.1)$$

Thus the firing rate at each position i is attributed to direction j in proportion to the amount of time the rat spent facing direction j at each position i to produce the predicted artefactual dependence on direction. The observed polar ratemap $f(\theta_j)$ can then be tested to see if it differs significantly from $f'(\theta_j)$ and is significantly modulated by direction. Muller et al successfully used this idea to show that place cells firing in an open cylinder were not directionally modulated. In addition, semi-partial correlation coefficients can be used to describe the amount of overall variance accounted for by one variable after taking into account the effects of other variables (Sharp, 1996). However, this procedure does not allow estimation and visualization of the relative effects of location and direction in cells for which there might be actual correlates of both. Nor is it clear how it could be extended to more than two behavioural dimensions.

Accounting for behavioural inhomogeneity becomes ever more important as the number of variables increases, since the more behavioural states a cell responds to, the greater the scope for introducing artefactual errors as described above. This chapter extends a previously defined maximum likelihood procedure (Burgess et al., 2005) to characterise a cell's response, in an unbiased sense to

any number (in theory) of behaviours. This method allows the creation of rate maps which provide robust estimation of the cell's simultaneous firing response for all specified behavioural variables. The procedure is applied to cells from the hippocampal CA1 field, head direction cells and theta-modulated place by direction cells in the dorsal presubiculum and grid-cells in the dorso-lateral medial entorhinal cortex. Of primary interest in this chapter will be the effect of speed on the firing rate of cells from across the hippocampal formation. In particular, the simultaneous effect of speed, location and head direction. Grid cells, presented in Chapter 4, head direction (HD) cells and theta-modulated place by direction (TPD) cells from the dorsal presubiculum and place cells recorded from CA1 are brought together here to investigate the nature of the hippocampal code for speed of movement. The hippocampal formation is implicated in performing path-integration (dead-reckoning), in the absence of sensory input. Speed information is critical in performing this function properly. In particular, the HF would need to combine heading direction and speed and continuously integrate them in order to provide an accurate estimate of its current position. Many of models presented in section 1.6 are dependent on the availability of this information in order to operate effectively (Samsonovich & McNaughton, 1997; Burgess et al., 2007; Blair et al., 2007).

3.2 Methods

3.2.1 Subjects

Fourteen male hooded Lister rats, weighing 280-400g at time of surgery were used as subjects in this study. Grid cell recordings presented in chapter 4 were also used in this chapter. See Cacucci *et al.* (2004) and methods in chapter 2 and 4 for more details.

3.2.2 Behavioural training

Experiments were conducted in a black-curtained, circular testing arena 2.3 m in diameter. Between trials, rats were kept on a holding platform outside the arena. Two identical circular-walled (diameter, 78 cm) and smooth, light-gray wooden cyclinders (all 50 cm high) were used, placed on a black, circular platform 90cm in diameter, raised 27 cm above the floor. This platform was cleaned before every trial. The centre of each box and the black platform always had the same location in the arena. An external cue card (102 cm high; 77 cm wide) suspended 25 cm inside the black-curtain rail provided directional constancy. The animals were carried along the same path between the environments, always facing the direction of travel, so that they were never purposefully disoriented. During eight minute trials, the rat searched for grains of sweetened rice, randomly thrown into the environment.

3.2.3 Firing-rate maps

Each arena was divided into 36×36 cm bins. For a given cell, firing rates in each bin were calculated by dividing the total number of action potentials fired during occupancy of the bin by the total duration of occupancy. The firing rate in each bin was smoothed using a 3×3 kernel, i.e. the firing rate for each bin was calculated as the average of the 3×3 bin kernel centred on that bin. The binning is coarser than usual for place-cell recording because the maximum likelihood (ML) algorithm (see below) requires a certain amount of sampling in each bin to converge successfully. The firing-rate maps are auto-scaled (red to dark blue), where the warmest colour represents peak firing and the coldest colour represents no firing. Unvisited bins are shown in white.

The directional firing characteristics of both HD and TPD cells are displayed as polar plots. The directional range (0-360°) is subdivided into 36 bins of 10° each.

The number of spikes that the cell fired when the animal was facing its head in a specific direction is divided by the time spent facing that direction. Directional ratemaps were smoothed by a 3×1 boxcar kernel, i.e. the value in each bin was calculated as the average value of itself and the bin either side of it (while accounting for the circularity of the data). The preferred direction of a cell is the direction at which firing rate is maximal.

Speed ratemaps were calculated slightly differently to account for the fact that the rat rarely spends much time running at high speeds and as a result usually very few spikes, if any, are fired in this range. Thus, instead of dividing speed into a certain number of bins of equal bin width, the width of each bin was chosen such the number of spikes the cell fired in each bin was approximately equal. No smoothing was performed on the speed ratemaps.

3.2.4 Criteria for data inclusion

Cells were selected on the basis of their locational and directional correlates, rhythmicity of their firing, and spike isolation. For a cell to be classified as an HD cell, it had to have a peak rate in the directional field exceeding 1 Hz and show no theta frequency modulation in the autocorrelogram. The second criterion follows from Sharp (1996), a study of postsubicular cells, in which none of the cells classified, using regression analysis in the HD category, showed any theta modulation. For a cell to be classified as TPD, it had to meet the following criteria: a peak rate in the locational field exceeding 1 Hz, a peak rate in the directional field exceeding 1 Hz, and clear theta modulation in the autocorrelogram. In addition, the cell had to be well isolated, with a 2 ms refractory period in its autocorrelogram. CA1 PCs were taken from Lever *et al.* (2002) and Wills T.J., Lever C., Cacucci F., Burgess N., & O'Keefe J. (2004) and had to show a peak rate in the locational field exceeding 1 Hz.

3.2.5 Maximum likelihood method

How does one assess how to associate a particular spike with a particular behavioural variable? A method outlined in Burgess *et al.* (2005) provides a maximum likelihood (ML) model to address this question. First let us define some notation to make the following derivations easier. Bold symbols

$\mathbf{r}_{i_k} = r_{i_1} r_{i_2} \dots r_{i_k} \dots r_{i_{K-1}} r_{i_K}$, the product of the variables r_{i_k} , where the i_k indexes

different behavioural variables (e.g. i_1 might index position r_{i_1} and i_2 might index direction r_{i_2}) while bold indices $\mathbf{i}_k = i_1 i_2 \dots i_k \dots i_{K-1} i_K$, where no product is implied. Let us now define the expected number of spikes in a given time interval as:

$$\lambda_{i_k} = E[n_{i_k}] = \mathbf{r}_{i_k} t_{i_k} \quad (3.2)$$

where n_{i_k} are the number of spikes observed in the interval combination

$\mathbf{i}_k = i_1 i_2 \dots i_k \dots i_K$ (where the index i_k runs from 1 to I_k , the total number of intervals, for example the total number of pixels an arena may be divided into).

\mathbf{r}_{i_k} are the model contributions to firing, due to the rat occupying a behavioural state defined by \mathbf{i}_k (e.g. position x_{i_1} , direction x_{i_2} and speed x_{i_3}) and t_{i_k} refers to the time spent in a given combination of behavioural states. The model of the expected number of spikes equation (3.2) is a ‘factorial’ model of the K variables – i.e. the contributions from each are multiplied. This need not be the case, they could for example be summed. However, in simulations the factorial model proved more successful in achieving the maximum likelihood value. The maximum likelihood method (see Dayan & Abbott (2002) chapter 3 for an introduction) is to choose the \mathbf{r}_{i_k} such that the probability of observing the data n_{i_k} is maximised. This \mathbf{r}_{i_k} then represents the best estimate of firing propensity in each behavioural state. In order to do this, the maximum likelihood approach requires a probabilistic model for the data (i.e. the spikes). A typical candidate is the Poisson model. It has been observed that variance of place cell firing on individual runs through a place field is generally a little greater than that predicted by the Poisson distribution (Fenton & Muller, 1998). The Poisson will be employed in any case, since it provides an excellent first order model for spiking stochasticity and remains tractable within the maximum likelihood framework. Hence, the likelihood of obtaining a particular number of spikes n_{i_k} is given by:

$$p(n_{i_k}) = \frac{\lambda_{i_k}^{n_{i_k}} e^{-\lambda_{i_k}}}{n_{i_k}!} \quad (3.3)$$

Assuming that the firing in each bin is independent then we can rewrite the probability as:

$$L = \prod_{i_k} p(n_{i_k}) \quad (3.4)$$

$$l = \sum_{i_k} n_{i_k} \log(r_{i_k} t_{i_k}) - r_{i_k} t_{i_k} - \log(n_{i_k}!) \quad (3.5)$$

Since the maximum of this function will occur whenever its derivative is zero we take partial derivatives with respect to each of the variables and find the values of the variables which set them to zero:

$$0 = \frac{\partial}{\partial r_{i_m}} = \sum_{i_k \neq i_m}^{I \neq I_m} n_{i_k} \frac{r_{i_1} r_{i_2} \dots r_{i_{m-1}} r_{i_{m+1}} \dots r_{i_{K-1}} r_{i_K}}{r_{i_k}} - r_{i_1} r_{i_2} \dots r_{i_{m-1}} r_{i_{m+1}} \dots r_{i_{K-1}} r_{i_K} t_{i_k} \quad (3.6)$$

$$\Rightarrow r_{i_m} = \frac{\sum_{i_k \neq i_m}^{I \neq I_m} n_{i_k}}{\sum_{i_k \neq i_m} r_{i_1} r_{i_2} \dots r_{i_{m-1}} r_{i_{m+1}} \dots r_{i_{K-1}} r_{i_K} t_{i_k}} \quad (3.7)$$

These produce $I = \sum_k I_k$ equations which can be iterated in to give the optimum

r_{i_k} given a sufficiently large number of data points n_{i_k} (in principle there can

be $\prod_k I_k$ observations n_{i_k} but in practice far fewer are sampled and many of

these will be zero). To illustrate with 2 variables, the recursive algorithm

proceeds as follows:

- 1) Given a uniform initial estimate of r_{i_1} , we estimate r_{i_2} with equation (3.7).
- 2) The log-likelihood is then calculated via equation (3.5).
- 3) Equation (3.7) can now be used to calculate r_{i_1} from the calculated value of r_{i_2} , this new value of r_{i_1} is then used to calculate r_{i_2} .

Step 2 is then repeated with the new values of r_{i_k} to update the likelihood and so on. When the difference between successive estimates of the likelihood are within a small predefined tolerance, the algorithm stops and reports the values r_{i_k} .

3.3 Results

From the dataset of chapter 4, all cells whether theta modulated or not were included. An additional three grid cells which were not used previously, due to lack of concurrently recorded EEG were now added – giving a total of 57 grid cells. A total of 46 TPD cells and 63 HD cells were recorded in Cacucci *et al.* (2004) and a further 45 place cells from Lever *et al.* (2002) and Wills T.J. *et al.* (2004) were added. Five of the TPD cells and one of the HD cells were unavailable for use in this analysis leaving a total of 41 TPD cells and 62 HD cells. Finally, the maximum likelihood method is sensitive to the total number of bins used, since the total number of parameters to be estimated is equal to the product of the number of bins in each variable and hence grows quickly with every additional variable. Successful convergence of the algorithm depends on their being a sufficient number of spikes fired to estimate these parameters. Resolution can usually be negotiated to allow the algorithm to converge for cells which exhibit sparse firing. In this case the small minority of cells (1 grid cell, 1 TPD cell and one HD cell), for which the algorithm failed to, were considered an acceptable trade-off for the given resolution and were not included in the final analysis. Finally, 56 grid cells, 40 TPD cells, 61 HD cells and 45 place cells were put forward for analysis.

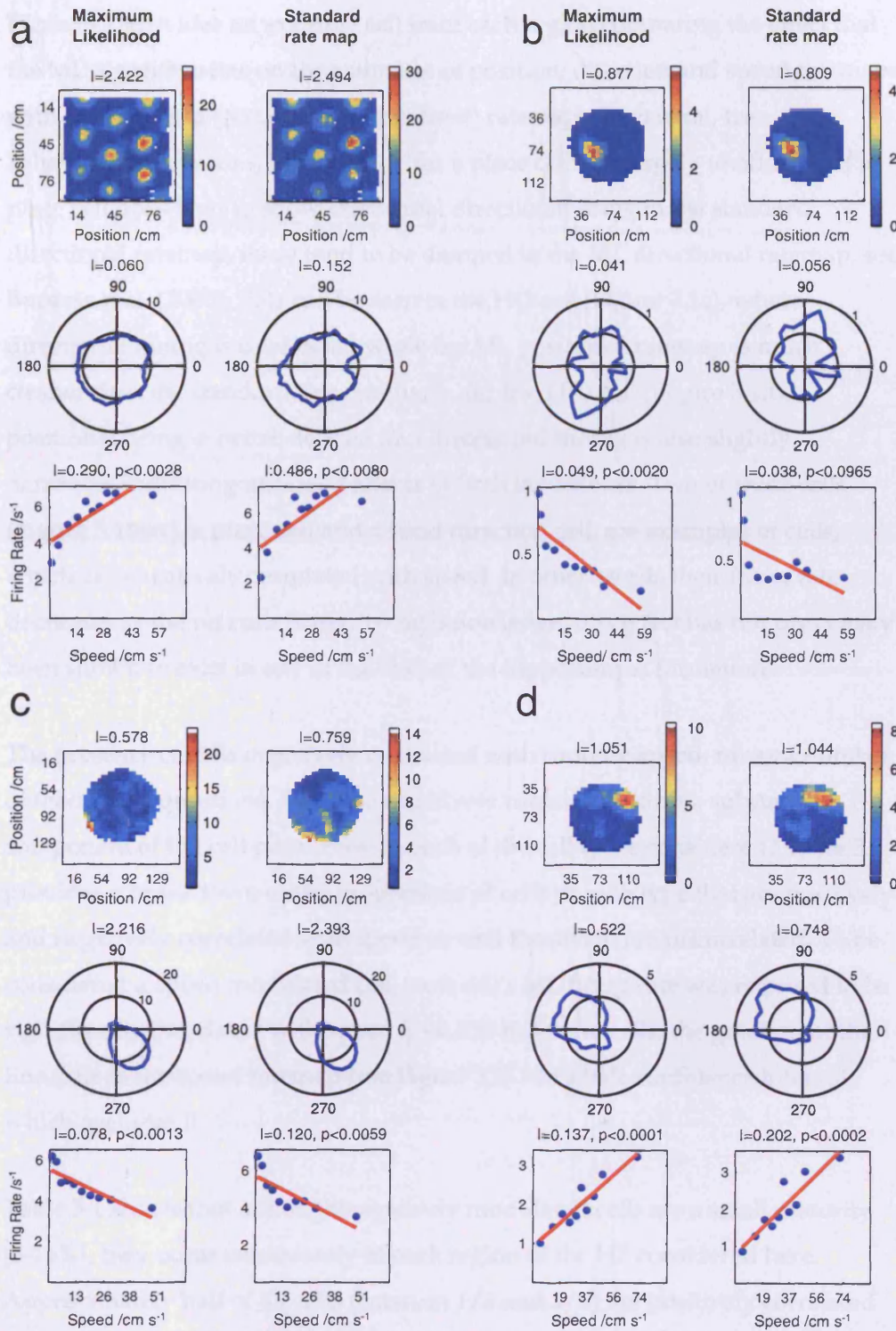


Figure 3.1 Example comparisons between ML (left column) and standard ratemaps (right columns). **a)** A non-directional grid cell with strong positive speed correlation. **b)** A CA1 place cell and **c)** A presubicular HD cell both showing negative speed correlation. Finally **d)** A TPD cell, which is positively correlated with speed. Positional firing rate (row 1) is colour coded according to the colourbar adjacent to the ratemap. The radius of each blue point in the directional (polar) ratemaps (row 2) implies magnitude of the firing rate when the rat's head is pointing in the direction of that radius. Red lines show a linear least squares fit to the data, whose significance is stated above the ratemap. 'I' denotes Skaggs Information in bits/s.

Figure 3.1 provides an example cell from each region comparing the effect that the ML algorithm has on the estimates of position, direction and speed ratemaps with the standard (occupancy normalised) ratemaps. In general, true behavioural correlates, like position for a place cell, are largely unaffected. If a place cell does tend to show artefactual directional firing in the standard directional ratemap, these tend to be damped in the ML directional ratemap, see Burgess *et al.* (2005). This can be seen in the HD cell (Figure 3.1c), where directional tuning is unaffected while the ML positional ratemap is much cleaner than the standard one. Similarly, for the TPD cell (Figure 3.1d), positional firing is better defined and directional tuning is also slightly narrower, indicating unbiased effects of both behaviours. Two of these cells (Figure 3.1b&c), a place cell and a head direction cell, are examples of cells, which are negatively correlated with speed. In other words their firing rate decreases as the rat runs faster. To my knowledge, this effect has not previously been shown to exist in any of the cells of the hippocampal formation.

The presence of cells negatively correlated with running speed, raises a number of theoretical questions. Do these negatively tuned cells form a substantial component of the cell population in each of the cell types considered? Table 3.1 provides a breakdown of the proportions of cells of each type that are positively and negatively correlated with speed as well those that are uncorrelated. To be considered a speed modulated cell, each cell's ML firing rate was required to be significantly correlated with speed ($p < 0.05$). For these cells, the gradient of the linear fit to the speed ratemap (see Figure 3.1) has a 95% confidence interval, which excludes 0.

Table 3.1 shows that although negatively modulated cells are a small minority (5-15%), they occur consistently in each region of the HF considered here. Approximately half of all cells (between 1/3 and 3/5) are positively correlated with speed while the remaining two-fifths (ranging from 1/3 to 1/2) do not pass criteria for satisfactory speed modulation. The majority of cells show a positive correlation with speed with a comparably large number of cells that have no strong inclination to alter their firing rates monotonically with changes in running speed. However, a small number of cells in each region display a strong negative correlation with speed.

Table 3.1 Proportions of cells in each region positively and negatively modulated by speed. Firing rate correlations with are required to be significantly correlated ($p < 0.05$). A small but consistent population of cells in each region appear to be strongly negatively correlated with speed.

Cell type	Analysis	Positively Correlated	Negatively Correlated	Uncorrelated	Total
Place Cells	ML ratemap	26 (58%)	3 (7%)	16 (35%)	45
	Standard ratemap	27 (60%)	1 (2%)	17 (38%)	45
Head Direction Cells	ML ratemap	26 (43%)	5 (8%)	30 (49%)	61
	Standard ratemap	25 (41%)	3 (5%)	33 (54%)	61
Place by Direction Cells	ML ratemap	13 (32.5%)	6 (15%)	21 (52.5%)	40
	Standard ratemap	17 (42.5%)	6 (15%)	17 (42.5%)	40
Grid Cells	ML ratemap	34 (55%)	7 (6%)	15 (39%)	56
	Standard ratemap	31 (61%)	3 (12%)	22 (27%)	56
Total	ML ratemap	99 (49%)	21 (10%)	82 (41%)	202
	Standard ratemap	100 (50%)	13 (6%)	89 (44%)	202

Figure 3.2 provides distributions of the correlation values from each cell type. They are far from uniform and a greater proportion of data lies in the tails (where correlations are greatest), albeit much more biased toward positive correlations, but with also a small preference for highly negative correlations.

Figure 3.3 shows data for all cells in each region. Here the ML speed ratemap for each cell has been normalised by the sum of firing rates in all speed bins so that firing rates across cells may be collated. Data from all positively (first column) or negatively (second column) correlated cells given in Figure 3.3, are plotted together. Segregating cells based on their firing characteristics shows how robustly a small population of cells can code for changes in running speed, indicating that speed information is readily and accurately available to the hippocampal formation.

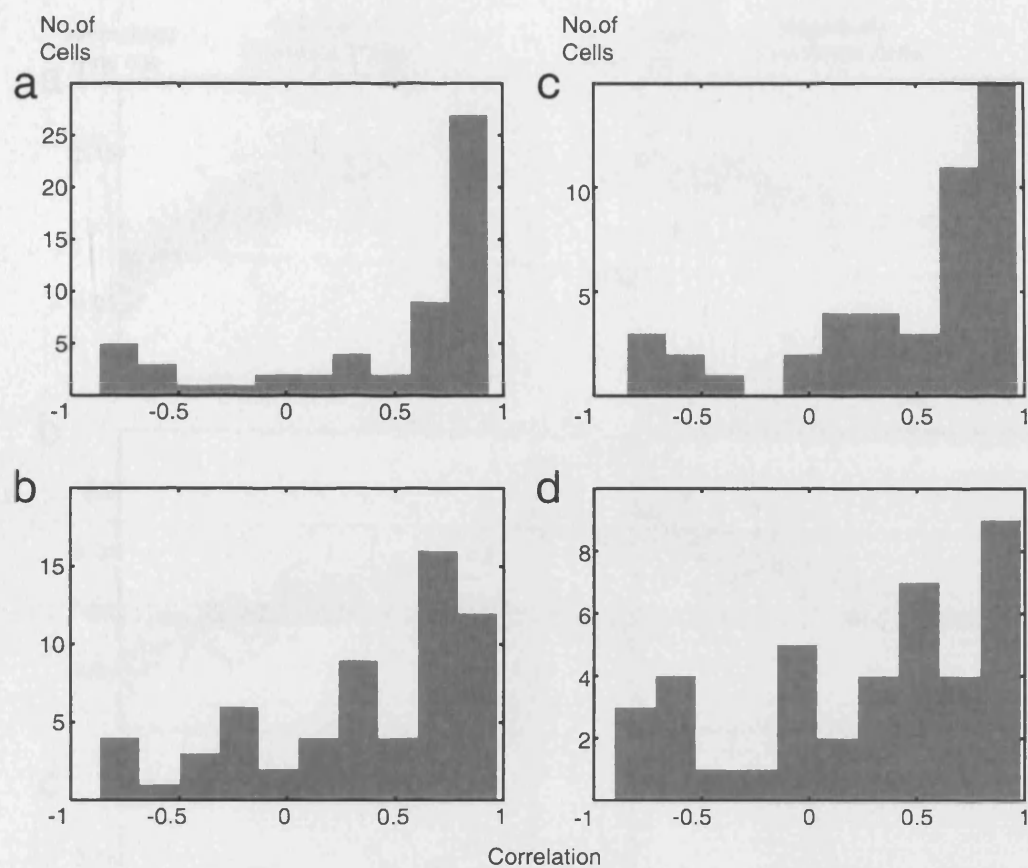


Figure 3.2 Distribution of R-values of linear fits to ML speed ratemaps. **a)** Grid cells, **b)** HD cells, **c)** place cells and **d)** TPD cells.

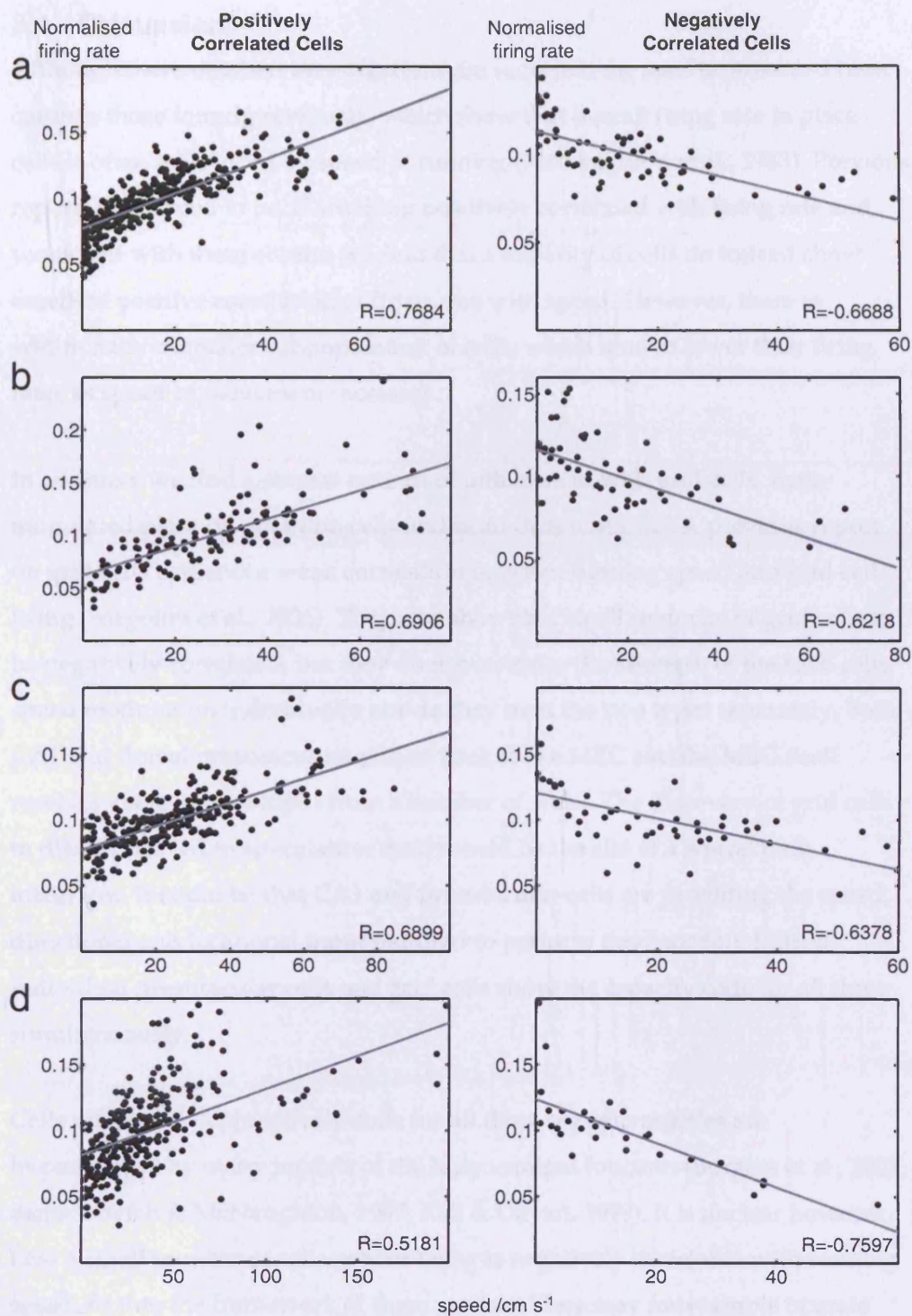


Figure 3.3 Normalised firing rate across multiple cells of each type. a) Grid cells, b) TPD cells, c) HD cells, and d) Place cells. Grey line shows linear least squares fit to the data. R value shown - lower right. Positive and negative speed modulation is similar for both negatively and positively correlated cells in different regions. In the case of TPD cells and HD cells, similar plots (not shown) produce very weak, just significant correlations, whose lines of best fit are effectively flat, with a y-intercept close to the mean.

3.4 Discussion

Although more detailed investigations are required, the results presented here, confirm those found previously, which show that overall firing rate in place cells is often influenced by speed of running (McNaughton et al., 1983). Previous reports find speed to be, if anything positively correlated with firing rate and consistent with these studies we find that a majority of cells do indeed show excellent positive correlation of firing rate with speed. However, there is additionally a smaller subpopulation of cells, which tend to lower their firing rates as speed of movement increases.

In addition, we find a similar pattern of influence in both grid cells, theta-modulated place by direction cells and head direction cells. A previous report on grid cells presents a weak correlation between running speed and grid cell firing (Sargolini et al., 2006). They also show that small minority of grid cells to be negatively correlated, but they do not consider the strength of the each cells speed modulation individually nor do they treat the two types separately. Both CA1 and dorsal presubiculum project back to the MEC and the MEC itself receives visuo-spatial input from a number of areas. The discovery of grid cells in dMEC has led to speculation that it could be the site of a neural path integrator. It could be that CA1 and presubicular cells are providing the speed, directional and locational input required to perform this function. Indeed, individual presubicular cells and grid cells show the capacity code for all three simultaneously.

Cells which can conjunctively code for all three spatial variables are hypothesised by many models of the hippocampal function (Burgess et al., 2007; Samsonovich & McNaughton, 1997; Kali & Dayan, 1999). It is unclear however, how a small number of cells, whose firing is negatively correlated with running speed, fit into the framework of these models. They may for example operate through a disinhibitory mechanism to achieve the same purpose or perhaps they are involved in supporting path-integration in an entirely novel way.

It is important to stress that the method used to disentangle the various spatial correlates is general and applicable to any potential correlates of cell firing and need not correspond to some physical behaviour. The main assumptions are

that the different correlates contribute to the average firing of a cell in a multiplicative manner and that the spike train statistics follow a Poisson distribution. Although this is not always the case, many if not most neurons do exhibit Poisson-like firing at least to first order. Indeed Fenton *et al.* (1998) have shown that CA1 pyramidal cells are usually more variable than would be predicted by Poisson statistics. This property could arise from the oscillatory interference model, as the precise history of movement since the last phase reset affects the resulting firing rate.

4 The oscillatory interference model predicts a relationship between grid cell firing patterns and theta activity at different running speeds

4.1 Introduction

Grid cells in the rodent medial entorhinal cortex fire in a remarkably regular spatial pattern. The peaks in the distribution of spikes fired by grid cells occur at the vertices of a triangular grid and tessellate any environment in which the rat is placed. This unique feature and their location at the origin of the perforant path projection to the hippocampus makes them critical actors in spatial cognitive function and demands a deeper physiological understanding of their characteristics at the cellular level. Interference models account for firing properties of hippocampal cells on the basis of oscillatory properties of the hippocampal formation. The importance of oscillations, in particular in the theta band, is well established in spatial and mnemonic tasks. Experimental evidence suggests that theta band oscillations play a key role in influencing the membrane potential of entorhinal stellate cells. Their firing is modulated at theta band frequencies and phase precession with respect to the theta rhythm has also been documented (Hafting et al., 2006). The frequency of sub-threshold membrane potential oscillations of cell somas and their dendrites are known to vary with input voltage (Kamondi, Acsady, Wang, & Buzsaki, 1998) and with their dorso-ventral location in the MEC (Giocomo, Zilli, Fransen, & Hasselmo, 2007). The variation in frequency with location correlates well with the known dorso-ventral increase in grid scale.

There are currently two types of interference model accounting for grid cell firing: the moiré interference model and the oscillatory interference model. The first provides an explanation of grid cell firing from the interference patterns produced by putative theta micro-grids. These micro-grid cells themselves have a hexagonally symmetric spatial pattern on a much finer scale. The scale varies with speed such that the frequency with which they fire as the rat moves through an environment corresponds to a frequency in the theta band. Interference between micro grids with slightly differing spatial frequency results in a moiré interference pattern, which replicates the same hexagonal symmetry on a larger scale (see Figure 4.7b). This resulting interference pattern

is the grid cell firing pattern and the mechanism by which it is generated results in a key prediction, namely that the frequency of modulation of spike firing (the intrinsic firing frequency of the cell) should vary with the direction in which the rat traverses the grid. Runs made in the direction of either of the six principal axes of the grid (*aligned* runs) or the six directions intermediate to them (*misaligned* runs) should respectively achieve the maximum or minimum intrinsic frequency. This difference is not small, the minimum frequency being a factor square root of three smaller than the maximum. Frequencies around the theta band should thus show a difference of 3-5Hz - well within detectable limits. The reason for this difference is that the 2D "carrier wave" of the moiré interference pattern itself forms a triangular grid. The likelihood of spike firing is maximal at the peaks of the carrier wave and the distance between peaks varies as a function of direction, thereby affecting the intrinsic frequency at which the cell fires.

The oscillatory interference model predicts that intrinsic firing frequency of grid cells exceeds the EEG theta frequency by an amount proportional to running speed and decreases with the spatial scale of the grid like firing pattern. The relationship with speed is evident in all variants of the model (see equation (1.1), (1.2), (1.11) or (1.12). Electrophysiologically, the frequency of the membrane potential oscillation should be reflected in the rhythm of cell firing. The baseline frequency is common across grid cells and should be reflected in the frequency of movement-related theta, a 7-11Hz rhythm which dominates the EEG of rats performing translational motion (Buzsaki, 2002; O'Keefe, 2006). How does the model relate these two measurable quantities with grid scale?

It is instructive here to recast the equations from section 1.5 in terms of the intrinsic firing frequency f_i and f_i' , the paired dendrites of the rectified model of equations (1.11) and (1.12). Here baseline frequency f_b is explicitly equated with the extracellularly recorded theta frequency f_θ .

$$2(f_i - f_\theta) = 2\Delta F = \beta s(t) \cos[\phi(t) - \phi_i]^+ \quad (4.1)$$

$$f(t) = H \left\{ \prod_{i=1}^n \cos \left(f_i t + \frac{\varphi_i}{2} \right) \cos \left([f_i - f_\theta] t + \frac{\varphi_i}{2} \right) + \cos \left(f'_i t + \frac{\varphi_i}{2} \right) \cos \left([f'_i - f_\theta] t + \frac{\varphi_i}{2} \right) \right\} \quad (4.2)$$

In the rectified model, dendritic frequency is only sensitive to directions within 180° of the preferred direction. As a result, the intrinsic frequency should never fall below the baseline frequency. Equation (4.2) shows explicitly that the carrier frequency under the model is equivalent to the intrinsic frequency and modulated by an envelope at the difference of the intrinsic and baseline frequencies.

The envelope of each interference pattern relates to the grid scale in the following sense. The model predicts that the distance between adjacent peaks, L , as the rat runs in any direction and at any speed, is proportional to running speed divided by the difference in dendritic and baseline frequencies, i.e. the spatial period is the speed at which the rat moves divided by the temporal period of the envelope.

$$L = s / (f_d - f_b) \quad (4.3)$$

This will be a fixed value set by β . This follows from the fact that the difference in frequencies is itself proportional to running speed and direction (equation (4.1)). Note that the dendritic frequency f_d is maximal f_d^{\max} when the rat is running along the preferred direction of the dendritic oscillator. When two or more interference patterns oriented at angles differing by 60° are multiplied together, the resulting pattern forms peaks at the nodes of a triangular grid. The orientation of the grid is at 30° from the preferred directions of the linear interference patterns. Therefore when runs are made in this direction, the distance between peaks given by equation (4.3) should equate to the grid scale, (equation (1.7)), which is the same as:

$$L_G = \frac{2s}{\sqrt{3}(f_d^{\max} - f_b)} \quad (4.4)$$

It is impossible to measure the actual dendritic membrane potential oscillation using *in vivo* multi-unit recording techniques. Measurements of intrinsic

frequency and theta are measured as single values over a trial and averaged over all directions sampled by the rat. Nevertheless, we can establish an approximate relationship between time-averaged measures of intrinsic firing frequency \bar{f}_i , theta frequency f_θ , and the f_i of the dendritic oscillator (equation (4.1) and (4.2)) and thus with grid scale. We can relate $(f_d^{\max} - f_b)$ to $(\bar{f}_i - f_\theta)$, since $(\bar{f}_i - f_\theta) = \langle f_d(t) - f_b(t) \rangle_{dir}$. For the rectified model (Figure 4.1c), $\langle f_d(t) - f_b(t) \rangle_{dir} = 2(f_d^{\max} - f_b)/\pi$, using equation (4.1), since on average: $1/\pi \int_{-\pi/2}^{\pi/2} \cos(\varphi - \varphi_i) d\varphi = 2/\pi$. Thus, replacing $(f_d^{\max} - f_b)$ with $\langle f_d(t) - f_b(t) \rangle_{dir}$ in equation (4.4) and combining the calculations above we obtain:

$$L_G = \frac{4\bar{s}}{\sqrt{3}\pi(\bar{f}_i - f_\theta)} \quad (4.5)$$

where \bar{f}_i is the measured intrinsic frequency. The predicted inverse relationship between intrinsic oscillatory frequencies and grid size (which increases dorso-ventrally with recording location (Hafting et al., 2005) is consistent with comparison of intrinsic intracellular oscillations in slices with the typical grid size for that slice's dorsoventral location (Giocomo et al., 2007).

In summary, interference patterns multiplying at the soma under the oscillatory interference model predict that intrinsic firing frequency always remains above theta frequency. Consistent with previous studies we would expect that the EEG theta frequency is modulated by speed and consequently so should the intrinsic frequency. Crucially, the difference between intrinsic frequency and theta frequency should also vary with speed in order to maintain a stable grid of fixed scale and finally measured grid scale itself should correlate well with theoretical grid scale predicted by the difference between intrinsic and theta frequencies. The moiré interference model predicts that intrinsic frequency measured in runs made along the principal axes of the grid should be factor square root of three times the frequency measured in runs made in the intermediate directions. By contrast, the 2-D oscillatory model (Burgess et al., 2007) predicts modulation of the difference between intrinsic and theta frequencies in the opposite direction (greater difference for *misaligned* than *aligned* runs) and by a much smaller factor: $2/\sqrt{3} = 1.15$.

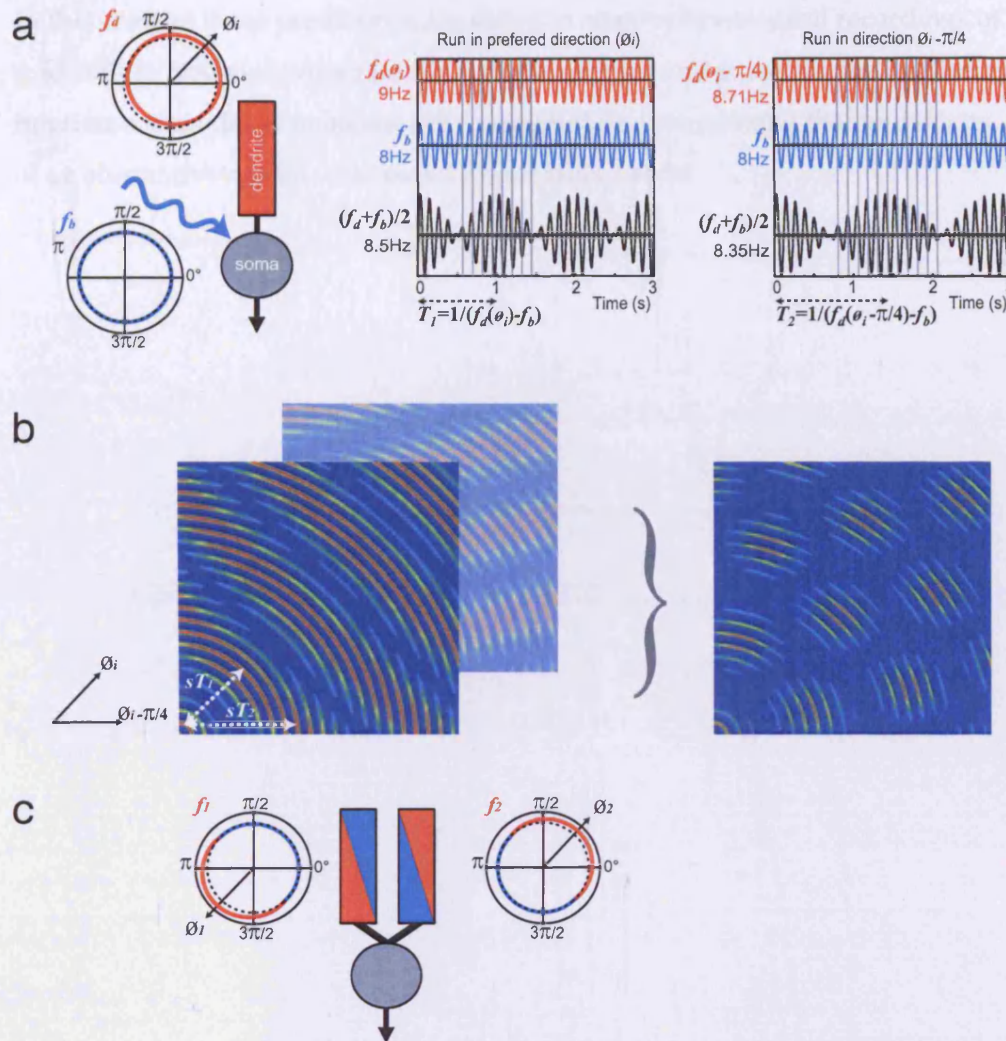


Figure 4.1 The 2D oscillatory interference model. **a)** Left. Schematic model, showing the soma and a single dendritic process. The somatic membrane potential is the sum of an input at baseline frequency (f_b) and a dendritic membrane potential oscillation at frequency f_d . The dendritic frequency varies from baseline according to the animal's running speed $s(t)$ and heading direction $\theta(t)$, reflecting presumed input from a head-direction cell with cosine tuning to a preferred direction θ_i , such that $f_d(t) = f_b(t) + \beta s(t) \cos(\theta(t) - \theta_i)$. Hence f_d is maximized for runs in the preferred direction (θ_i) and minimized for runs in the opposite direction. Right. The somatic membrane potential follows the interference pattern of the two frequencies, as shown for straight runs in the preferred direction θ_i , and at $\theta_i - 45^\circ$ ($\pi/4$ radians): f_d is higher for the run in the preferred direction (9Hz vs. 8.7Hz); f_b and s are assumed to be constant (8Hz and 30cm s^{-1} respectively). The time between the peaks of amplitude of the membrane potential is $T = 1/(f_d - f_b)$, which is minimum for the runs in the preferred direction. Spikes are fired at the peaks of the somatic membrane potential and show 'phase precession' relative to f_b , (zero crossings marked by vertical grey lines). The constant β sets the spatial scale of the firing patterns. **b)** Spatial firing patterns predicted by the model as the rat makes straight runs from the origin (bottom left; blue: no firing; red: maximum firing). Left. Firing from the model cell in a). The interference pattern is evident as bands of firing lying perpendicular to the preferred direction θ_i . The distance between bands is $sT = s/(f_d - f_b)$. The panel behind shows the firing pattern generated by a dendrite receiving input with preferred direction at 60° ($\pi/3$ rads) to θ_i . The result of both dendrites impinging on the same cell, modelled as the product of the two interference patterns, exhibits the regular, hexagonal pattern typical of mEC grids (right). **c)** An alternative 'rectified' model, in which two dendritic membrane potential oscillations vary from baseline frequency (f_b) according to input from head-direction cells with rectified cosine tuning to opposite preferred directions (θ_1 and θ_2 where $\theta_1 = \theta_2 + \pi$). That is: $f_1 = f_b + \beta s(t) H(\cos(\theta(t) - \theta_1))$ and $f_2 = f_b + \beta s(t) H(\cos(\theta(t) - \theta_2))$, where H is the threshold-linear function ($H(x) = 0$ if $x < 0$; $H(x) = x$ if $x \geq 0$). This model, in which intrinsic oscillations always equal or exceed f_b , produces an identical banded-spatial envelope of firing as the basic model shown in a).

In this chapter these predictions are tested in electrophysiological recordings of grid cells in freely-moving rats. The results support and constrain the oscillatory interference model of neuronal processing, while contradicting the predictions of an alternative model – the moiré interference model.

4.2 Methods

4.2.1 Animals

Five male Lister Hooded rats (250-400g in weight and three to six months of age at implantation) were used in this study². See Chapter 2 – General Methods for details of surgical procedures, single unit recording cell isolation and histology.

4.2.2 Behavioural training

Entorhinal activity was recorded while animals foraged for sweetened rice in a 100cm x 100cm square enclosure placed centrally on the floor of the experimental room. Four interchangeable 120 x 50cm Perspex sheets, held in place with corner clamps, were used to create walls 100cm in length and 50cm high. The position and height of the walls afforded animals a clear view of orientation cues. For three animals (nos. 1, 2 & 3) the Perspex walls were coated with white plastic, a fourth (no. 4) experienced walls covered with masking tape, and for the final animal (no. 5) thin sheets of black painted hardboard were fixed in front of the Perspex. Polyvinyl sheeting light-grey for four animals (nos. 1-4) and black for one (no. 5), covered the floor of the enclosure. Between trials, the recording enclosure was disassembled and reassembled with the walls in random positions; similarly the floor was cleaned with water and rotated by multiples of 90°.

Before data collection, rats were familiarised with the enclosure with three or more 20 minute exposures on separate days. Subsequent screening for grid cells took place in the same enclosure. A full recording session was run when cells with an apparently grid-like firing were isolated. Each full session consisted of multiple 20 minute trials in different environmental configurations; however, for the purposes of the present paper, only the data from the first trial, which was always run in the 'familiar' enclosure, were used. The tetrode movement protocol, spike waveforms and the locations of peak firing were used to ensure that each cell was submitted for analysis once only.

² In total 6 rats were implanted for the study by (Barry et al., 2007), 5 by Dr. Caswell Barry and a further 1 by Dr. Robin Hayman. Data from 3 of the 6 rats and a further 2 rats (implanted by Dr. Caswell Barry following a similar protocol up to the 1st trial, (unpublished)) were used in this study. Only first trial data from these last two rats were used in this chapter.

4.2.3 Data analysis

In total 73 putative grid cells and concurrent EEG were recorded during 43 trials (i.e. more than one cell was recorded on some trials).

Gridness, grid scale and grid orientation

Spatial autocorrelograms of rate maps (Hafting et al., 2005; Sargolini et al., 2006) were used to assess the periodicity, regularity and orientation of cells with multiple firing fields. Spatial autocorrelograms were estimated using unsmoothed rate maps. Specifically the spatial autocorrelogram was defined as:

$$r(\tau_x, \tau_y) = \frac{n \sum \lambda_{xy} \lambda_{x-\tau_x, y-\tau_y} - \sum \lambda_{xy} \sum \lambda_{x-\tau_x, y-\tau_y}}{\sqrt{n \sum \lambda_{xy}^2 - (\sum \lambda_{xy})^2} \sqrt{n \sum \lambda_{x-\tau_x, y-\tau_y}^2 - (\sum \lambda_{x-\tau_x, y-\tau_y})^2}} \quad (4.6)$$

Where $r(\tau_x, \tau_y)$ is the autocorrelation between bins with spatial offset of τ_x and τ_y . $\lambda(x, y)$ is the firing rate in bin at (x, y) and n is the number of bins over which the estimate was made. The autocorrelogram was then smoothed with a two dimensional Gaussian kernel of width 2.5 bins. The six peaks surrounding the central peak on the autocorrelogram were considered to be the local maxima closest to, but excluding, the central peak. The extent of each peak was defined as the contiguous set of bins around the peak with a value greater than half the value of the peak bin. The spatial autocorrelograms, constructed from the combined unsmoothed baseline rate maps, were used to estimate the orientation, gridness, and grid scale of each cell, following refs. (Sargolini et al., 2006; Hafting et al., 2005). The orientation of the grid was the angle between a nominal horizontal reference line and an axis defined by the centre of the spatial autocorrelogram and the peak closest to the reference line in an anti-clockwise direction. Grid scale, or grid length, was the median distance from the central peak to the six surrounding peaks. Gridness, a measure of spatial periodicity, was calculated by first defining a mask of the spatial autocorrelation centred on but excluding the central peak and bounded by a circle passing around the outside edge of the outermost of the six central peaks. Next, this area was rotated in 30° increments up to 150°, and for each rotation the Pearson product moment correlation coefficient was calculated against the un-rotated mask. Gridness was then expressed as the lowest correlation obtained for rotations of 60° and 120° minus the highest correlation obtained at 30°, 90° or 150°. Cells with

gridness of 0.3 or greater were classified as grid cells ($n=54$), a threshold that closely matched the experimenter's subjective judgment. Cells that fired fewer than 500 spikes in the 20 minute trial ($n=7$), were removed from the analysis reducing the number to 47.

Spectral analysis

Estimates of the intrinsic frequency of cell firing (f_i) and the frequency of the theta rhythm (f_θ) were obtained, respectively, from the spike-train of each cell and the concurrently recorded extracellular EEG in continuous 'runs' of at least 0.5s during which the animal's speed consistently exceeded 5cm/s. This minimum speed was chosen to exclude non-theta behaviours such as rearing, grooming and chewing. This subset of runs are henceforth referred to as *all* runs to differentiate them from *slow*, *fast*, *aligned* or *misaligned* runs defined below.

For analyses of the effect of running speed, *fast* and *slow* runs were defined as continuous periods of at least 0.5s, running at a speed between s_{min} and s_{max} . For *slow* runs $s_{min} = 5$ cm/s and $s_{max} = s_M$, for *fast* runs $s_{min} = s_M$ and $s_{max} = \text{infinity}$, where s_M is the mean of the speeds at which spikes were fired when running at above 5cm/s. For analyses of running direction, *aligned* and *misaligned* runs were defined as continuous periods of at least 0.5s running at above 5cm/s in a direction within $\pm 15^\circ$ of the grid's six principal axes (*aligned* runs), or $\pm 15^\circ$ of the six *misaligned* directions, (see Figure 4.7b).

The theta rhythm, f_θ , was estimated as follows. EEG segments corresponding to runs were concatenated and zero padded to 2^{19} elements. Zero-padding does not affect the spectral content of the signal, since it doesn't change the input sampling rate, while at the same allows the use of fast and efficient algorithms for calculating the FFT. Artefacts resulting from concatenation may occur due to differences in mean signal amplitude or from sharp discontinuities between runs. However, these would respectively occur at frequencies far lower or higher than the range of interest. Power spectra were constructed by performing a fast Fourier transform (FFT) on the resulting sequence, where the square-modulus of each Fourier frequency coefficient represents the signal power at that frequency. The power spectrum was smoothed using a Gaussian kernel with standard deviation 0.375Hz (results were robust to variations in kernel size

and shape), and f_0 defined as the frequency of the peak in the power spectrum between 7 and 11 Hz.

As an example of the robustness to smoothing let us take the two cells given in Figure 4.3 and calculate values for *all*, *slow*, and *fast* runs for different values of standard deviation for the smoothing kernel and for different values of a boxcar smoothing kernel. In every case the values produced have a standard deviation much less than 0.1 and thus far smaller than the variance in the data. For the cell in Figure 4.3a, these are 0.02 Hz, 0.06 Hz and 0.07 Hz and for the cell in Figure 4.3b they are 0.02 Hz, 0.05 Hz and 0.05 Hz for *all*, *slow* and *fast* respectively. The power spectra in each of these cases are shown in Figure 4.2 for the cell described in Figure 4.3b as an example.

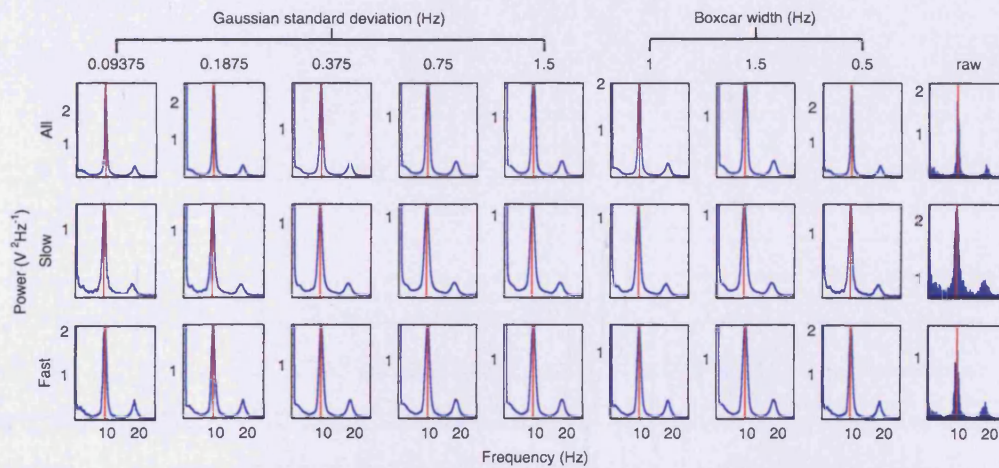


Figure 4.2 Robustness of frequency estimates to variations in smoothing characteristics. Each column displays the power spectra for differing values of standard deviation of a Gaussian kernel and a boxcar kernel as indicated for *all* (row 1) *slow* (row 2) and *fast* (row 3) runs. The last column presents the raw power spectrum without any smoothing.

A cell's intrinsic frequency (f_i) was estimated from the power spectrum of its spike train autocorrelogram. The spike-train for each run was used to construct a temporal autocorrelogram (bin width 2 ms), using 'unbiased' normalization by the number of bins at each lag. The average autocorrelogram was calculated from the autocorrelograms from each run, weighted by the duration of the run. The average autocorrelogram was truncated to the first 0.5s, zero-padded to 2^{16} elements, its power spectrum found, and f_i defined as the frequency of the peak power spectrum between 7 and 11 Hz.

To be sure of accurate estimation of frequencies, we restricted our analyses to those cells with clear peaks in the power spectra derived from their spike-train autocorrelogram and from the concurrently recorded EEG. A clear peak was defined as having mean power with 1 Hz of the peak at least 50% greater than mean spectral power. Clear peaks were required for both intrinsic firing frequency and theta frequency. No trials were rejected due to absence of a clear theta frequency, but 19 cells were rejected due to absence of a clear intrinsic firing frequency.

Instantaneous frequency analysis

A second analysis was performed to compare directly the effect of speed of movement on momentary intrinsic and EEG frequencies. This was done as follows. The recorded EEG signal was filtered using a 6-12Hz, 251-tap, Blackman windowed, band-pass *sinc* (sine cardinal) filter. Windowing the filter achieves good stop-band attenuation and small pass-band ripple. An analytic signal was then constructed using the Hilbert transform and takes the form $s_a(t_k) = s(t_k) + i\mathcal{H}[s(t_k)]$, where \mathcal{H} specifies the Hilbert transform, $s(t_k)$ is the filtered EEG signal, $t_k = k\Delta$, where $k = 1, \dots, K$ indexes the time-step and Δ is the inverse of the sampling rate. The phase of the analytic signal $\varphi(t_k)$ gives the phase of the EEG at t_k . Each spike was assigned a phase $\varphi(t_k)$ if it fell in the interval $[t_k - \Delta/2, t_k + \Delta/2]$. The analytic signal was filtered to remove periods of low quality EEG by discarding those regions with low signal power. Average power was calculated for each cycle in the analytic signal, where the start of each cycle was defined at those points where the analytic phase difference with the previous point fell below $-\pi$. Cycles with power below the 15th percentile in each trial and the spikes falling within them were discarded.

By default the analytic function assigns zero phase to the peaks of the signal. This assignment is arbitrary and for our purposes, zero phase or the start of the EEG cycle is redefined separately for each cell, as the phase at which fewest spikes were fired. In each theta cycle where spikes were fired, the circular mean phase of those spikes was calculated and recorded as the nearest $\varphi(t_k)$ of the analytic signal. Instantaneous intrinsic frequency was calculated as the inverse of the time between the mean phase of spikes in successive cycles. Spikes are not always observed on every theta cycle on every traversal through a field and

gaps of up to three empty cycles were allowed. The time taken for three theta cycles ($<0.5s$), is still considerably less than the timescale of behavioural changes, e.g. the time taken for the rat to go from one sub-field of the grid to the next. In this way many hundreds of instantaneous frequency measurements were obtained from each cell. For each measurement, the average speed measured between the mean phase of spikes in successive cycles was recorded. Similarly, the EEG frequency was measured as the average instantaneous frequency of the EEG between the same points. Instantaneous frequency is calculated as the change in phase between each EEG sample multiplied by the sampling rate and divided by 2π . Thus, concurrent measurements of speed, EEG frequency and intrinsic frequency were produced at theta frequency timescales (around 100 – 200 ms).

Results are stated as mean \pm s.e.m. and tested with paired two-tailed t-tests unless stated otherwise.

4.3 Results

73 putative grid cells were recorded with concurrent EEG from layers II and III of dorso-lateral mEC of 5 rats during foraging for food in a familiar square enclosure (1m², 20 minute trials). Of these, 54 cells had a sufficiently high gridness score to be defined as grid cells. Accurate estimation of intrinsic frequency requires sufficient spikes and clear rhythmic modulation of firing. Accordingly, cells firing fewer than 500 spikes (7 cells) were excluded, as were an additional 19 cells lacking clear theta-band modulation (i.e., mean power within 1Hz of the theta-band peak not exceeding 50% of mean spectral power). The remaining 28 grid cells, recorded in 24 trials, entered the analysis.

Figure 4.3 examines the temporal properties of grid cell firing and concurrently recorded EEG in an example of a grid cell with a small grid scale (Figure 4.3a) and one with large grid scale (Figure 4.3b). Differences in theta frequency between *slow* and *fast* runs were sometimes noticeable in example traces of raw EEG see Figure 4.3a, first row and often in the EEG power spectra Figure 4.3 a and b, row 2. Similarly, changes in intrinsic frequency were visually detectable on many examples of both the spike train autocorrelograms (Figure 4.3 a & b, row 3) and their power spectra (Figure 4.3 a & b, row 3). The translucent grey bars transcending rows 2 and 3 in Figure 4.3 a & b, highlight the difference between the EEG frequency and the cell's intrinsic firing frequency, as measured by the peaks in the power spectra and how this difference increases between *slow* and *fast* runs. Crucially these effects are far more pronounced in the cell with a small grid scale (Figure 4.3a), where the model predicts large frequency differences than they are in the cell with a much larger grid (Figure 4.3b), where the differences are predicted to be small.

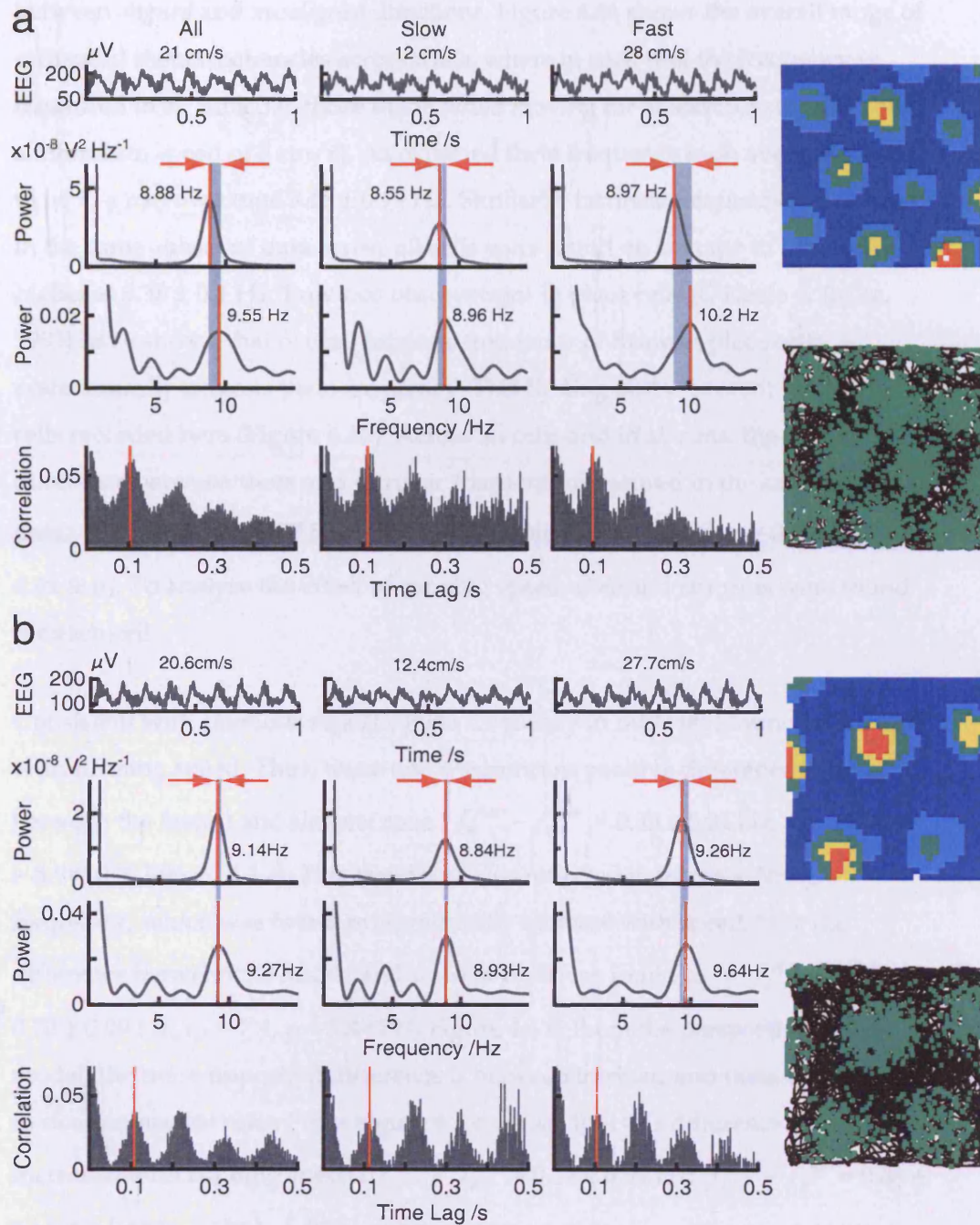


Figure 4.3 The temporal characteristics of grid cell firing. Two example cells, one with small grid scale (a) and one with large grid scale (b). Left: Examples of raw EEG (top), EEG power spectra (upper middle), autocorrelogram power spectra (lower middle) and spike-train autocorrelograms (bottom) for *all* runs at above 5cm/s (1st column) and for *slow* (2nd column) and *fast* runs (3rd column). Right: smoothed grid cell firing rate map (100x100cm box; top) raw traces below showing the rat's path in black and spike locations in green (bottom). Note that, as predicted by the model, the intrinsic firing frequency exceeds the theta frequency and by a greater amount during *fast* than *slow* runs and is greater for grid cells of smaller scale than for those of larger scale (red arrows and grey shading).

To quantify these effects in the recorded cell population, the means across cells were compared for theta and intrinsic frequencies in *fast*, *slow* and *all* runs and

between *aligned* and *misaligned* directions. Figure 4.4a shows the overall range of measured theta frequencies across trials, where in each trial the frequency is measured in *all* runs (i.e. those made while moving for at least 0.5 seconds above a minimum speed of 5 cm/s). As expected theta frequency is on average found to be in a narrow range 9.19 ± 0.19 Hz. Similarly, intrinsic frequencies measured in the same subset of data across all cells were found on average to be a little higher at 9.38 ± 0.1 Hz. Previous observations in place cells (O'Keefe & Recce, 1993) have shown that overall intrinsic frequency of firing in place cells systematically exceeds theta frequency. This finding is also present in the grid cells recorded here (Figure 4.4b). Across all cells and in *all* runs, the paired difference between theta and intrinsic frequency measured in the same subset of data, $f_i - f_\theta = 0.22 \pm 0.07$ Hz, was highly significant: $t_{27} = 3.08$, $p = 0.0047$ (Figure 4.4a & b). To analyse the effect of running speed, *slow* and *fast* runs were found for each cell

Consistent with previous reports, theta frequency in mEC was found to increase with running speed. Thus, there was a significant positive difference in theta between the fastest and slowest runs ($f_\theta^{fast} - f_\theta^{slow} = 0.35 \pm 0.02$ Hz, $t_3 = 16.00$, $p = 5.9 \times 10^{-14}$, Figure 4.4 c). This trend was also reflected in intrinsic firing frequency, which was found to significantly increase with speed, here the difference between the fastest and slowest runs was found to be $f_i^{fast} - f_i^{slow} = 0.70 \pm 0.09$ Hz, $t_{27} = 7.4$, $p = 5.4 \times 10^{-8}$, Figure 4.4 c. From the perspective of the model, the more important difference is between intrinsic and theta frequencies in *slow* versus *fast* runs. From Figure 4.4 c we see that this difference also increased with running speed ($f_i^{slow} - f_\theta^{slow} = 0.12 \pm 0.09$ Hz; $f_i^{fast} - f_\theta^{fast} = 0.48 \pm 0.12$ Hz; $(f_i^{fast} - f_\theta^{fast}) - (f_i^{slow} - f_\theta^{slow}) = 0.35 \pm 0.09$ Hz, $t_{27} = 3.81$, $p = 0.00073$).

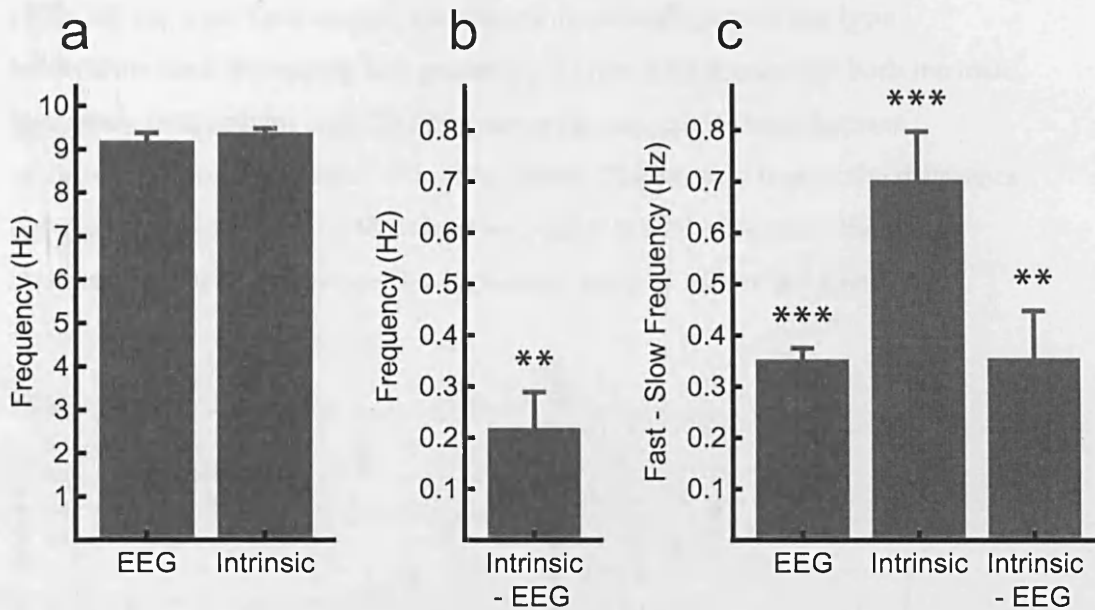


Figure 4.4 Differences between intrinsic and EEG frequencies and the effect of running speed across cells. Grid cell intrinsic firing frequency, f_i , systematically exceeds the concurrently recorded EEG theta frequency, f_θ . a) All runs over 5cm/s. b) The intrinsic firing frequency is significantly higher than the concurrent theta frequency ((b) shows mean \pm s.e.m. of the paired difference between intrinsic and theta) c) The difference between intrinsic firing frequency and theta frequency is greater for *fast* runs than for *slow* runs. Both frequencies increase with running speed but intrinsic firing frequency increases by more, so that the difference between intrinsic and theta frequencies also increases with running speed. * denotes $p < 0.05$; ** $p < 0.005$.

The oscillatory interference model predicts that the relationship between speed and intrinsic/EEG frequency and the difference between them in particular varies instantaneously with speed. Measuring the instantaneous EEG frequency is relatively difficult and even more so in the case of intrinsic firing frequency. To attempt a more fine-grained analysis aimed at relating these quantities instantaneously, intrinsic frequency was measured as the inverse of the time between spikes fired on subsequent cycles, with concurrent EEG frequency obtained from the analytic signal and concurrent speed from the recorded trajectory time-series as described in the methods above. The EEG and intrinsic frequencies obtained this way were subtracted by the mean EEG frequencies measured within the trial in which they were recorded. This allowed for between trial and rat variation. The EEG and intrinsic frequencies obtained this way from all cells are shown in Figure 4.5a as a function of speed of running. Rats do not often run at the highest running speeds and these are generally poorly represented. Therefore the speed data were divided into 5 equal parts and in Figure 4.5 each point represents 20% of the available data. In addition, higher running speeds are confounded by head shake and reflections of the

LEDs off the wall. Low speeds are also confounded by non-theta type behaviours such as rearing and grooming. Figure 4.5a shows that both intrinsic frequency (red points) and EEG frequency (green points) have a linear relationship which saturates at higher speeds. The same is true of the difference between the two (Figure 4.5b). However, there is a lot of noise in the data, especially at the highest speeds which don't seem to follow the trend.

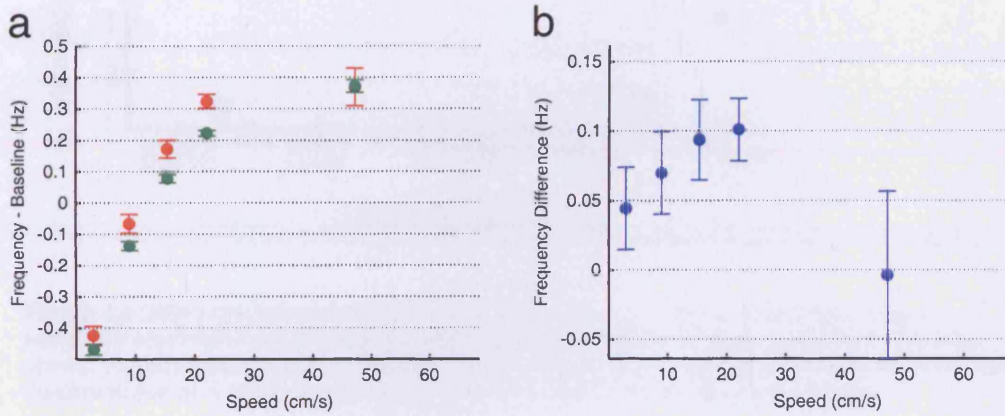


Figure 4.5 Instantaneous intrinsic and EEG frequencies as a function of speed. Each point represents 20% of all data (mean \pm sem). (a) Intrinsic frequency (red) and EEG frequency (green) (green), where the mean of all measured EEG frequencies within a trial has been subtracted from all data points. (b) Difference between concurrently measured, instantaneous EEG and intrinsic frequency plotted as a function of speed.

Finally, the relationship between the difference in frequencies, speed, and the spatial scale of the grids was examined. Since the greatest measurement error occurs in the estimate of the small difference $f_i - f_\theta$ rather than the estimate of L , we correlated $(f_i - f_\theta)/\bar{s}$ with $1/L$, where \bar{s} the mean speed of the runs in a trial and L is the measured grid scale, see Figure 4.6. We thus, find a good linear correlation to support the predicted relationship in equation (4.5).

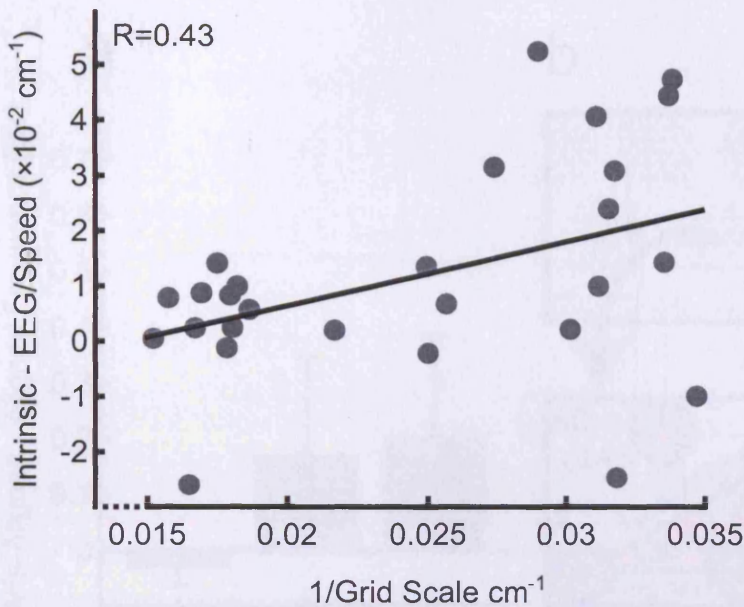


Figure 4.6 Difference between intrinsic and EEG frequencies and the relationship to grid scale. The predicted inverse grid scale (difference in intrinsic and theta frequencies divided by speed, y axis) correlates with the measured inverse grid scale (x axis). The inverse of the spatial scale is shown to avoid divide by zero errors in the (noisy) difference in frequencies.

A related interference model (Blair et al., 2007) posits micro-grid firing patterns (grid-like patches of firing at the scale of the distance run during one theta cycle), with the observed (large-scale) grids resulting from moiré interference between micro-grids with slightly different scales or orientations. The moiré interference model predicts significantly higher intrinsic firing frequencies for runs *aligned* with the principal axes of the grid than for *misaligned* runs (by a factor $\sqrt{3} \approx 1.73$), reflecting the different frequencies at which firing patches occur along these directions (Figure 4.7 b). By contrast, the oscillatory interference model predicts similar firing frequencies for *aligned* and *misaligned* runs. This is due to the related prediction that the intrinsic frequency will exceed theta by more for *misaligned* than *aligned* runs by the small

Figure 4.7 Directional modulation of frequencies with respect to the moiré interference model. a) Analysis of frequencies in runs *aligned* or *misaligned* with the grid. No significant difference was found for either frequency between *aligned* and *misaligned* runs, with intrinsic frequency actually slightly lower for *aligned* than *misaligned* runs, contrary to the prediction of a moiré interference model (see (b), and Blair *et al.* (2007)). The difference between intrinsic and theta frequencies also did not vary significantly between *aligned* and *misaligned* runs, and was slightly larger for *misaligned* compared to *aligned* runs, consistent with the oscillatory interference model (Burgess *et al.*, 2007), albeit non-significantly.

factor $1/\cos(30^\circ) \approx 1.15$, since runs *aligned* with grid nodes are at 30° from the preferred direction of a linear interference pattern. Accordingly, *aligned* and *misaligned* runs of at least 0.5s duration were extracted from the data within which intrinsic firing and theta frequencies were measured. No significant differences between *aligned* versus *misaligned* runs in intrinsic firing frequency, theta frequency, or in the difference between the two frequencies were found

$$(f_{\theta}^{\text{misaligned}} - f_{\theta}^{\text{aligned}} = 0.03 \pm 0.03 \text{ Hz}, p = 0.36; f_i^{\text{misaligned}} - f_i^{\text{aligned}} = 0.17 \pm 0.17 \text{ Hz}, p = 0.53; (f_i^{\text{misaligned}} - f_{\theta}^{\text{aligned}}) - (f_i^{\text{misaligned}} - f_{\theta}^{\text{aligned}}) = 0.21 \pm 0.18 \text{ Hz}, p = 0.26).$$

The direction of change in intrinsic frequency with running direction is incompatible with the moiré interference model prediction, while the direction of change of the difference between intrinsic and theta frequencies is compatible with the oscillatory interference prediction, see Figure 4.7.

4.4 Discussion

The findings of this study are both consistent with existing literature on the effects of speed on EEG theta frequency and provide support in favour of an oscillatory interference model of grid cell firing (Burgess et al., 2007), see also Giocomo *et al.* (2007). Predictions relating the difference between intrinsic firing frequency and theta frequency to running speed and grid size were upheld. Theta frequency increased with speed as did intrinsic frequency but more importantly intrinsic frequency is found to be higher than theta frequency at both *fast* and *slow* speeds. This observation has an interesting implication for the oscillatory interference model. In order to maintain an intrinsic firing frequency greater than or equal to the concurrent theta frequency, dendritic subunits must also maintain their intrinsic sub-threshold oscillation frequency above that of theta. This effectively constrains this type of model to those variants such as the rectified model of Figure 4.1c where this is indeed the case (Burgess et al., 2007). This finding is reminiscent of that found in 1D phase precession (O'Keefe & Recce, 1993), raising the possibility that this phenomenon exists also in at least a subset of entorhinal cortical cells. There is already some evidence that entorhinal cortical layer II neurons are capable of phase precession (Hafting et al., 2006).

The relationship between theta frequency and running speed argues against versions of the model (Burgess et al., 2007; Giocomo et al., 2007) in which β is proportional to theta frequency. This would result in a non-linear relationship between the difference $f_d - f_b$ and speed. The net of effect of this would be that grid scale would vary with speed, since β in equation (4.1) and thus the difference $f_d - f_b$ would be a function of theta which is itself a function of speed. The data are consistent with the predicted linear relationship between frequency differences and running speed. However, they can neither specify the slope of this relationship nor exclude the possibility of other increasing relationships. The determination of these key constraints was precluded by the small numbers of spikes remaining in each behavioural interval when speed was divided into further subintervals (e.g., into *slow*, *medium* and *fast* runs).

However, a more detailed analysis into the relationship between frequency and speed (Figure 4.5) shows that these quantities can indeed be related linearly and compares the association between speed, intrinsic frequency, EEG frequency

and the difference between them on a moment-by-moment basis. This is a more direct and compelling test of the predictions of the oscillatory interference model, which requires continuously changing, trajectory-dependent frequencies.

Finally, our data do not support the related spatial (moiré) interference model of grid cell firing (Blair et al., 2007); showing no sign of the predicted dependence of intrinsic frequency on running direction. This model predicts that intrinsic frequency measured in runs *aligned* with the principal axes of the grid should be greater by a factor $\sqrt{3}$ than those made in *misaligned* runs. Not only is this prediction of the moiré interference model unsubstantiated by the results, the mean difference is in fact in the opposite direction to that predicted. Although this difference is not significantly different from zero, it is compatible with the oscillatory interference model, which predicts *misaligned* runs to be $2/\sqrt{3}$ greater than *aligned* runs. We note however, that the magnitude of this difference does not compare well with the expected magnitude which would be of the order of 1 Hz rather than the 0.21 Hz actually found.

Although the model's basic mechanism for the production of grid-like firing patterns from oscillatory interference was supported, further work is required to relate the model to many aspects of the emerging literature on grid cell firing. Firstly 19 of 54 grid cells isolated were rejected on the basis of poor theta modulation. It is unclear how the model relates to this subset of non-modulated cells or whether oscillatory interference of sub-threshold oscillations can result in firing that isn't modulated at the theta rhythm. In addition to this grid cells may be further categorised on the basis of their functional characteristics and cell morphology. For example, deeper layers III, V and VI of entorhinal cortex contain conjunctive cells, whose firing is modulated by position and head direction (Sargolini et al., 2006), while layer II cells are largely only position modulated. Furthermore, different cell types exist in different proportions throughout the layers; deeper layers contain pyramidal neurons as well as stellate cells.

It is important to acknowledge the existence of oscillations other than movement-related theta such as the lower-frequency atropine-sensitive theta

(Buzsaki, 2002; O'Keefe, 2006); and the intracellular somatic oscillations recorded in vitro (Giocomo et al., 2007). Further investigation is required to establish the effect of these oscillations and the extent and context of their relevance for the model. Finally, how does the oscillatory interference model relate to alternative grid cell models based on recurrent connectivity (McNaughton et al., 2006; Fuhs & Touretzky, 2006)? The oscillatory interference model may be complementary to the recurrent connectivity model, in that it might provide the initial firing pattern required to allow the formation of appropriate recurrent connectivity to stabilise grids relative to other grids (McNaughton et al., 2006; Fuhs & Touretzky, 2006) or relative to the environment (via connectivity with place cells Burgess *et al.* (2007)). More generally, our findings support a radical model of neuronal processing based on interfering sub-threshold oscillations, extending results in hippocampus (O'Keefe & Recce, 1993; Lengyel et al., 2003; Maurer et al., 2005) to entorhinal neocortex.

5 Environmental novelty is associated with reduction of the hippocampal theta frequency

5.1 Introduction

Detection of novelty is a function of fundamental importance in the operation of any competent memory system. It alerts an organism to changes, often subtle, in sensory input, which may be critical to its survival. In addition, efficient encoding of events into memory requires the ability to differentiate between that which has not changed (familiar) and that which has (novel). The hippocampal formation, which has a critical role in episodic/declarative memory, (Cohen & Eichenbaum, 1993; Squire & Zola-Morgan, 1991; O'Keefe & Nadel, 1978) has long been linked with novelty detection (Sokolov, 1963; Aggleton & Brown, 1999; Strange, Fletcher, Henson, Friston, & Dolan, 1999; Kohler, Danckert, Gati, & Menon, 2005), especially where experience differs from expectation (Vinogradova, 2001; Gray & McNaughton, 2000; Honey, Watt, & Good, 1998; Kumaran & Maguire, 2006). These ideas are variously known as contextual or relational novelty, associative mismatch or comparator processing.

Determining the electrophysiological correlates of contextual novelty has been a principal focus of human memory research. A number of human intracranial event-related potential studies (Knight, 1996; Grunwald, Lehnertz, Heinze, Helmstaedter, & Elger, 1998; Grunwald & Kurthen, 2006) and single unit studies (Halgren, Squires, Wilson, Rohrbaugh, Babb, & Crandall, 1980; Fried, MacDonald, & Wilson, 1997; Rutishauser, Mamelak, & Schuman, 2006), (see (Axmacher, Mormann, Fernandez, Elger, & Fell, 2006; Rugg & Coles, 1995) for a review) have implicated the HF in novelty processing, finding increased amplitudes in ERPs relating to greater neuronal synchronisation and selective neuronal discharge relating to novel versus familiar stimuli.

Cholinergic and GABAergic innervation of the hippocampal formation via the medial septum is known to be critical in generating the theta rhythm. Furthermore, both the septo-hippocampal pathway (Givens & Olton, 1995) and theta oscillations themselves (Sederberg, Kahana, Howard, Donner, & Madsen, 2003; Jacobs, Hwang, Curran, & Kahana, 2006; Ekstrom, Caplan, Ho, Shattuck, Fried, & Kahana, 2005; Osipova, Takashima, Oostenveld, Fernandez, Maris, &

Jensen, 2006; Rizzuto, Madsen, Bromfield, Schulze-Bonhage, & Kahana, 2006; Mormann, Fell, Axmacher, Weber, Lehnertz, Elger, & Fernandez, 2005; Fell, Dietl, Grunwald, Kurthen, Klaver, Trautner, Schaller, Elger, & Fernandez, 2004; McCartney, Johnson, Weil, & Givens, 2004) are important for a wide variety of mnemonic functions. Correspondingly, a number of theoretical mechanisms have been proposed to underlie these processes. These have focussed either on models of neuropharmacological control, which emphasise the role of acetylcholine (Yu & Dayan, 2005; Myers, Ermita, Harris, Hasselmo, Solomon, & Gluck, 1996) or dopamine or acetylcholine and both theta and gamma oscillations (Lisman & Otmakhova, 2001; Hasselmo, 2006), see (Ranganath & Rainer, 2003; Gray & McNaughton, 2000) for reviews. Despite extensive theoretical investigation into novelty detection, the precise mechanisms remain elusive.

Environmental novelty is a pertinent form of contextual novelty for foraging mammals, and the HF both represents environmental layout, via the firing of 'place cells' (O'Keefe & Nadel, 1978; Muller, 1996) and directs exploration of spatial alterations to environmental layout – i.e. of unexpected rearrangement or absence of objects, but not replacement of an object by a new one (O'Keefe & Nadel, 1978; Save, Poucet, Foreman, & Buhot, 1992; Save, Buhot, Foreman, & Thinus-Blanc, 1992; Lee, Hunsaker, & Kesner, 2005). This exploration is thought to enable environmental representations to be updated (O'Keefe & Nadel, 1978) and seems to result from discrepancy between current experience and a stored (spatial) representation rather than the absolute novelty of individual stimuli. Indeed some place cells ('misplace' cells) specifically fire at the location of an unexpectedly displaced or missing object (O'Keefe, 1976; Fyhn, Molden, Hollup, Moser, & Moser, 2002; Lenck-Santini et al., 2005), but not when an object is replaced by a new one "mirroring the effects of lesions;" (Lenck-Santini et al., 2005). In addition, a sufficiently changed environment induces rapid global 'remapping' of the entire place cell representation (Bostock et al., 1991; Wills, Lever, Cacucci, Burgess, & O'Keefe, 2005; Fyhn et al., 2007) producing a new attractor state in memory (Wills et al., 2005; Nakazawa et al., 2002; Leutgeb, Leutgeb, Treves, Meyer, Barnes, McNaughton, Moser, & Moser, 2005).

Given the importance of the theta rhythm in memory operations and the salience of environmental novelty for foraging mammals, this chapter examines the link between the two. In addition, we specifically set out to test a prediction of the oscillatory interference model of grid cell firing: that environmental novelty might be signalled by a drop in theta frequency (Burgess et al., 2007).

5.2 Materials and Methods

5.2.1 Subjects

Seven male Lister Hooded rats, weighing 315-390g at time of surgery, were used as subjects. They were maintained on a 12:12 hour light:dark schedule (with lights off at 15:00). See chapter 2 – General Methods and references therein for details of animal housing, surgical procedure, basic recording strategy, spike sorting, and histology.

5.2.2 Electrode implants and localisation

Seven rats were implanted: 5 rats had two microdrives, one each in CA1 and subiculum, one rat had two microdrives, both in CA1 and one rat had a single microdrive implanted in the subiculum. In one double-implanted rat, cells were recorded from subiculum only. Recording sites were in anterodorsal CA1 and dorsal subiculum in all cases, verified by inspection of histological material.

CA1 tetrode implants were centred on the following anterior-posterior and medio-lateral coordinates: a) 3.0-3.1mm posterior to bregma, 1.8-2.0 mm lateral to the midline, and b) 3.8-4.0 mm posterior to bregma, and 2.4-2.6 mm lateral to the midline. Tetrodes were positioned 500-800 μm above the CA1 layer at surgery. Subicular tetrode implants were centred on the following anterior-posterior and medio-lateral coordinates: 5.8-6.2 mm posterior to bregma, 2.8-3.1 mm lateral to the midline. Tetrodes were positioned 500-800 μm above the subiculum at surgery.

5.2.3 Screening and training procedures before the test trials

Before the period of formal recording of the test trial series, rats were screened and acclimatised to recording apparatus and rice-foraging, in a room separate from both the home cage room and the testing lab. Electrode activity was monitored over a 2-5 week period. During screening, the rat rested on a square holding platform (39 cm sides, 5 cm high ridges) containing sawdust. Rats were pre-trained in this screening room to forage for rice on a black square platform (94 cm sides, 2 cm high ridges). Each rat was given a few sessions (10-20 minutes long) of training until it had acquired the random foraging task such that it spent most of its time moving over all areas of the platform. These training procedures were done so that, as far as possible, the novelty afforded

by the first exposures to environment 'a' did not include non-environmental novelty associated with rice-related cues/contingencies, continuously locomoting with the headstage, and so on. Once electrodes were appropriately positioned and acclimatization complete, the rat was brought to the testing lab, and placed on a holding platform (similar to the one in the screening room), see Figure 5.1a. All the rats had two to three hours of exposure to the holding platform in the testing lab over one to two days before beginning the test trial series.

5.2.4 Test trial series

A diagram of the environments used and order of testing in the test trial series is shown in Figure 5.1a & b. Experiments were conducted within a black-curtained circular testing arena 2.3 m in diameter (except that the curtains were opened for environment 'b', as described below). The centre of each testing environment had the same location relative to the arena. An external white cue card (102 cm high, 77 cm wide), which was prominently visible from the testing arena provided directional constancy throughout the test trial series, as did standardized procedures for translating the rat and placing it into the box and various background cues. For every trial, the rat was passively displaced, facing 'lab north', about 2 metres in the 'lab north' direction, and placed at the centre of the given environment. During trials the rat searched for grains of sweetened rice randomly thrown into the box about every 30 seconds. At the end of each trial, the rat was removed from the given recording environment and placed back on the holding platform. Rats were kept on a holding platform outside the arena before and after every trial. The inter-trial interval was 20 minutes.

Three environments were used in the test trial series. Environment 'a' was a square 'morph' box, as previously described (Lever et al., 2002), with 62 cm sides. The black curtains were fully drawn so as to surround environment 'a'. Environment 'b' was a circular-walled, wooden light-grey enclosure, 79 cm in diameter, with seams at 'lab-north' and 'lab-south'. For environment 'b', the black curtains were opened, such that various extra-arena cues were visible. The 'floor' of environments 'a' and 'b' was a circular black platform, raised 27 cm above the actual floor of the testing arena. Environment 'c' consisted simply of this circular open platform, which was 90cm in diameter, with the arena

curtains fully drawn as for environment 'a'. The platform was thus the floor for all three environments, and was cleaned before every trial.

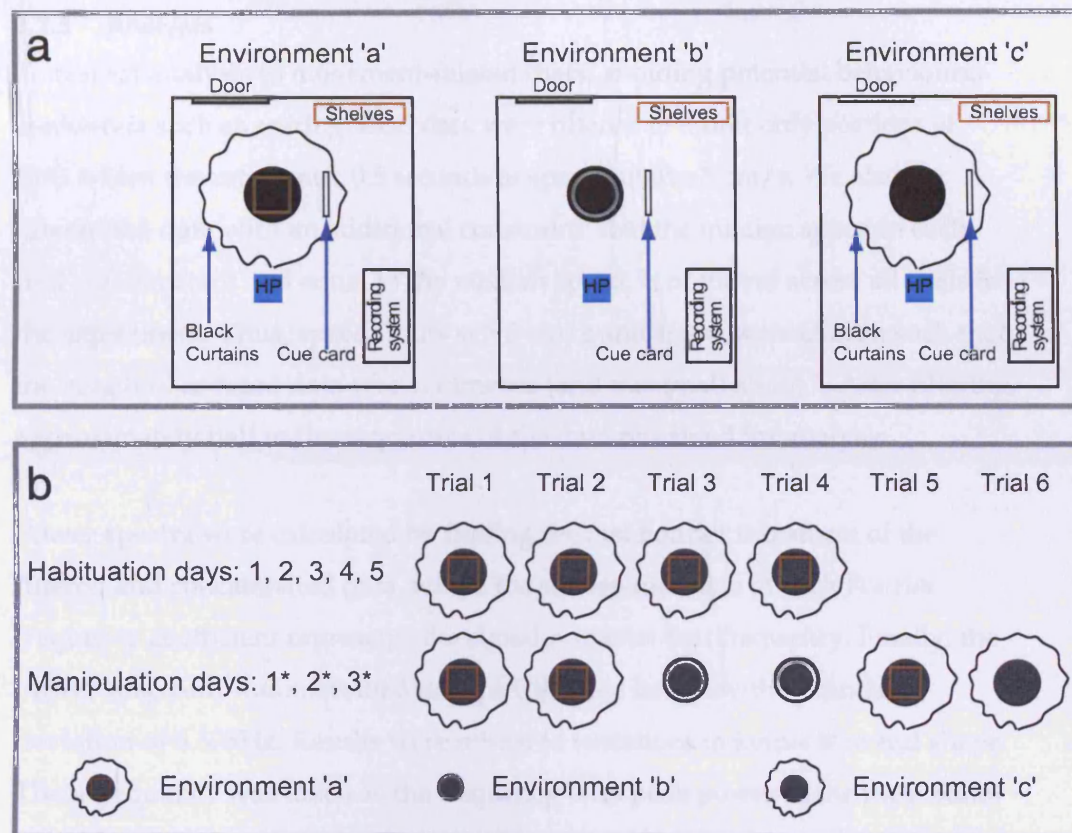


Figure 5.1 Experimental paradigm for collection of data used in chapter 5 and 6. a) Description of environments. Environment 'a' is a brown, square, walled environment with curtains drawn closed, environment 'b' is a white, cylindrical, walled environment with curtains drawn open, while environment 'c' is simply the raised black circular platform (which forms the floor for all environments), with the curtains drawn closed again. HP refers to the holding platform. All environments share the same prominent cue card in the same position. (b) Shows the procedure for each day. On days 1-5, rats were exposed to 4 20 minute trials in environment 'a'. On the 6th, 8th and 10th day (days 1*, 2* and 3*), rats experienced environment 'b' in place of 'a' on the 3rd and 4th trials and subsequently experienced a further trial in environment 'a' followed by 1 trial in environment 'c'.

During the habituation phase (days 1-5) there were 4 trials per day, all in environment 'a'. This was followed by the manipulation phase, on days 6, 8 and 10 (referred to as days 1*, 2* and 3* respectively, where the asterisk indicates day within the manipulation phase). No testing was performed on days 7 and 9. There were 6 trials on days 1*-3*, organised as follows. Trials 1, 2 and 5 were conducted in environment 'a', trials 3 and 4 in environment 'b', and trial 6 in environment 'c'. The black curtains were opened 90 seconds before the beginning of trial 3, and closed 90 seconds after the end of trial 4. We took care that testing time was similar for all rats and similar across the test trial series for

a given rat. Across all days and all rats, the starting time of the day's first trial ranged from 2.25 pm to 4.25pm.

5.2.5 Analysis

To restrict analysis to movement-related theta, avoiding potential behavioural confounds such as rearing, EEG data were filtered to admit only portions of EEG where the rat spent ≥ 0.5 seconds at speeds above 5 cm/s. We also re-filtered the data with an additional constraint: that the median speed in each trial was constant and equal to the median speed, k , of the rat across all trials in the experiment. Thus, speed limits $s_1 > 5$ cm/s and $s_2 < \infty$ were chosen such that the length of ordered data was symmetric (and maximal) about k . After filtering, approximately half to three-quarters of the data remained for analysis.

Power spectra were calculated by finding the fast Fourier transform of the filtered and concatenated data, where the square-modulus of each Fourier frequency coefficient represents the signal power at that frequency. Finally, the power spectrum was smoothed using a Gaussian kernel with a standard deviation of 0.375Hz. Results were robust to variations in kernel size and shape. Theta frequency was taken as the frequency with peak power in the theta band (5–11Hz). All analysis was conducted using MatLab R12.1, (The MathWorks, Inc.).

In order to collate data across rats, systematic variation in theta frequency between them must be accounted for. Thus, a baseline theta frequency for each rat was defined as the mean of theta over trials in habituation days 2-5. The baseline for each rat was then subtracted from the frequency per trial measured in that rat.

Due to technical problems, EEG data were unavailable for Rat 3 on day 4. Missing values for these trials were replaced by the average over the same trials on days 2, 3 and 5 (day 1 was not included, since theta frequency was much lower on this day compared to the others). Hence, four rats were included in the ANOVA showing the effect of familiarity in days 1-5 see below. (The significant effect of day in this ANOVA remains significant if data from Rat 3 are excluded). In addition, the test trial series for Rat 1 was terminated at the end of change day 1*, thus data for days 2* and 3* are missing for this rat. As a result,

all ANOVAs involving effects over days 1*-3* only include data from the remaining 3 rats. See Figure 5.2 for all data.

5.3 Results

Of the seven rats used in this experiment, one had no available EEG. Two of the remaining six, in both of whom designated EEG channels were in the subiculum, showed relatively low power in the theta band compared to the other four rats, all of which had EEG electrodes in CA1. In addition, power spectra in these two rats had noisy peaks and showed frequent double peaking in the theta band, which we attribute to flutter Nerd & Bilkey (2005). These two rats were also excluded. Of the four rats included in the analysis Rat 4 is missing EEG data for day 4.

Theta frequencies measured for each rat and for each trial are shown in column 1 of Figure 5.2. The effect of novel trials on the theta frequency of each rat is clearly visible. Points in black mark values measured in novel environments 'b' and 'c', while gray points show trials in environment 'a'. In each rat, the frequency measured in environment 'a' on day 1, is visibly lower compared to subsequent days. The same is true in novel environments in rats 2 and 3. The most notable behavioural correlate of theta frequency, speed, which has been reported in some previous studies but not others, is shown in the second column. We see that speed increases in general throughout the experiment, possibly reflecting the rats overall confidence within the environment or with the task, despite large changes in environmental context. We note however, that there is a drop in speed, restricted only to the very first exposure to environment 'b' when compared to the previous exposure in environment 'a', which quickly vanishes. Novel contexts are often associated with slower movements as the rat explores more carefully the changes to its environment. Thus, in this section we explore these effects in greater detail and attempt to rule out any possible effects of speed on the theta frequency changes with novelty.

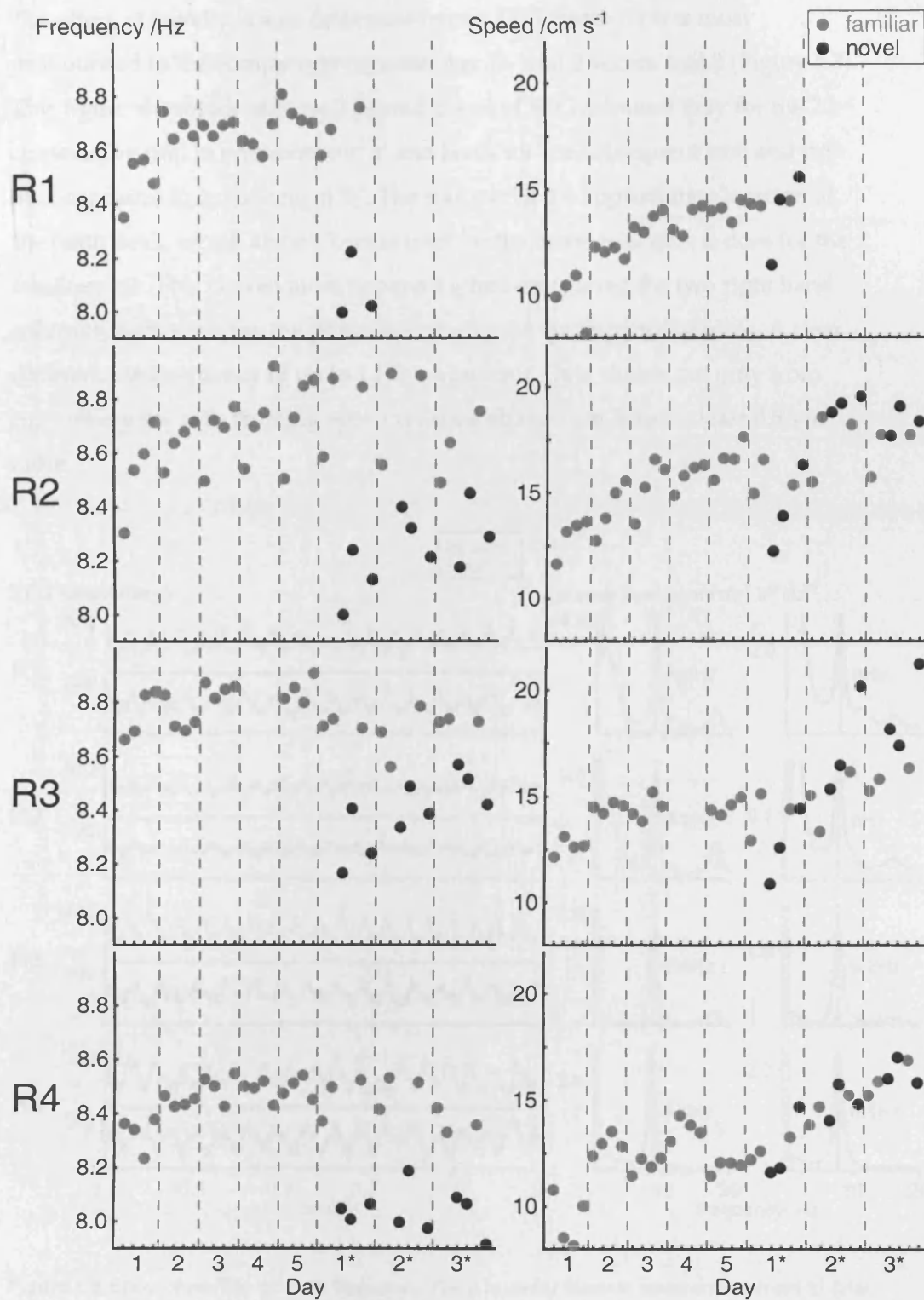


Figure 5.2 EEG frequencies and speeds for individual rats and trials Left column: Theta frequency (baseline frequencies: R1 - 8.68 Hz, R2 - 8.67 Hz, R3 - 8.81 Hz, R4 - 8.48 Hz) Right column: Median speed (baseline speeds: R1 - 12.94 cm s⁻¹, R2 - 15.93 cm s⁻¹, R3 - 14.48 cm s⁻¹, R4 - 13.18 cm s⁻¹). Baselines were calculated in exactly the same way for theta frequency and speed, see section 4.2.5.

The effect of novelty is also detectable in raw EEG traces. This is most pronounced in the comparison between day 1*, trial 2 versus trial 3 (Figure 5.3). This figure shows for each rat 2 second traces of EEG coloured gray for the 22nd consecutive trial in environment 'a' and black for the subsequent trial and first ever exposure to environment 'b'. The star marks the approximate location of the tenth peak, which always occurs later for the novel trial than it does for the familiar one. This is even more apparent when comparing the two right hand columns, each showing the power spectra for the corresponding trials. A clear difference in frequency of up to 1 Hz is apparent. Data shown are only from runs where the rat's running speed remains above 5 cm/s for at least 0.5 s or more.

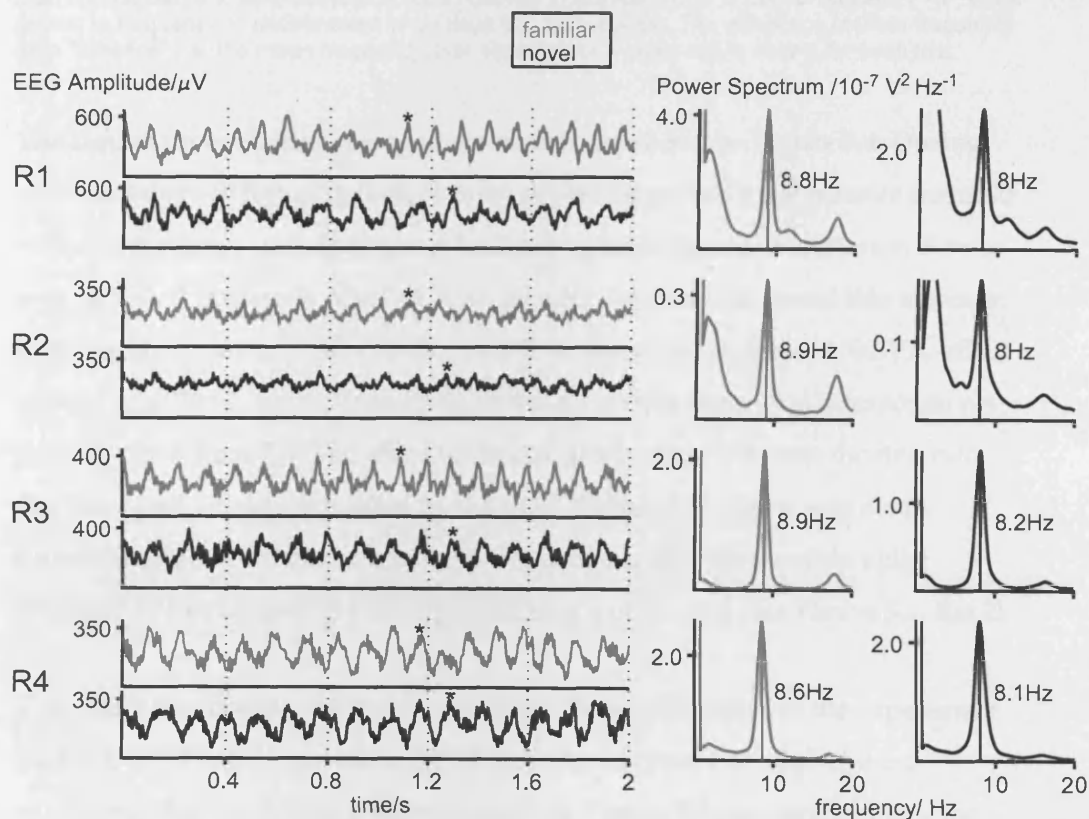


Figure 5.3 Effect of novelty on theta frequency. Theta is visibly faster in novel environment 'b' (trial 3, black lines) than familiar environment 'a' (trial 2, grey lines) on day 1*: individual traces from each rat (left, asterisk marks 10th cycle); power spectra for whole trial (right).

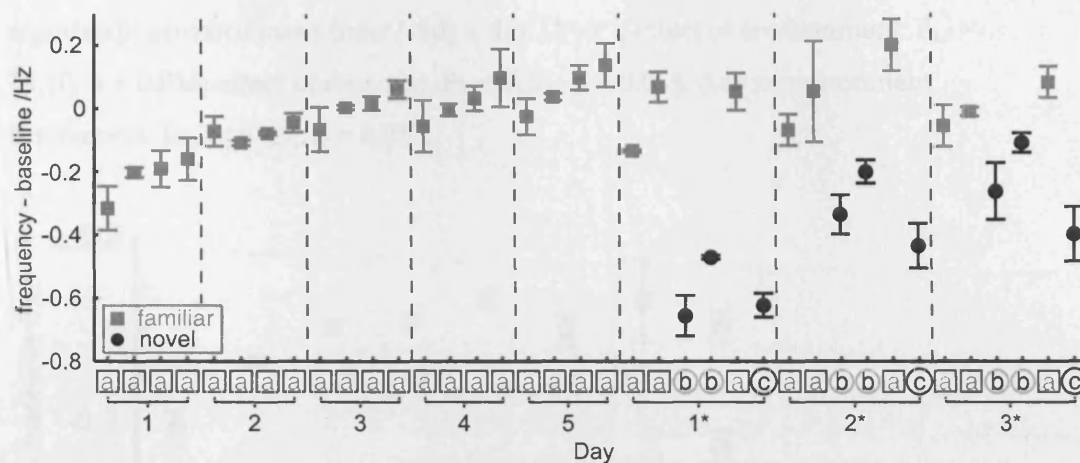


Figure 5.4 Average over rats of baseline-adjusted theta frequency for each trial in the experiment. Theta frequency increases with days of experience in environment 'a' (days 1-5), and change to an environment within a common setting produces an even greater initial decrease in frequency than first exposure to environment 'a' (cf. frequency in environments 'b' and 'c' on days 1*-3*, black points, to frequency in environment 'a' on days 1-3, grey points). The difference in theta frequency from 'baseline' (i.e. the mean frequency over days 2-5 for a given rat) is shown for each trial.

The results for each trial averaged across rats are shown in Figure 5.4. During the first 5 days of foraging in the brown square there was a progressive increase in theta frequency with increasing familiarity across days of experience. A two-way repeated measures ANOVA with factors, day and trial found this increase to be highly significant (day (1-5) x trial (1-4) repeated measures ANOVA, effect of day: $F_{4,12}=24.82$, $p<0.001$; effect of trial: n.s., $p=0.26$; day x trial interaction n.s., $p=0.39$), see Figure 5.4. The effect was most pronounced between the first two days and had already saturated by the third (Figure 5.5). There was a non-significant hint of an increase in theta frequency across trials within a day (Figure 5.4) due largely to a strong effect in one of the rats (see Figure 5.2, Rat 2).

This effect was complemented by results in the second phase of the experiment (days 1*, 2*, 3*), during trials in which new environments 'b' and 'c' were substituted for the expected brown square. In Figure 5.5 gray points mark the average over environment 'a' trials within a day, whereas black points mark the average over trials in environments 'b' and 'c'. This comparison unambiguously illustrates the sharp decrease in theta in new environments. This decrease lessened over days and while the effect of day was not quite significant, the relative change in frequency between environment type and day was, as shown by the interaction these two factors. A two-way repeated measures ANOVA performed on data from the second phase found the effect of environment to be

significant (environment (new/old) x day (1*-3*), effect of environment: $F_{1,2} = 62.10$, $p = 0.016$; effect of day: n.s., $F_{2,4} = 6.51$, $p = 0.055$; day x environment interaction: $F_{2,4} = 10.27$, $p = 0.027$).

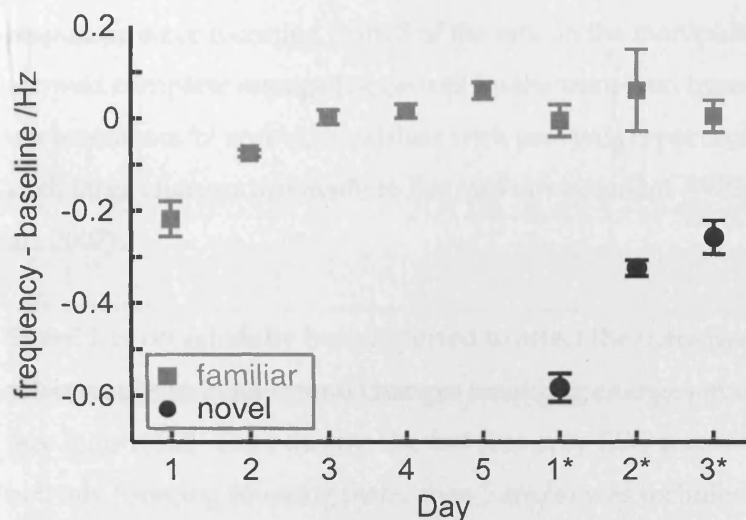


Figure 5.5 Effect over days on baseline-adjusted theta frequency. The novelty effect is shown most clearly when each day's trials within familiar environment 'a' (grey points) or novel environments 'b' and 'c' are averaged (black points). Points show the mean across rats, error bars show s.e.m.

Frequency measured in the new environments (over days 1*-3*) was far lower than that measured on comparable days (1-3) in environment 'a'. In addition, the rate at which theta approached baseline in the new environments was significantly greater than that associated with the first days of exposure in the brown square. A three-way ANOVA, comparing initial exposure in environments 'a' and 'b' and using only the first two trials in each day was performed (environment (b vs a) x day (1*-3* in b, 1-3 in a) x trial (1-2), effect of environment: $F_{1,2} = 30.00$, $p = 0.032$; effect of day: $F_{2,4} = 38.94$, $p = 0.002$; effect of trial n.s., $p = 0.147$; environment x day interaction: $F_{2,4} = 9.00$, $p = 0.033$).

In environment 'b' alone the effect over days is significant (c.f. effect of day in environments 'b' and 'c' combined above). The significant interaction between environment and day indicates attenuation of this differential effect over days (see Figure 5.5) i.e. theta frequency increases with days of exposure in both the initial environment 'a' and the new one 'b', but more so in 'b'. More importantly the effect of environment was significant, i.e. the effect of unexpectedly experiencing environment 'b' in place of environment 'a' produced a greater reduction than the initial exposure to environment 'a', when compared to

baseline. This may reflect the need for a stronger contextual novelty signal when existing environmental representations need to be changed, i.e. when a prior expectation is violated, as compared to the effect of absolute novelty, when an environmental representation needs to be set up for the first time. CA1 place cell responses were recorded from 3 of the rats on the manipulation days 1*-3* and showed complete remapping caused by the transition from environment 'a' to environments 'b' and 'c', consistent with previous reports of remapping when such large changes are made to the rat's environment (Wills et al., 2005; Fyhn et al., 2007).

Speed has occasionally been reported to affect the theta frequency and novelty often results in behavioural changes including changes in overall running speed (see Figure 5.2). Thus despite the fact that only EEG recorded while rats were actively foraging (moving faster than 5 cm/s) was included, novelty related changes in theta frequency might reflect or be modulated to some extent by novelty-related changes in behaviour. In order to test for any indirect effects of the average running speed in a trial on theta frequency, such as might be mediated by body temperature (Whishaw & Vanderwolf, 1971), a linear model was fit to theta frequency as a function of median speed per trial across the entire dataset for each rat. The effects of speed on frequency, as measured by the correlation between the two, were non-significant for each rat but varied in strength across rats ($r^2 = 0.006-0.097$; $p=0.06-0.65$ see Table 5.1 for details). The linear model was used to control for any potential confounds produced by running speed on the effect of novelty on theta frequency. The effect of speed on frequency, as indicated by the regression analysis was subtracted, and the ANOVAs above were repeated on the frequency residuals. This manipulation left all of the main results effectively unchanged. The effect of gradually increasing experience over the first five days was still significant (effect of day: $F_{4,12}=28.82$, $p<0.001$; effect of trial: n.s., $p=0.25$; day x trial interaction n.s., $p=0.26$). The same was true of the effect of environmental novelty on days 1*-3* (environment (new/old) x day (1*-3*), effect of environment: $F_{1,2} = 61.35$, $p = 0.016$; effect of day: n.s., $p = 0.26$; day x environment interaction: $F_{2,4} = 9.53$, $p = 0.03$). Thus, new environments still provided significantly lower measurements of theta compared with familiar environments experienced on the same days (1*-3*), even after all indirect effects of speed are removed. The greater effect of

unexpected environment 'b' on days 1*-3* compared to the initially novel environment 'a' on days 1-3 increased slightly and attenuated more slowly over days (effect of environment: $F_{1,2}=145.01$, $p=0.007$; effect of day: $F_{2,4}=12.44$, $p=0.026$; Environment x Day interaction: $F_{2,4}=2.56$, $p=0.193$; effect of Trial: n.s., $p=0.101$, all other interactions: not significant). This demonstrates the robustness of these results to possible novelty-related changes in running speed.

Table 5.1 Correlation between median running speed and theta frequency per trial per rat.

Rat	r^2	p	n (trials)
Rat 1	0.097	0.12	26
Rat 2	0.096	0.06	38
Rat 3	0.006	0.65	34
Rat 4	0.012	0.51	38

This would not however, account for direct correlation of speed with the concurrently recorded EEG. To account for any such potential confound, theta frequency was calculated in subsets of data from each trial, chosen so that the median running speed was constant in each trial for a given rat. The median speed was chosen to be the median of all speeds sampled in the rat during the entire experiment. These sub-sampled data are shown in Figure 5.6 and the analysis performed above was repeated on these data. As before the effect of days of experience over days 1-5 remained ($F_{4,12}=12.44$, $p<0.001$, no effect of trial or interaction), as did the effect of environmental novelty on days 1*-3* ($F_{1,2}=73.00$; $p=0.013$, no effect of trial or interaction). The effect of initial novelty in environment 'a' being slightly reduced compared to the greater effect of unexpected environment 'b' on days 1*-3*, which increased slightly as it did with the previous control for speed ($F_{1,2}=124.83$, $p=0.008$) and showed less attenuation over days (Environment x Day interaction: $F_{2,4}=0.33$, $p=0.738$; effect of Trial: n.s., $p=0.30$; no other significant interactions).

Overall, controlling for variation in running speed slightly weakened the increase in theta frequency seen over the first five days of experience within a given environment and slightly strengthened the theta frequency reduction on encountering the unexpected environments on change days 1*-3*. The effect of novel environments remained approximately constant across both control manipulations for speed.

Environmental novelty may induce stress in the animal. Stress has been also reported to affect theta frequency, but tends to increase it (Fontani, Farabollini, & Carli, 1984), consistent with the effects of anxiolytics in decreasing theta frequency (Gray & McNaughton, 2000), so that any novelty-induced stress could only have weakened the novelty-related decrease in frequency effects reported here.

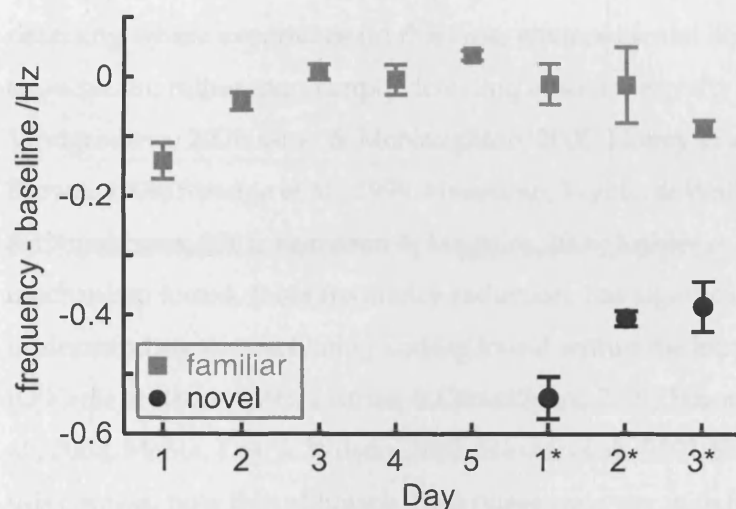


Figure 5.6 Effects over days on baseline-adjusted theta frequency in data sub-sampled to maintain constant median running speed. The effect of novelty on theta frequency does not reflect variations in running speed. Data from each trial were sub-sampled to remove any differences in median speed across trials in the sub-sampled data. Mean theta frequency is shown versus days of experience in familiar environment 'a' (grey points) or novel environments 'b' and 'c' (black points) in sub-sampled data for which median speed is constant across trials. Points show the mean across rats, error bars show s.e.m.

5.4 Discussion

The results suggest that environmental novelty is signalled by a reduced HF theta frequency compared to that in a familiar environment. Intriguingly, an unexpected change to a familiar environment within a common arena setting causes a greater reduction than first exposure to an entirely novel setting. As well as suggesting a new mechanism for signalling novelty, the results support the suggestion that the hippocampus performs a comparator function in detecting where experience (in this case, environmental layout) differs from expectation, rather than simply detecting absolute novelty *per se* (Sokolov, 1963; Vinogradova, 2001; Gray & McNaughton, 2000; Honey et al., 1998; Aggleton & Brown, 1999; Strange et al., 1999; Hasselmo, Wyble, & Wallenstein, 1996; Lisman & Otmakhova, 2001; Kumaran & Maguire, 2006; Kohler et al., 2005). The specific mechanism found, theta frequency reduction, has significant implications for understanding the oscillatory coding found within the hippocampal system (O'Keefe & Recce, 1993; Lisman & Otmakhova, 2001; Hasselmo, 2006; Harris et al., 2002; Mehta, Lee, & Wilson, 2002; Huxter et al., 2003; Skaggs et al., 1996). In this context, note that although theta phase can vary with location across the HF, theta frequency is constant (Buzsaki, 2002) and thus suitable for mediating a generic signal such as contextual novelty. Since gamma power is higher during theta-associated behaviours, relates to hippocampal memory function, is strongly modulated by theta phase in the HF and neocortex in rats and humans, and theta frequency and gamma frequency co-vary (Bragin, Jando, Nadasdy, Hetke, Wise, & Buzsaki, 1995; Chrobak & Buzsaki, 1998; Canolty, Edwards, Dalal, Soltani, Nagarajan, Kirsch, Berger, Barbaro, & Knight, 2006; Jensen & Colgin, 2007; Montgomery & Buzsaki, 2007), our findings have implications for models of oscillatory encoding in memory that involve both the theta and gamma ranges (Lisman & Otmakhova, 2001; Mormann et al., 2005; Sederberg et al., 2003; Jacobs et al., 2006; Osipova et al., 2006; Rizzuto et al., 2006; Lisman & Idiart, 1995).

What could be the neural mechanism that mediates this contextual novelty dependent effect on HF theta frequency? We know that there appear to be two components to HF theta: the movement-related cholinergically independent theta with frequency 8-9Hz, and a lower frequency atropine-sensitive (i.e. cholinergically mediated) frequency of around 6Hz (Klink & Alonso, 1997;

Kramis et al., 1975). The medial septum sets the pace of HF theta and provides both GABAergic and cholinergic inputs, for reviews see (Buzsaki, 2002; O'Keefe, 2006). Increase in cholinergic input to the hippocampus, as seen during exploration of a novel environment (Giovannini, Rakovska, Benton, Pazzagli, Bianchi, & Pepeu, 2001; Thiel, Huston, & Schwarting, 1998), results in a reduction of hippocampal theta frequency (Givens & Olton, 1995). The results support the idea that the GABAergic input sets baseline theta frequency during motion, with increased cholinergic input mediating a reduction in overall frequency in response to novelty. This would be consistent with the rapid and slow synaptic actions of GABA and acetylcholine respectively, and with the proposed involvement of acetylcholine in signalling novelty (Hasselmo, 2006; Meeter, Murre, & Talamini, 2004; Carlton, 1968; Hasselmo, Schnell, & Barkai, 1995). This interpretation is less obviously consistent with a proposed role of acetylcholine in 'expected uncertainty', as compared with 'unexpected uncertainty' (Yu & Dayan, 2005), but the random foraging task used here precludes any direct correspondence to this proposal. The trigger for increased cholinergic innervation from the medial septum might arise from the HF itself, on the basis of the comparison of the stored representation of an environment with the altered input (Sokolov, 1963; Vinogradova, 2001; O'Keefe & Nadel, 1978; Lisman & Otmakhova, 2001; Gray & McNaughton, 2000; Hasselmo et al., 1996; Borisyuk, Denham, Hoppensteadt, Kazanovich, & Vinogradova, 2001; Meeter et al., 2004; Myers et al., 1996).

An electrophysiological signature of contextual novelty has been identified in the human hippocampus (e.g., the 'MTL-P300 Knight, 1996; Grunwald et al., 1998; Grunwald & Kurthen, 2006; Halgren et al., 1980; Rugg & Coles, 1995). The cause of these event-related potentials is the subject of much speculation: as well as synaptic/neuronal activity triggered by the novel event, further suggested contributions include non-time-locked 'induced' activity, event-triggered phase alignment of ongoing oscillations and increased power at specific frequencies (Makeig, Westerfield, Jung, Enghoff, Townsend, Courchesne, & Sejnowski, 2002; Duzel, Neufang, & Heinze, 2005; Fell et al., 2004; Rizzuto, Madsen, Bromfield, Schulze-Bonhage, Seelig, Aschenbrenner-Scheibe, & Kahana, 2003; McCartney et al., 2004; Axmacher et al., 2006). The results presented here imply that a fourth

mechanism may play a role: namely stimulus-induced changes in characteristic frequencies such as theta.

The proposed relationship between novelty and theta frequency has implications for, but is not necessarily incompatible with, current models in which theta provides separate phases for encoding and retrieval (Hasselmo, 2006; Meeter et al., 2004; Borisyuk et al., 2001; Hasselmo, Bodelon, & Wyble, 2002), interacts with gamma frequency oscillations to organize memory for sequences (Lisman & Otmakhova, 2001; Lisman & Idiart, 1995; Jensen & Colgin, 2007) or provides a clock signal against which information is encoded by firing phase in hippocampus (O'Keefe & Recce, 1993; Skaggs et al., 1996) or entorhinal cortex (Burgess et al., 2007). More specifically, the results support the oscillatory interference model (Burgess et al., 2007) of firing of medial entorhinal grid cells (Hafting et al., 2005), which predicts that a change in the frequency of movement-related theta underlies the increase in the spatial scale of the firing pattern of grid cells seen in novel environments (Fyhn, Hafting, Treves, Moser, & Moser, 2006). This in turn might contribute to changes in place cell firing when the rat experiences a novel environment ('remapping' (Bostock et al., 1991)), by causing a mismatch between the grid cells' inputs to place cells and environmental sensory information from lateral entorhinal cortex (Burgess et al., 2007). This model requires further experimental investigation to determine its relationship to mechanisms supporting the effects of novelty, e.g. the potential roles acetylcholine and atropine-sensitive theta but predicted the result presented here and suggests a new mechanism by which environmental novelty might trigger the formation of new hippocampal representations.

In conclusion, these findings demonstrate a new potential mechanism for signalling of environmental novelty: a reduction in the theta frequency generated by hippocampal formation. The results have important implications for the interpretation of event-related potentials, and support the idea that the hippocampal formation plays a greater role in 'contextual novelty' or 'comparator' processing than absolute novelty *per se*. In addition, they provide indirect support for the hypothesis of a cholinergically-mediated mechanism for novelty detection, and the oscillatory interference model of grid cell firing.

6 Functional organisation of the HF: is the subiculum an input or an output stage?

6.1 Introduction

The precise details of how the different subregions of the hippocampal formation and their distinct properties contribute to the functions they perform have yet to be uncovered. Previous chapters have developed ideas from the perspective of the oscillatory properties of the hippocampal formation. One of the more obvious roles of an oscillation such as theta, whose frequency is constant throughout the HF, is to act as a global synchronising mechanism, a clock against which neural events across different regions can be related. Note that although theta varies in both phase and amplitude throughout the HF, simultaneous EEG recordings at comparable locations (e.g. CA1 pyramidal layer) are found to be in synchrony across large parts of the hippocampal formation (Mitchell & Ranck, Jr., 1980; Fox et al., 1986; Bullock et al., 1990). Insights into the interplay between different subregions of the HF have recently been provided by simultaneous single-unit recording experiments on rats performing behavioural and mnemonic tasks. Comparisons of CA3 and CA1 for example, show a differential response between these regions, in the emergence place fields in response to novelty (Leutgeb et al., 2004) and functional heterogeneity in response to the rotation of environmental cues (Lee, Rao, & Knierim, 2004). Some studies have tested potential contributions to the function of pattern separation/completion, proposed to occur in the dentate gyrus and CA3 (Leutgeb, Leutgeb, Moser, & Moser, 2007; McHugh, Jones, Quinn, Balthasar, Coppari, Elmquist, Lowell, Fanselow, Wilson, & Tonegawa, 2007). Others have looked at CA1 and entorhinal cortex (Frank, Brown, & Wilson, 2000; Fyhn et al., 2007), and CA1 and prefrontal cortex (Jones & Wilson, 2005).

The region regarded as CA1's major efferent, the subiculum, receives less attention despite fMRI studies in humans which indicate enhanced recruitment of subiculum in retrieval processes (Zeineh, Engel, Thompson, & Bookheimer, 2003; Small, Nava, Perera, Delapaz, & Stern, 2000; Gabrieli, Brewer, Desmond, & Glover, 1997). The traditional view of the subiculum is as 'the last step in the large loop of processing through the HF' (Amaral & Lavenex, 2007), i.e. as hippocampal output together with the deeper layers of the entorhinal cortex

(Witter & Moser, 2006), to which both subiculum and CA1 project. This stance reflects the massive, unidirectional, CA1 projection to the subiculum, which is considered its major excitatory input (Amaral & Lavenex, 2007), and relatively less detailed understanding of its functional neurophysiology. It is therefore considered as the 'final relay' further to the trisynaptic loop (Huang & Kandel, 2005).

However, subicular firing may not be simply relaying its CA1 input. Subicular and CA1 responses are often dissociated. In response to large environmental changes CA1 cells often remap, while subicular cells are far less affected (Sharp, 1997). This dissociation was also reflected by differential temporal responses between the two regions in a delayed non-match to sample task (Deadwyler & Hampson, 2004). Most interestingly perhaps is the idea that subicular firing could actually lead firing in CA1. Collating data from different studies, Sharp used timeshift analysis of spatial signals (Muller & Kubie, 1989) and reported that the subiculum was, surprisingly, *more* anticipatory than CA1 (Sharp, 1999). In these types of analyses spike train time series are shifted relative to the position time series in small steps (of the order of milliseconds), in order to minimise the size of place fields or maximise information rate.

The results presented in this chapter extend work done in the previous chapter on the same dataset. Using largely simultaneous recordings, we focus here on the temporal relationships between CA1 and subiculum, by characterising each region's spike firing relative to the theta oscillation, and by re-examining spatial anticipatory firing. The temporal relationships between these regions are further explored under the novelty conditions described in the previous chapter. As discussed earlier the HF is involved in novelty detection, particularly where current context or stimuli differs from expectation (Hasselmo et al., 1996; Lisman & Otmakhova, 2001; O'Keefe & Nadel, 1978; Gray & McNaughton, 2000), consistent with its role in context-dependent episodic memory (O'Keefe & Nadel, 1978; Eichenbaum, 2004). While most theoretical literature has implicated CA1 in comparator processing, this function has also been ascribed to the subiculum (Naber, Witter, & Lopes Silva, 2000; Gray & McNaughton, 2000).

6.2 Materials and Methods

6.2.1 Subjects

Seven male Lister Hooded rats, weighing 315-390g at time of surgery, were used as subjects. See Chapter 2 – General Methods and references therein for details of animal housing, surgical procedure, basic recording strategy, spike sorting, and histology. See section 4.2 for details on electrode implantation in different rats, pre-experimental behavioural training procedures and details of the experimental paradigm.

6.2.2 Data Analysis

Cross-Correlation

Spike times from all cells in simultaneously-recorded ensembles (minimum 3 cells) were concatenated to form a single spiketrain (1ms bins). Cross-correlations between the subiculum and CA1 spiketrain in each trial were calculated for lags between -200 and +200 ms at 1ms intervals. The spiketrains were normalised such that the auto-correlations at zero lag were equal to 1. Cross-correlograms were smoothed with a Gaussian kernel ($\sigma = 5\text{ms}$). To obtain an overview of the cross-correlation between CA1 and subiculum, cross-correlograms from 52 available trials were averaged to find the mean \pm s.e.m. at each point in a ‘population’ cross-correlogram (Figure 6.1).

Anticipatory spatial firing using timeshifts

Locational firing rate maps were constructed from 2.4×2.4 cm binned data smoothed using a 5×5 bin square around each bin. Spike count divided by dwell time gave firing rate per bin. In timeshift analysis (Muller & Kubie, 1989), the spike data series is shifted forwards and backwards relative to the position data series. The spatial information rate for each timeshift was calculated according to the formula derived in Skaggs, McNaughton, & Gothard (1993). Timeshift analysis was performed in the -700 to +700ms range, in 10 ms steps. The resulting information rate series was smoothed by a 70ms boxcar kernel. Optimal timeshift was defined as that timeshift which maximised the cell’s information rate. A positive (negative) optimal timeshift implies the cell best indicates the rat’s future (past) position (relative to the position of the headstage LEDs). We excluded cell/trial data points where a cell fired with a peak rate (after smoothing) of less than 1.0 Hz or had an information rate < 0.1 bits per

second. The regional ensemble value was simply the mean optimal timeshift of the cells in that ensemble (minimum $n = 2$). Anticipatory firing analysis based on spatial translation requires good sampling and broadly similar behaviour across compared environments. Behaviour was different in the walled environments 'a' and 'b' vs. unwall environment 'c', with exploration in the unwall environment characterised largely by head-dipping, each bout varying more in duration than rearing in environments 'a' and 'b'. Further, since novel changes had already taken place, characterising the degree of novelty/surprise of environment 'c' in our sequence was somewhat unclear. Given these interpretative issues, apart from preliminary analyses indicating that the CA1-to-subiculum anticipatory lag was seen in environment 'c', we explored anticipatory firing in this environment no further.

Theta phase

The recorded EEG signal was filtered using a 6-12Hz, 251-tap, Blackman windowed, band-pass *sinc* (sine cardinal) filter. Windowing the filter achieves good stop-band attenuation and small pass-band ripple. An analytic signal was then constructed using the Hilbert transform and takes the form $s_a(t_k) = s(t_k) + i\mathcal{H}[s(t_k)]$, where \mathcal{H} specifies the Hilbert transform, $s(t_k)$ is the filtered EEG signal, $t_k = k\Delta$, where $k = 1, \dots, K$ indexes the time-step and Δ is the inverse of the sampling rate. The phase of the analytic signal $\phi(t_k)$ gives the phase of the EEG at t_k . Each spike was assigned a phase $\phi(t_k)$ if it fell in the interval $[t_k - \Delta/2, t_k + \Delta/2]$. The analytic signal was filtered to remove periods of low quality EEG by discarding those regions with low signal power. Average power was calculated for each cycle in the analytic signal, where the start of each cycle was defined at those points where the analytic phase difference with the previous point fell below $-\pi$. Cycles with power below the 15th percentile in each trial and the spikes falling within them were discarded.

Theta phase at any particular septo-temporal or proximo-distal location varies across the radial axis (i.e. depending on where in the cell layer the electrode is positioned). Since EEG electrode position was changed on some days to maximise cell isolation, absolute theta phase of spikes is not comparable across days or rats. However, it is still possible to compare relative phase between simultaneously recorded subiculum and CA1 spikes on the same day. Note that

phase of spikes from both regions is measured against theta recorded from one EEG electrode (which may be in CA1 or subiculum). In addition, within a region, it is possible to compare differences between trials in the same environment or between novel and familiar environments (on the same day) by comparing the phase of spikes against a reference phase.

Thus, in comparisons between regions, the mean phase of all CA1 spikes measured in the last trial of the day in a given environment is defined as the reference. This reference phase is subsequently subtracted from the phase of all spikes – CA1 and subicular – used in these analyses. All spike phases now have a common zero. Where comparisons are being made between both region and environment, a common reference is chosen as the mean phase of CA1 spikes in the last trial of the day in environment ‘a’ (note that in this case no distinction is made between environments ‘b’ and ‘c’, which are considered collectively as “novel”). In analyses within region, the same procedure is applied separately for subiculum and CA1. In other words, in the same trials as before, one reference phase is calculated for CA1 as the mean phase of all CA1 spikes and one reference phase is calculated for subiculum as the mean phase of all subicular spikes. The CA1 reference is subsequently subtracted from all CA1 spikes entering the analyses and the subiculum reference is subsequently subtracted from all subicular spikes entering these analyses. Each of the trials in these analyses contributes a minimum of two cells from each region. The day’s last trial in environment ‘a’ is trial 4 on days 1 and 2, and trial 3 on day 1*). The last trial in the novel environments is trial 6 on day 1*.

Behaviour

Rearing frequency was counted during each trial, using in most cases two cell counters (for rearing up against vs. without walls, data combined). Running speed was calculated from 50 Hz position tracking data, with 400ms boxcar smoothing.

6.3 Results

Over the first three habituation days (days 1-3) and the first manipulation day (day 1*) (see Figure 4.1 for an explanation of the experimental procedure), the available dataset comprised 242 CA1 and 139 subicular neurons, see Table 6.1 below. No attempt was made to exclude a minority of cells, which may have been resampled. The results focus almost entirely on days 1-3 and 1* despite data being collected on days 4, 5, 2* and 3*. Data on these days was generally sparse, with few if any cells in most rats, in particular rats in which data was simultaneously recorded, often had no cells in one or other region. For example on day 4, only 5 subicular cells were recorded (4 from one rat) and only 4 of seven rats had any cells. On day 3*, only two rats showed any cells and no subicular cells were recorded. In addition one of the simultaneous rats had no EEG recorded from it throughout the experiment and was excluded from the analysis on theta phase.

Table 6.1 Number of putative pyramidal cells recorded from each region at key stages of the test trial series. Number in parentheses shows number of cells recorded simultaneously with cells from the other region.

Day	CA1	Subiculum	Total
Day 1	69 (33)	42 (28)	111 (61)
Day 2	54 (31)	39 (23)	93 (54)
Day 3	48 (25)	26 (18)	74 (43)
Change Day 1 (Day 1*)	71 (50)	32 (24)	103 (74)
Total	242 (139)	139 (93)	381 (232)

Cross-correlation analysis: subiculum spikes tended to precede CA1 spikes

To get an idea of the overall temporal relationship between CA1 and subicular firing between-region cross-correlograms (-200 ms to +200 ms range, bin width = 1 ms) were constructed for 52 available trials from 4 rats over the four test days. Given a subicular spike at 0 ms, the cross-correlation indicates the relative likelihood of seeing a CA1 spike in the preceding or succeeding 200 ms. The trials were selected such that each contributed at least 3 cells from each region to their respective "regional" spike trains. Figure 6.1 shows the averaged cross-correlogram. There are two features of note. Firstly, principal cell types in both regions demonstrate often very prominent theta-modulation, apparent in the spike train auto-correlogram (Sharp & Green, 1994). Figure 6.1 shows that this relationship is still apparent between regions, hinting at the ability of the theta

rhythm to organise cell populations across the medial temporal lobe. Secondly the cross-correlogram displays evident, right-shifted asymmetry about the centre, indicating a greater propensity for subicular spiking to anticipate CA1 spiking. The range of greatest interest in terms of time-lag is between -50 ms and +50 ms. This is the about the upper limit of the time-scale one might expect for information to flow around the hippocampal circuit, i.e. from CA1 to subiculum/entorhinal cortex and back to CA1 either directly or via intermediate structures. The two troughs at -40 ms and +91 ms), indicated by red circles on Figure 6.1, define the period of the central “wave” in the cross-correlogram. The position of the centre of mass of this wave occurs at +25.3 ms signifying its average right-shift (red dashed line Figure 6.1).

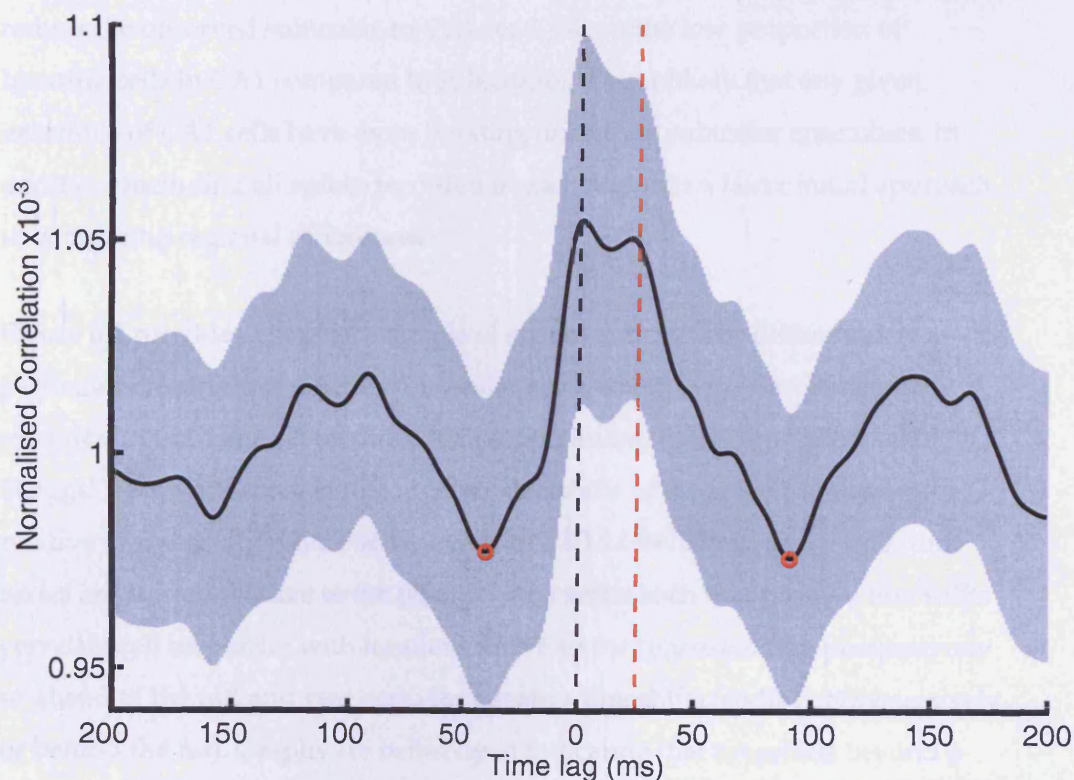


Figure 6.1 Cross-correlogram between subicular and CA1 spike trains, averaged over 52 trials, each contributing at least 3 cells to respective spike trains from each region (black line). 0 ms time lag represents the firing of subicular spikes. Grey region shows the s.e.m. at each point. Open red circles mark locations of the first minima either side of 0 ms. Red dashed line indicates location centre of mass of central peak.

Recent evidence (Jarsky, Mady, Kennedy, & Spruston, 2008) shows that there is a varying distribution of bursting cells along the proximo-distal axis of the hippocampal formation. Bursting units fire with high-frequency bursts of action

potentials and all subicular neurons tend to show a range of bursting behaviour proposed to be mediated by a slowly inactivating, D-type potassium current (Staff, Jung, Thiagarajan, Yao, & Spruston, 2000). Proportions of bursting units are found to vary in a graded manner from around 10% in proximal CA1 to 50% in distal subiculum. Potential confounds from differentially sampled bursting and non-bursting cells should, if anything reduce the effect seen in Figure 6.1. For example, a regular spiking subicular cell, whose action potentials are on average followed by a CA1 spike 10ms later, would show a peak in the cross-correlogram at +10ms. If instead the subicular cell was a bursting cell and the CA1 cell now fired 10ms after the onset of the each burst, each subsequent spike in a burst as well as the first spike would contribute to the cross-correlogram, broadening the peak in the negative direction. In other words, this would reduce the observed subicular-to-CA1 lead. Given the low proportion of bursting cells in CA1 compared to subiculum, it is unlikely that any given ensemble of CA1 cells have more bursting units than subicular ensembles. In addition, including all spikes recorded in each region is a fairer initial approach to comparing regional differences.

Figure 6.2 provides a typical example of spatial anticipatory differences in a particular ensemble of CA1 and subicular cells, which were simultaneously recorded in the same rat on day 2 of the experiment. Each graph shows the Skaggs' Information calculated at 10 ms timeshifts of the spike train series relative to the position time series between $-700 \leq t \leq +700$ ms. Spike train time series are shifted relative to the position time series such that positive timeshifts correlate cell responses with locations t ms into the future (coding prospectively or ahead of the rat) and vice versa for negative timeshifts (coding retrospectively or behind the rat). Graphs are bell-shaped indicating that timeshifts beyond a certain amount in either direction provide relatively little information about the relationship between the spike train and the animal's spatial location and are unlikely to be coding for this either prospectively or retrospectively. Under assumptions of efficient coding, timeshifts that maximise spatial information are most likely to indicate the extent of prospective or retrospective coding of space. These points are indicated by the black vertical lines and maximum information in subicular cells (gray curves) clearly occurs at larger anticipatory timeshifts than analogous points in CA1 cells (black curves), in almost every case. The

ensemble difference for this trial is 76 ms (i.e. the spikes anticipate the animal's location by 201 ms in subiculum and by 125 ms in CA1).

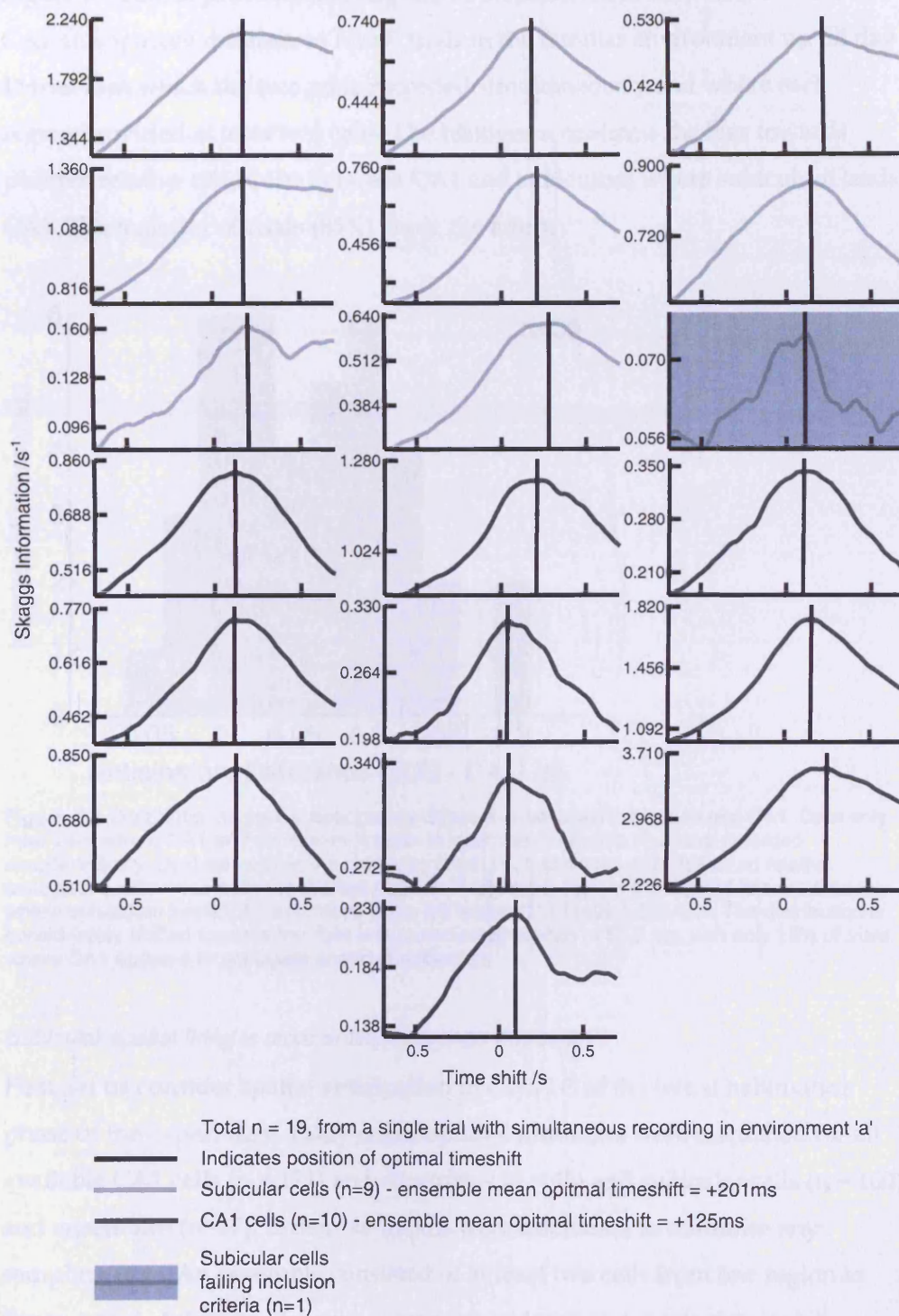


Figure 6.2 An example of spatial anticipatory differences in a simultaneously recorded CA1 and subicular ensemble of cells from day 2. Graphs show bell-shaped curves of Skaggs Information (Skaggs, McNaughton, & Gothard, 1993) as a function of relative timeshift between position and spike timeseries. Black vertical lines indicate the optimum timeshift (i.e. that which maximises Skaggs' Information). Gray lines show subicular cells (n=9), of which one fails criteria (shaded).

Black lines show CA1 cells ($n=10$). Peaks in the information curve of subicular cells are evidently right -shifted (i.e. more anticipatory) compared to CA1 cells in virtually every case.

Figure 6.3 below, provides a histogram of the differences between subicular and CA1 anticipatory differences for all trials in the familiar environment up till day 1* trial 2, in which the two were recorded simultaneously and where each region provided at least two cells. The histogram confirms the bias towards positive relative timeshifts between CA1 and subiculum where subiculum leads CA1. The majority of trials (85%) show the effect.

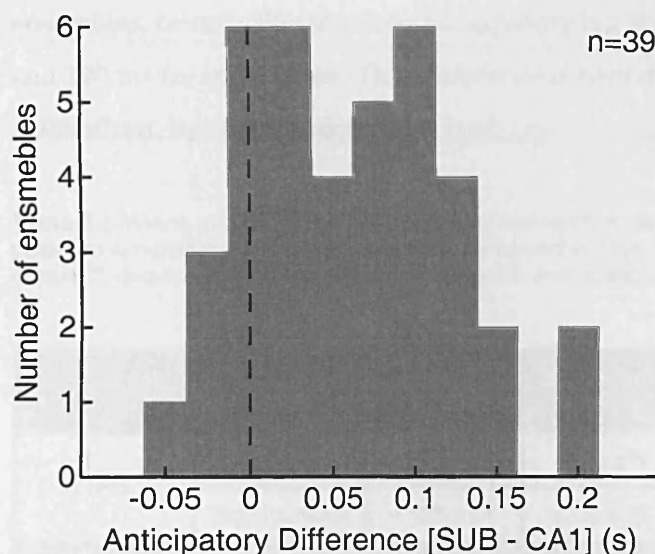


Figure 6.3 Distribution of spatial anticipatory differences between subiculum and CA1. Data only from trials where CA1 and subiculum provide at least two cells each and were recorded simultaneously. Dashed vertical line highlights 0 ms, i.e. those trials with little or no relative anticipatory difference between the two regions. Trials to the right of the dashed line are those where subiculum leads CA1 and those to the left where CA1 leads subiculum. The distribution is considerably shifted towards the right with a median difference of 62.5 ms, with only 15% of trials where CA1 appears to anticipate ahead of subiculum.

Subicular spatial firing is more anticipatory than that in CA1

First, let us consider spatial anticipation in days 1-3 of the initial habituation phase of the experiment. Daily mean optimal timeshifts were calculated for all available CA1 cells ($n = 171$) and ensembles ($n = 45$) and subicular cells ($n = 100$) and ensembles ($n=47$). Ensemble means were calculated to minimise any sampling bias. An ensemble consisted of at least two cells from one region to fire in a trial. Additionally, each rat was considered as a single data point. Where possible, results were calculated using all available data and additionally, only the subset of data where subicular and CA1 recordings were performed simultaneously. Table 6.2 summarises this data over the first three

days of the experiment. Mean optimal timeshifts in ensembles of subicular neurons ($+185 \pm 8$ ms) were clearly more anticipatory than those in CA1 ($+133 \pm 7$ ms), $t_{97} = 4.30$, $p = 7.2 \times 10^{-6}$ (all tests use two-sample, two-tailed t-tests unless specified otherwise), see Figure 6.4a. Restricting the data to only simultaneously recorded ensembles gives a similar result (SUB: $+188 \pm 10$, CA1: $+136 \pm 9$, $t_{73} = 3.51$, $p = 2.8 \times 10^{-4}$). A consistent and significant difference of the order of around +50 ms to +70 ms was measured between subicular and CA1 anticipatory firing. This occurred in groups of cells recorded simultaneously from the two regions and was not affected by analyzing the data following subdivision into cells, ensembles, or rats. The absolute anticipatory lag was around 130 ms for CA1 and 190 ms for subiculum. This difference is henceforth referred to as the ‘subiculum -to - CA1 anticipatory lead’.

Table 6.2 Means and s.e.m. for relative spatial anticipation between CA1 and Subiculum for all data and simultaneous recorded data only, measured in days 1-3 and divided by cells, ensembles or rats. Subiculum shows robust increased spatial anticipation with respect to CA1.

Day 1-3, Environment 'a'	Rats	CA1 /ms	Subiculum /ms	Relative Timeshift /ms	t test
Cells	All	$+127 \pm 9$	$+196 \pm 8$	+69	$t_{269} = 5.04$, $p = 2.6 \times 10^{-7}$
	Simultaneous	$+128 \pm 11$	$+200 \pm 10$	+72	$t_{153} = 4.27$, $p = 1.2 \times 10^{-5}$
Ensembles	All	$+133 \pm 7$	$+185 \pm 8$	+52	$t_{97} = 4.30$, $p = 7.2 \times 10^{-6}$
	Simultaneous	$+134 \pm 9$	$+204 \pm 12$	+52	$t_{60} = 3.99$, $p = 2.3 \times 10^{-5}$
Rat	All	$+127 \pm 12$	$+206 \pm 22$	+79	$t_9 = 2.37$, $p = 0.026$
	Simultaneous	$+128 \pm 18$	$+189 \pm 25$	+61	paired $t_3 = 4.23$, $p = 0.024$

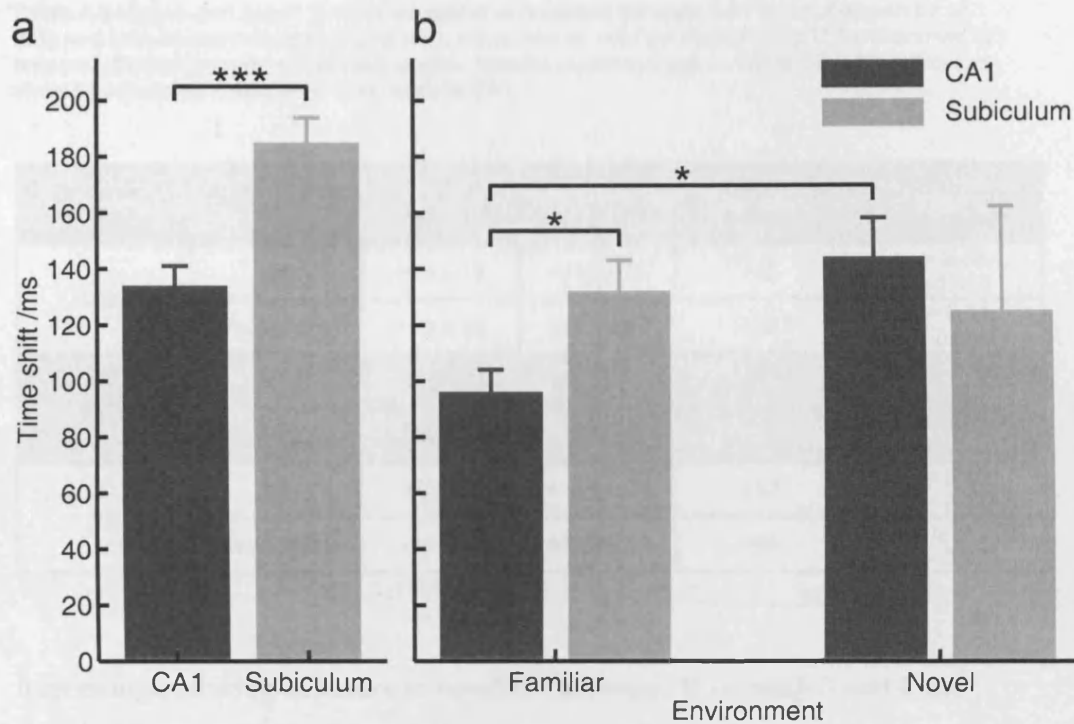


Figure 6.4 Differences in ensemble mean spatial anticipation. a) Subicular recordings (light grey) show increased mean spatial anticipation compared with CA1 (dark grey), over the first three days of recording in environment 'a'. b) Data from day 1*, In the familiar condition difference in (a) is replicated albeit with lower absolute levels. No significant differences between subiculum and CA1 when exposed to novelty. The loss of subiculum-to-CA1 anticipatory lead is due to increased spatial anticipation of CA1 in the novel environment versus the familiar. *: $p < 0.05$; ***: $p < 0.0005$.

Anticipatory coding in the novelty/surprise condition

The next question was whether the subiculum-to-CA1 anticipatory lead was altered by exposure to environment 'b', which first occurred on day 1*, trials 3 and 4. It was assumed that after twenty-two trials in environment 'a' using highly standardised procedures, environment 'b' would have elements of novelty and expectation-violation. We first confirmed that the anticipatory lead of subiculum over CA1 remained in the first two trials in the familiar environment 'a' on day 1*, albeit with lower levels of absolute anticipation and slightly smaller in magnitude (SUB: $+132 \pm 11$ ms, CA1: $+95 \pm 8$ ms, $t_{18} = 2.36$, $p = 0.014$). The same result was found using only simultaneously recorded data (SUB: $+137 \pm 13$ ms, CA1: $+97 \pm 10$ ms, $t_{14} = 2.09$, $p = 0.031$), see Figure 6.4b. Again this difference was robust and significant, however the data were divided, with one exception where it only just fails to reach significance, see Table 6.3 for details.

Table 6.3 Means and s.e.m. for relative spatial anticipation between CA1 and Subiculum for all data and simultaneous recorded data only, measured on only the first two day 1* (environment 'a') only and divided by cells, ensembles or rats. Results replicate those in **Table 6.2**, with subiculum showing increased anticipation compared to CA1.

Day 1*, Environment 'a'	Rats	CA1 /ms	Subiculum /ms	Relative Timeshift /ms	t test
Cells	All	+85 ± 13	+138 ± 12	+52	$t_{75} = 2.58$, $p = 0.009$
	Simultaneous	+83 ± 18	+141 ± 15	+58	$t_{52} = 2.11$, $p = 0.034$
Ensembles	All	+95 ± 8	+132 ± 11	+37	$t_{18} = 2.36$, $p = 0.014$
	Simultaneous	+97 ± 10	+137 ± 13	+40	$t_{14} = 2.09$, $p = 0.031$
Rat	All	+92 ± 7	+149 ± 19	+57	$t_9 = 2.25$, $p = 0.04$
	Simultaneous	+93 ± 11	+137 ± 15	+54	paired $t_3 = 2.78$, $p = 0.07$

Interestingly, during exposure to novel environment 'b' on trials 3 and 4, the anticipatory difference between the two regions narrowed, such that optimal timeshifts were now reversed and were somewhat more anticipatory in CA1 than in subiculum. The mean ensemble optimal timeshifts were now +125 ± 37 ms in subiculum and +144 ± 14 ms in CA1, while in simultaneously recorded data they were +141 ± 44 ms in subiculum and +156 ± 12 ms in CA1. The differences between subiculum and CA1 were no longer significant in environment 'b', (see Figure 6.4 b and Table 6.3 for details). The loss of the standard subiculum-to- CA1 anticipatory lead reflected an *increased* anticipatory coding of CA1 ensembles in the novel environment compared with the familiar. In other words, while subicular anticipatory coding remains unchanged between environments, CA1 anticipatory coding increased from that in the familiar environment to match the subiculum in the novel environment (Figure 6.4). This difference in CA1 ensemble means in environment 'b' (144 ± 14 ms) versus environment 'a' (95 ± 8 ms) was significant, (difference: 49 ms, $t_{18} = 2.53$, $p = 0.007$). No such difference was apparent between subicular ensembles in the two environments (SUB in environment 'b': 125 ± 37 ms, SUB in environment 'a': 132 ± 11 ms, difference: -7 ms, $t_9 = -0.18$, $p = 0.86$). The result is similar for data divided by individual rats.

Table 6.4 Means and s.e.m. for relative spatial anticipation between CA1 and Subiculum for all data and simultaneous recorded data only, measured on only the 3rd and 4th trial of day 1* (environment 'b') only and divided by cells, ensembles or rats. CA1 spatial anticipation has now increased to match that in subiculum.

Day 1*, Environment 'b'	Rats	CA1 /ms	Subiculum /ms	Relative Timeshift /ms	t test
Cells	All	+139 ± 35	+117 ± 30	-22	$t_{70} = 0.46$, $p = 0.65$
	Simultaneous	+143 ± 44	+141 ± 35	-2	$t_{50} = 0.03$, $p = 0.98$
Ensembles	All	+144 ± 14	+125 ± 37	-19	$t_{18} = 0.49$, $p = 0.64$
	Simultaneous	+156 ± 12	+141 ± 44	-15	$t_{14} = 0.33$, $p = 0.75$
Rat	All	+141 ± 6	+140 ± 35	-1	$t_9 = 0.03$, $p = 0.98$
	Simultaneous	+144 ± 9	+154 ± 49	+10	paired $t_3 = 0.2$, $p = 0.85$

Accordingly, changes in CA1 anticipatory coding were explored further. The increased anticipatory spatial coding in CA1 in environment 'b' appeared to be relatively transient. On day 2* optimal timeshifts in CA1 did not increase (indeed decreased) in the two environment 'b' trials (45 CA1 cells, 3 rats, (6 ensembles in each), $+102 \pm 14$ ms in environment 'a' vs. $+79 \pm 19$ ms in environment 'b', paired $t_{10} = 0.32$, $p = 0.36$). Thus, increased CA1 spatial anticipation on the rats' first day in environment 'b' was related to novelty, and not due to any specific physical features or peculiarities of environment 'b' relative to environment 'a'.

Could other variables explain these effects? Sharp found that hippocampal place cell optimal timeshifts were negatively correlated with trial running speed ($r = -0.24$, $p = 0.01$), while no correlation was found for subicular timeshifts (Sharp, 1999). Accordingly, in the first phase of the experiment (days 1-3, in environment 'a' only), regression analyses were used to determine whether or not behavioural or experimental variables could be responsible for observed relative difference in CA1 and subicular *ensemble* timeshifts. Two behavioural variables; speed and rearing frequency and two experimental variables; trial order and day were used as predictor variables (see Table 6.5). In this dataset, these variables did not account significantly for any of the variance in spatial anticipatory lag between regions, arguing strongly for an innate regional difference in spatial anticipation.

In order to assess the potential effects of these variables on the results from the second phase of the experiment, CA1 ensembles from the three environment 'a' and two environment 'b' trials on day 1* (n = 25, 5 rats) were entered in two separate stepwise multiple regressions. In the first, the effects of predictor variables rearing frequency and environment ('a', 'b') were considered and in the second, trial order (1, 2, 3, 4, 5) and environment ('a', 'b'). Rearing frequency and trial order made no significant unique contribution to optimal timeshift variance beyond that of environment (Beta p values = 0.90 (rearing frequency) and 0.13 (trial order)). The resultant regression model for the effect of environment on CA1 timeshifts was: $R = 0.52$, adjusted $R^2 = 0.24$, $p = 0.008$. As previously, running speed was not correlated with CA1 timeshifts ($r = -0.23$, $p = 0.27$).

Table 6.5 Regressing ensemble optimal timeshift with the either behavioural or experimental variables did not explain difference in optimal timeshifts between CA1 and subiculum.

Region	Running speed			Rearing frequency		Trial order		Day	
	N	R	p	r	p	R	p	r	p
CA1	45	0.02	0.90	-0.19	0.21	0.20	0.19	-0.14	0.36
Subiculum	47	0.18	0.24	-0.12	0.44	0.02	0.92	0.01	0.95

Theta-phase of firing

The phase of firing of subicular and CA1 cells relative to the EEG theta waves provides another indication of their temporal relationship. A Rayleigh's-Z and Watson's-U² test was performed for all spikes in each regional ensemble for a given trial; in every ensemble, the phase distribution was significantly non-uniform. For convenience, the ensemble's trial mean phase is called the 'preferred phase'. We did not obtain data on day 3 from one of the rats with simultaneous subicular and CA1 recordings; accordingly, the analysis in environment 'a' is restricted to days 1 and 2 only.

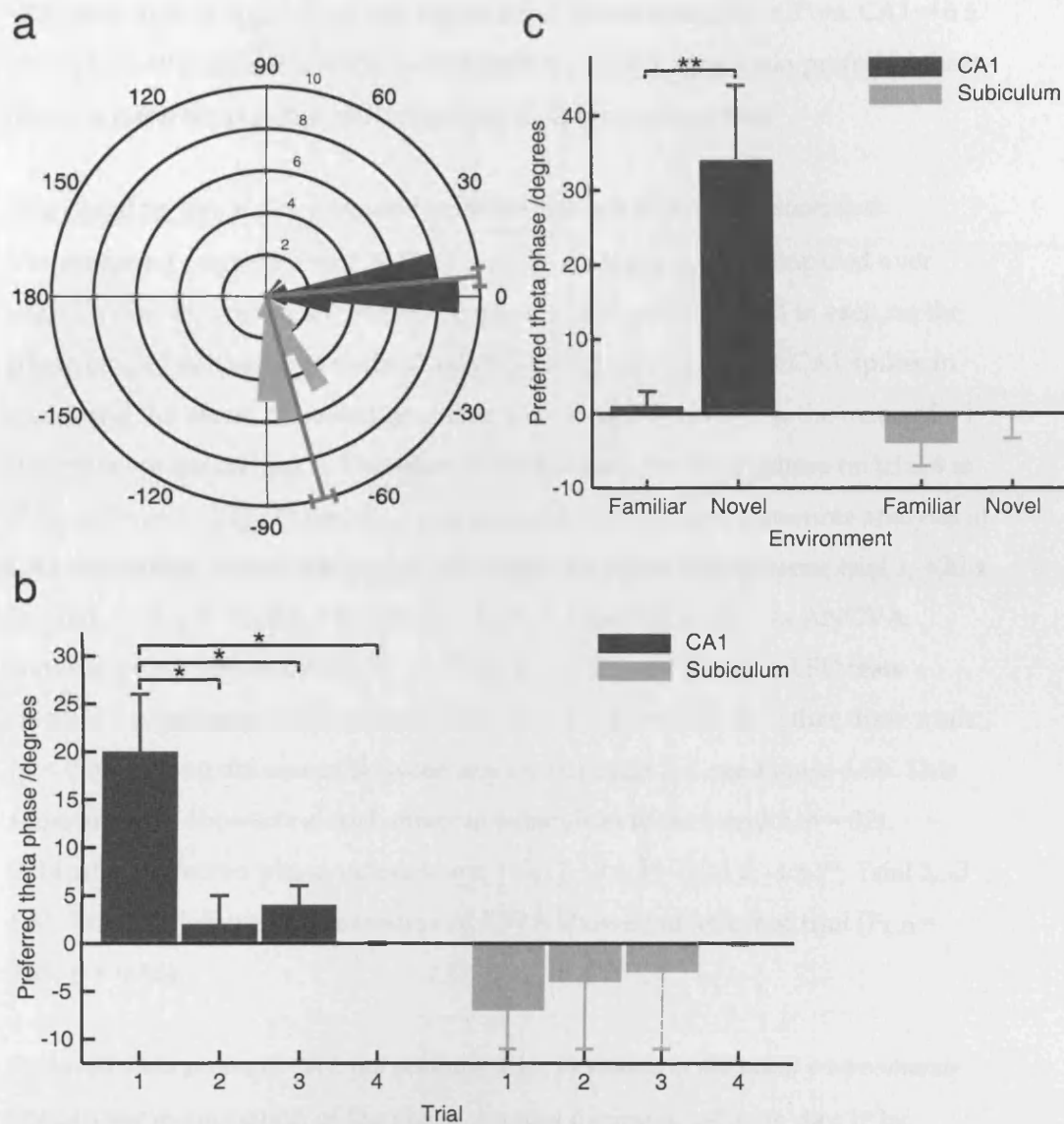


Figure 6.5 Results from theta phase analysis. a) Rose plot showing the difference in preferred mean phase with respect to the ongoing theta rhythm of CA1 and subicular ensembles. Subicular ensembles tend to prefer firing almost a quarter of a theta cycle ahead of CA1 ensembles. b) Effect of trial order in CA1 but not subiculum. CA1 ensembles consistently fire later only in the first trial of every day, compared to other trials, an effect not seen in subiculum. c) In simultaneously recorded data novelty results in CA1 ensembles' preferred phase increasing significantly by 30°. *: $p < 0.05$; **: $p < 0.005$.

CA1 spikes occur later in the theta cycle than subicular spikes

We compared theta phase of spiking in CA1 and subiculum in three rats with simultaneously recorded data from CA1 and subiculum on days 1 and 2 (8 trials per rat). On each of these days, in each rat, the mean phase of CA1 spikes in trial 4, was defined as the reference phase relative to which the phase of all spikes in all trials were defined. Preferred phase was significantly increased in CA1 relative to subiculum for each of 24 trials. On average spiking in CA1 occurred

+80° later than in subiculum, see Figure 6.5 a, (Subiculum: $-76 \pm 3^\circ$ vs. CA1: $+6 \pm 3^\circ$, Watson-Williams $F_{1,46} = 322$, $p < 0.000001$). This difference in preferred theta phase is referred to as the 'subiculum-to- CA1 theta-phase lead'.

First trial of the day shows increased preferred phase in CA1 but not subiculum

The preferred phase of firing in CA1 and the subiculum was compared over trials on two separate days in environment 'a'. On each day and in each rat the phase of CA1 spikes were defined relative to the mean phase of CA1 spikes in trial 4 and the phase of subicular spikes were defined relative to the mean of subicular spikes on trial 4. Therefore in each region the mean phase on trial 4 is 0° by definition. There were four rats available for repeated measures analysis of CA1 ensembles (days 1 and 2, $n = 32$). Preferred phase values were: trial 1, $+20 \pm 6^\circ$; trial 2, $+2 \pm 3^\circ$; trial 3, $+4 \pm 2^\circ$; trial 4, 0°. A repeated measures ANOVA showed a clear effect of trial ($F_{3,21} = 7.93$, $p = 0.001$) and Fisher's LSD tests showed a significant difference between trial 1 and each of the other three trials ($p < 0.03$) but no difference between any two of trials 2-4, see Figure 6.5b. This same analysis showed no such effect in subiculum (days 1 and 2, $n = 32$). Subicular preferred phase values were: Trial 1, $-7 \pm 3^\circ$; Trial 2, $-4 \pm 7^\circ$; Trial 3, $-3 \pm 8^\circ$; Trial 4, 0°. Repeated measures ANOVA showed no effect of trial ($F_{3,21} = 0.25$, $p = 0.86$).

Preferred theta phase in CA1, but not subiculum, increased in the novel environments

I began my examination of the phase changes during novelty on day 1* by checking that the change in phase across the familiar trials of this day replicated the findings on days 1 and 2. The subiculum -to-CA1 theta-phase lead was present in the three environment 'a' trials on day 1*, albeit slightly less so (49°) – Subiculum: $-44 \pm 14^\circ$, CA1: $+5 \pm 4^\circ$; Watson-Williams $F_{1,16} = 14.80$, $p = 0.001$. In this case all spikes from both regions and all trials were defined relative to the mean phase of CA1 spikes recorded in trial 5 on day 1*. Phase data recorded on day 1*, also showed average CA1 firing phase to occur later in the first trial in environment 'a' than in subsequent trials in that environment, as it had on days 1-2 (same reference phase as in previous analysis) – 4 rats: environment 'a', trial 1 = $+21 \pm 4^\circ$; trial 2 = $+3 \pm 8^\circ$; trial 3 = 0° ; effect of trial, $F_{2,6} = 6.60$, $p = 0.03$; Fisher's LSD tests: trial 1 vs. 3, $p = 0.01$; trial 1 vs. 2, $p = 0.06$). Again, no such effect was seen in subiculum ($F_{2,6} = 1.77$, $p = 0.25$).

As CA1 was found to exhibit an increased preferred phase in the first trial on day 1*, this trial was not used as a comparison trial in the following familiar versus novel environment comparison. Rather, environment 'b' and 'c' trials were paired with the most temporally-adjacent environment 'a' trials (3 paired trials for each of 4 rats: trial 2 ('a') vs. trial 3 ('b'), trial 5 ('a') vs. trial 4 ('b'), trial 5 ('a') vs. trial 6 ('c'); phase referenced to each rat's regional trial 5 value. The paired t tests showed that mean preferred phase of CA1 spikes occurred 33° later in environment 'b' and 'c' trials, see Figure 6.5c (environment 'a': $+1 \pm 2^\circ$ vs. environments 'b' and 'c': $+34 \pm 10^\circ$, $t_{11} = 3.63$, $p = 0.004$), while there was no such effect in subiculum (4 rats, environment 'a': $-3 \pm 3^\circ$ vs. environments 'b' and 'c': $-1 \pm 3^\circ$, paired $t_{11} = 0.70$, $p = 0.50$). That is to say that the subiculum in fact led CA1 more in novel environments than it did in familiar environments, in contrast to the effect found in spatial anticipation.

Note that even if environment 'a' trial 1 is used as a comparison trial (3 paired trials for each of 4 rats: trial 1 ('a') vs. trial 3 ('b'), trial 2 ('a') vs. trial 4 ('b'), trial 5 ('a') vs. trial 6 ('c')), this novel environment-induced preferred phase-increase effect is still observed. Trials are now matched according to trial order, such that the first trial in the familiar environment is matched with the first trial in the novel environment etc. In this case the mean preferred phase of CA1 spikes increased by 27° in environment 'b' and 'c' trials (paired $t_{11} = 2.60$, $p = 0.02$); there was no such effect in subiculum (paired $t_{11} = 0.86$, $p = 0.41$).

Theta phase and global firing rate

Theta phase may control excitability thresholds; for instance, the discharge probability of CA1 pyramidal cells is maximal around or just after the trough of the theta wave recorded locally from the pyramidal layer (Kamondi et al., 1998; Csicsvari, Hirase, Czurko, Mamiya, & Buzsaki, 1999). In the present dataset firing rate was generally lower in novelty conditions. Accordingly, we tested for relationships between preferred theta phase and global firing rate, the latter intended as a measure of the level of general excitation in CA1. Global firing rate was calculated by dividing all spikes in a trial by the total number of cells active on that day, and dividing this by trial length.

First, let us examine the dataset on day 1* demonstrating the phase-increase effect associated with novel environments. There is no correlation between preferred phase (referenced to trial 5 preferred phase) and normalized global firing rate ($n = 24$, $r = -0.06$, $p = 0.72$). The sample size is sufficient to see an effect of note.

Secondly, could global firing rate affect the phase-increase effect associated with the day's first trial? Over days 1-2, as expected, a negative correlation was seen between preferred phase and trial order (trial 1 vs. trial 2, 3 and 4, $n = 32$, $r = -0.649$, $p = 0.00006$). There was no significant correlation between preferred phase and global firing rate ($r = -0.18$, $p = 0.33$). Further, stepwise linear regression showed that global firing rate made no significant unique contribution to preferred theta-phase variance beyond that of trial order. Over day 1*, as expected, a negative correlation was seen between preferred phase and trial order (trial 1 vs. trial 2 and 5, $n = 12$, $r = -0.717$, $p = 0.009$), but there was no correlation between preferred phase and global firing rate ($r = -0.47$, $p = 0.12$). In conclusion, we saw no evidence that theta phase determined rate, or vice versa.

6.4 Discussion

The principal results from this study are that first, the co-spiking relationship of CA1 and subiculum shows that on average subicular spiking correlates best with CA1 spiking that follows about 25 ms later. Second, subicular anticipatory firing is found typically to lead the CA1, by about 30-70ms. Consistent with both of these results, the mean theta phase of subicular spiking also leads the CA1 by about 45-90° of a theta cycle, which equates to approximately 15-30 ms if the theta frequency is 8Hz. Both the lead in anticipatory firing and the preferred theta phase of spiking of subiculum versus CA1 are modifiable, being affected by environmental novelty. Interestingly, the site of change is in CA1 for both spatial anticipation and preferred theta phase of spiking; subicular processing is apparently little altered. Preferred theta phase of spiking seemed to be sensitive to two types of novelty. One of these, the first trial on any day, consistently elicited CA1 spikes later in the theta cycle, while the subiculum was unaffected. Similarly, first exposure to new environments resulted in CA1 spikes firing later on average in the theta cycle than they did in the familiar environment; again no change was seen in the subiculum. Spatial anticipation in CA1 was insensitive to the “novelty” of the first trial of the day. The first exposure to a novel or surprising environment, however, elicited a more advanced spatial anticipatory coding in CA1 – equivalent to subicular levels (which were unchanged from that in the familiar environment). Thus, there seems to be a conflict between results seen in the preferred phase of spiking and those in spatial anticipation, which is that they appear to change in opposite directions to each other under conditions of novelty, whereas one would expect them to be in the same direction (but see Figure 6.6 and text below).

The simplest interpretation of the spatial anticipatory and theta-phase timing results in the familiar environment is that subicular firing represents an earlier processing stage than CA1 firing. This is perhaps surprising given the well-established view that the subiculum acts as the ‘final staging post’ of hippocampal processing (Amaral & Lavenex, 2007). These two lines of evidence are supported by the cross-correlation analysis, which suggests that subicular firing succeeds CA1 by approximately 25 ms. The regional difference in preferred theta phase, may be interpreted as either subiculum leading CA1 by a sixth to a quarter of a cycle (approximately 20 – 30 ms @8Hz) or CA1 leading

subiculum by a three-quarters to five-sixths of a cycle (approximately 90 – 105 ms @8Hz). This seems unlikely; such a long hypothetical lag (90ms at 8Hz theta frequency) does not fit easily with candidate indirect routes through the entorhinal cortex and makes no more sense of the massive, monosynaptic CA1 to subiculum projection known to link the two regions. In addition, the central peak in the averaged cross-correlogram is higher than those at around -100 and +150 ms peaks. Taken together, results from the three complementary approaches run counter to traditional view of information flow in the hippocampal circuit (Amaral & Lavenex, 2007), suggesting instead that on average the subiculum is informed about the external/ideothetic spatial world before CA1. More speculatively, an average lead of 25 ms may mean that subiculum can inform CA1, via re-entrant processing, e.g. (Kloosterman, van Haeften, Witter, & Lopes da Silva, 2003; Naber et al., 2000). This possibility has important implications, suggesting for example how relatively context-invariant, environmental-boundary coding in the subiculum might act as indirect input to plastic, context-sensitive, 'remapping' place cells (Barry et al., 2006; Sharp, 1997). In unpublished spatial-field analysis of the present experiment, replicating Sharp's (Sharp, 1997) striking findings, many subicular cells show continuity of coding across environments that CA1 completely remaps, consistent with the notion of a more 'sensory' subiculum input (Sharp, 1997).

The novelty-induced changes in preferred theta phase demonstrated here support and inform theoretical models of memory concerned with efficient shifting between encoding and retrieval modes, particularly those suggesting different theta phases for novel and familiar information (Hasselmo et al., 1996; Hasselmo et al., 2002). The present study provides data about both the magnitude and direction of phase change; the novelty of a novel environment elicited a somewhat larger change than that of the day's first trial, and novelty consistently resulted in CA1's preferred firing phase to occur later in the theta cycle. The latter effect is consistent with the first experiment of Manns, Zilli, Ong, Hasselmo, & Eichenbaum (2007), where non-match items were associated with a CA1 mean phase increase of about 25°.

What drives this change in preferred theta phase? The results of chapter 5 demonstrate a decrease in the theta frequency in novelty, particularly in the novel environments 'b' and 'c' (Jeewajee, Lever, Burton, O'Keefe, & Burgess, 2008). However, since theta frequency is the same throughout the HF (Buzsaki, 2002), it is unclear if theta-frequency reduction could somehow affect preferred phase in CA1 but not subiculum. The increased phase in CA1 in environment 'b' might seem contradictory to CA1's more advanced anticipatory spatial firing in environment 'b' trials but preferred theta phase and cross-correlation reflect 'pure' temporal relationships; spatial anticipatory differences may not simply reflect same-signal processing delays. Spatial, environmental signals are complex and spatial anticipation may reflect a range of different types of input, for example path-integrative or environmental and sensory, with varying levels of influence in familiar and novel conditions. However, there are grounds to speculate a similar mechanism may underlie both changes if: in novelty, the input balance to CA1 shifts in favour of entorhinal cortex over CA3 (Hasselmo et al., 1995); CA1 cells are *more* anticipatory than CA3 cells (Muller & Kubie, 1989); and CA1 cells are *less* anticipatory than their spatial entorhinal cell inputs. This last assumption makes a clear prediction regarding the relative anticipatory lead of entorhinal cortical cells. Novelty-driven neuromodulation could also support plasticity at CA1 synapses, such that CA3 cells become, with increasing familiarity, increasingly dominant in driving CA1 cell firing, in line with the many more CA3-CA1 than entorhinal-CA1 synapses (Witter & Moser, 2006; Hasselmo et al., 1995). Entorhinal-dominant CA1 spiking would not only be more spatially anticipatory, but also show a theta mean phase difference from CA3-dominated CA1 spiking, since synaptic input from entorhinal cortex is strongest at hippocampal fissure theta troughs, while that from CA3 is strongest at theta peaks in the fissure, (see discussion (Manns, Zilli, Ong, Hasselmo, & Eichenbaum, 2007)). Figure 6.6 provides a schematic of this speculative model involving the entorhinal cortex and CA3 which may be able to explain these findings.

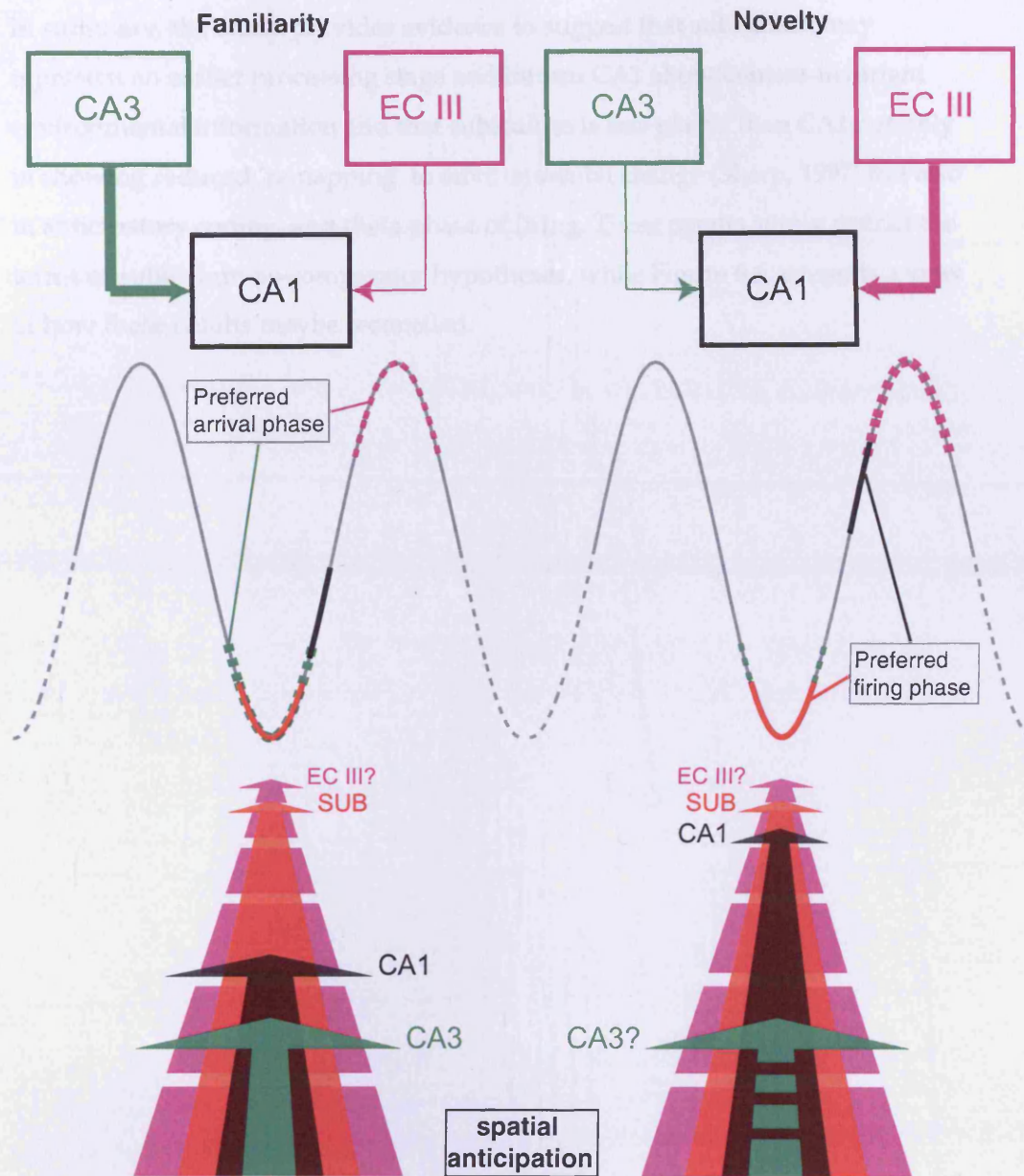


Figure 6.6 Speculative model of the organisation hippocampal activity during familiarity (left) and novelty (right). Theta phase of firing in CA1 (black) lags that in subiculum (red), and increases with environmental novelty, such that its preferred phase occurs later in the theta cycle. It is possible that similar mechanisms underlie both changes in preferred theta phase and changes in spatial anticipatory firing in CA1. This speculative model assumes that: a) in novelty, the input balance to CA1 shifts in favour of entorhinal over CA3 input (Hasselmo et al., 1996), while CA3 dominates in familiar conditions; b) In familiar conditions CA1 cells are more anticipatory than CA3 cells (Muller & Kubie, 1989); c) CA1 cells are less anticipatory than their spatial entorhinal cell inputs (a prediction); d) CA1 phase increase reflects more entorhinal input. Both more advanced spatial anticipation, and firing later in theta cycle, could reflect entorhinal-dominant, as opposed to CA3-dominant, CA1 spiking. It has been suggested that the peaks of synaptic input from entorhinal cortex and CA3 may be separated by about half a theta cycle ((Brankack et al., 1993), see discussion in (Manns et al., 2007)). Novelty-dependent neuromodulation could also support plasticity at CA1 synapses, such that CA3 cells become, with increasing familiarity, increasingly dominant in driving CA1 cell firing (see section 1.6.4).

In summary, the study provides evidence to suggest that subiculum may represent an earlier processing stage and inform CA1 about context-invariant environmental information and that subiculum is less plastic than CA1 not only in showing reduced 'remapping' to environmental change (Sharp, 1997) but also in anticipatory coding, and theta phase of firing. These results surely restrict the terms of subiculum-as-comparator hypotheses, while Figure 6.6, presents a view of how these results maybe reconciled.

7 General Discussion

The aim of this thesis was to explore the neural code of the hippocampal formation and in particular to explore the multitude of ways in which oscillations can affect and organise this code during spatial exploratory behaviour and under conditions of contextual novelty. What role do oscillations play in establishing and maintaining the firing fields of grid cells? Do they in fact act as a system for organising activity between regions or as a clock signal for timing spikes or both? And what role do they play in the important function of detecting novelty? In order to investigate these questions single unit recording data, from rats exploring novel and familiar environments while cells and EEG were recorded from different regions of the hippocampal formation were analysed in depth. In chapter 4, I reported results concerning models using oscillatory mechanisms for producing grid cell firing patterns. In chapter, 5 a study investigating the effects of environmental novelty and expectation violation on the hippocampal theta frequency were presented. Finally the sixth chapter extended the study of this dataset to compare the differences in the timing of spikes between the CA1 field of the hippocampus and the subiculum.

7.1 Grid cell firing in the oscillatory interference model

The oscillatory interference model provides a mechanism by which principal cells of the entorhinal cortex produce their outstanding, hexagonally symmetric firing pattern. At the same time, this mechanism, based on interfering sub-threshold membrane potentials offers a means of explaining the remarkable property of theta phase precession. Although, the details of this model are not complete, there is continuing experimental support for a fundamental role for sub-threshold and local field potential oscillations in neural function ((O'Keefe & Recce, 1993; Giocomo et al., 2007; Kamondi et al., 1998); something cognitive). In order to gain a deeper understanding of how oscillatory mechanisms might support the firing of grid cells, I analysed intrinsic and concomitantly recorded local field theta oscillations in a set of grid cells. The results of chapter 4 inform, support and constrain this type of model. The predictions of the model are borne out in the data. Theta frequency, intrinsic frequency and the difference between them all increase with speed as predicted. The latter relationship in particular is required to maintain the stability of the grid field under conditions of varying speed. The difference between theta and intrinsic frequencies should increase with the inverse of the grid scale and this prediction is also confirmed. Finally, an alternative oscillatory model of grid cells is ruled out by the results. The moiré interference model predicts a directionally modulated intrinsic frequency with a large difference between the frequency recorded in *aligned* and *misaligned* runs. The data show no evidence that such a difference exists in runs divided in this way.

What are the implications of these findings? Firstly, they assert the validity of the oscillatory interference model. At the very least they indicate that oscillatory activity in both the intrinsic sub-threshold membrane potential of individual cells and the population activity as measured by the extracellularly recorded EEG, play a major part in influencing the firing characteristics of grid cells. At the same time they set limits on the framework of models using oscillatory interference as a basis for their operation. Further work is required to establish the details of interactions between oscillations in membrane potentials in different compartments with each other and with the theta rhythm. Uncovering these details should lead to further clarification of the model framework and the

precise manner in which oscillations are involved in the producing the features of hippocampal formation cells.

7.2 Novelty and the theta rhythm

What are the physiological correlates of novelty in the brain? The results in chapter 5 show that the theta oscillation is clearly involved and changes in the theta oscillations correlate better with novelty and unexpected change than with other behavioural controls. EEG studies implicate evoked potentials, originating at the temporal lobes in detecting novelty in humans (Knight, 1996; Grunwald et al., 1998; Grunwald & Kurthen, 2006). In rats, recording large-scale neural activity *in vivo*, is far easier and hippocampal theta rhythm is both prominent and known to be critical for performing spatial and mnemonic functions. Thus, I analysed changes in theta rhythm while rats performed activity known to elicit movement-related θ . Surprisingly, conditions of novelty lower the frequency of the theta rhythm. Moreover, this reduction was greater when the rat experienced an environment that it was not expecting and is robust to behavioural controls for speed and stands in contrast to changes reported due to stress.

These findings have wide ranging implications for research across species, on novelty detection, neuromodulation and modelling of the hippocampal system. How might a drop in the theta frequency affect the properties of the system? This finding has a number of implications for models of hippocampal function. Novelty is associated with higher levels of acetylcholine release (Giovannini et al., 2001) and is also responsible for the slower α -theta. It is unclear how a lowering of the frequency would affect models which rely on separate phases of theta for storage and recall or how it might aid in the storage of novel information. It may be that lower α frequency impacts the network through differential effects on different classes of interneurons, which are known to be θ -modulated but at different phase lags (Somogyi & Klausberger, 2005).

Novelty has also been shown to result in an increase in spatial scale of grid cells. A reduction in theta frequency in variants of the oscillatory interference model could support this observation (see section 1.6.2 and Burgess *et al.* (2007)). Blair *et al.* (2007) argue that grid cells form a basis set much like the Fourier basis set and can be combined appropriately to create place cell firing and more generally scale-invariant representations of other cognitive modalities. If this is

indeed the case then, such a mechanism might underlie global remapping of place cells via a transient increase in spatial scale which alter spatial input to place cells and cause subsequent reorganisation of synaptic weights.

7.3 Organisation of hippocampal activity

Oscillations have long been thought to organise brain activity and one of the analyses presented in Chapter 6 probes precisely this function. In simultaneous recordings of subiculum and CA1 as rats first became familiarised to one environment and then exposed to another completely different one in its place, I looked at the timing of spikes from subicular and CA1 principal cells. The most intriguing result from this study concerns the idea first proposed by Sharp (1999) that subiculum may act as an input to the hippocampal formation. Subicular cells both anticipate position further ahead of the rat in space and on average fire earlier in the theta cycle. Both these results are consistent with the cross-correlation, which shows that CA1 spikes tend to fire somewhat later than subicular spikes. Subiculum is heavily connected with a number of subcortical structures, the amygdaloid complex and perirhinal cortex, though there is a paucity of information regarding cortical input. The subiculum may be informing and or modulating the EC and thence the hippocampus with respect to these inputs.

In novelty however, changes reflected in CA1 appear to be in conflict. While CA1 increases its anticipation of space to match that or even exceed that in the subiculum, it also happens to fire even later in the theta cycle compared to subiculum than in the familiar environment. This result is counterintuitive and difficult to interpret. In particular how do these effects interact with the reported reduction of the theta frequency in novelty? Could they perhaps be dependent on one another? Further experimental and computational investigations are required to resolve the many questions raised by these results.

7.4 Conclusions

In conclusion the findings presented here suggest that the oscillatory properties of the hippocampal formation are supporting the hippocampus in performing spatial and episodic functions. The detection of novelty, the formation of grid cells and a system for organising hippocampal activity are some of the wide ranging tasks in which they are critically involved. Understanding the details of interactions between oscillatory mechanisms and various components of the hippocampal formation will be important for understanding principles involved in neural function.

Reference List

- Aggleton, J. P. & Brown, M. W.** (1999). Episodic memory, amnesia, and the hippocampal-anterior thalamic axis. *Behav.Brain.Res.*, **22**, 425-490.
- Agnihotri, N. T., Hawkins, R. D., Kandel, E. R., & Kentros, C.** (2004). The long-term stability of new hippocampal place fields requires new protein synthesis. *Proc.Natl.Acad.Sci.U.S.A.* **101**[10], 3656-3661.
- Alonso, A. & Llinas, R. R.** (1989). Subthreshold Na⁺-dependent theta-like rhythmicity in stellate cells of entorhinal cortex layer II. *Nature*, **342**, 175-177.
- Amaral, D. G. & Lavenex, P.** (2007). Hippocampal neuroanatomy. In *The hippocampus book* (pp. 37-114). Oxford University Press.
- Amaral, D. G. & Witter, M. P.** (1995). The Hippocampus. In G.Paxinos (Ed.), (2nd ed., pp. 443-493). New York: Academic Press.
- Amaral, D. G. & Witter, M. P.** (1989). The three-dimensional organization of the hippocampal formation: A review of anatomical data. *Neuroscience* **31**[3], 571-591.
- Amit, D. H.** (1989). *Modelling Brain Function*. Cambridge University Press.
- Andersen, P., Bliss, T. V., & Skrede, K. K.** (1971). Lamellar organisation of hippocampal excitatory pathways. *Exp.Brain Res.* **13**, 222-238.
- Anderson, M. I., Hayman, R. A., Chakraborty, S., & Jeffery, K. J.** (2003). The representation of spatial context. In K.J.Jeffery (Ed.), (1st ed., pp. 274-294). Oxford: Oxford University Press.
- Axmacher, N., Mormann, F., Fernandez, G., Elger, C. E., & Fell, J.** (2006). Memory formation by neuronal synchronization. *Brain Res.Rev.*, **52**, 170-182.
- Barry, C.** (2008). *Terra Cognita: Representations of Space in the Entorhinal Cortex.*, Ph.D Thesis, University College London.
- Barry, C. & Burgess, N.** (2007). Learning in a geometric model of place cell firing. *Hippocampus*, **17**, 786-800.
- Barry, C., Hayman, R., Burgess, N., & Jeffery, K. J.** (2007). Experience-dependent rescaling of entorhinal grids. *Nat.Neurosci.*, **10**, 682-684.
- Barry, C., Lever, C., Hayman, R., Hartley, T., Burton, S., O'Keefe, J. et al.** (2006). The boundary vector cell model of place cell firing and spatial memory. *Rev.Neurosci.*, **17**, 71-97.
- Bassett, J. P. & Taube, J. S.** (2001). Neural correlates for angular head velocity in the rat dorsal tegmental nucleus. *J.Neurosci.*, **21**, 5740-5751.
- Bayer, S. A., Yackel, J. W., & Puri, P. S.** (1982). Neurons in the rat dentate gyrus granular layer substantially increase during juvenile and adult life. *Science*, **216**, 890-892.
- Best, P. J. & Thompson, L. T.** (1984). Hippocampal cells which have place field activity also show changes in activity during classical conditioning. *Soc.Neurosci.Abst.* **10**[125].

- Best, P. J. & Thompson, L. T.** (1989). Persistence, reticence, and opportunism of place-field activity in hippocampal neurons. *Psychobiology*, **17**, 230-235.
- Bingman, V. P., Siegel, J. J., Gagliardo, A., & Erichsen, J. T.** (2006). Representing the richness of avian spatial cognition: properties of a lateralized homing pigeon hippocampus. *Rev. Neurosci.* **17**[1-2], 17-28.
- Blackstad, T. W.** (1956). Commissural connections of the hippocampal region in the rat, with special reference to their mode of termination. *J. Comp. Neurol.*, **105**, 417-537.
- Blair, H. T., Cho, J., & Sharp, P. E.** (1998). Role of the lateral mammillary nucleus in the rat head direction circuit: a combined single unit recording and lesion study. *Neuron*, **21**, 1387-1397.
- Blair, H. T. & Sharp, P. E.** (1995). Anticipatory head direction signals in anterior thalamus: evidence for a thalamocortical circuit that integrates angular head motion to compute head direction. *J. Neurosci.*, **15**, 6260-6270.
- Blair, H. T., Welday, A. C., & Zhang, K.** (2007). Scale-invariant memory representations emerge from Moire interference between grid fields that produce theta oscillations: a computational model. *J. Neurosci.*, **27**, 3211-3229.
- Bland, B. H., Trepel, C., Oddie, S. D., & Kirk, I. J.** (1996). Intraseptal microinfusion of muscimol: effects on hippocampal formation theta field activity and phasic theta-ON cell discharges. *Exp. Neurol.*, **138**, 286-297.
- Borisjuk, R., Denham, M., Hoppensteadt, F., Kazanovich, Y., & Vinogradova, O.** (2001). Oscillatory model of novelty detection. *Network.*, **12**, 1-20.
- Bostock, E., Muller, R. U., & Kubie, J. L.** (1991). Experience-dependent modifications of hippocampal place cell firing. *Hippocampus*, **1**, 193-205.
- Bragin, A., Jando, G., Nadasdy, Z., Hetke, J., Wise, K., & Buzsaki, G.** (1995). Gamma (40-100 Hz) oscillation in the hippocampus of the behaving rat. *J. Neurosci.*, **15**, 47-60.
- Brankack, J., Stewart, M., & Fox, S. E.** (1993). Current source density analysis of the hippocampal theta rhythm: associated sustained potentials and candidate synaptic generators. *Brain Res.*, **615**, 310-327.
- Brun, V. H., Otnass, M. K., Molden, S., Steffenach, H. A., Witter, M. P., Moser, M. B. et al.** (2002). Place cells and place recognition maintained by direct entorhinal-hippocampal circuitry. *Science*, **296**, 2243-2246.
- Brunel, N. & Trullier, O.** (1998). Plasticity of directional place fields in a model of rodent CA3. *Hippocampus*, **8**, 651-665.
- Bullock, T. H., Buzsaki, G., & McClune, M. C.** (1990). Coherence of compound field potentials reveals discontinuities in the CA1-subiculum of the hippocampus in freely-moving rats. *Neuroscience*, **38**, 609-619.
- Burak, Y. & Fiete, I.** (2006). Do we understand the emergent dynamics of grid cell activity? *J. Neurosci.*, **26**, 9352-9354.
- Burgess N.** (2007). Computational Models of the Spatial and Mnemonic Functions of the Hippocampus. In P. Andersen, R. G. M. Morris, D. G. Amaral, T. V. Bliss, & J. O'Keefe (Eds.), (1st ed., pp. 715-749). Oxford: Oxford University Press.

- Burgess, N., Recce, M., & O'Keefe, J.** (1994). A model of hippocampal function. *Neural Netw.*, **7**, 1065-1081.
- Burgess, N., Barry, C., & O'Keefe, J.** (2007). An oscillatory interference model of grid cell firing. *Hippocampus*, **17**, 801-812.
- Burgess, N., Cacucci, F., Lever, C., & O'Keefe, J.** (2005). Characterizing multiple independent behavioral correlates of cell firing in freely moving animals. *Hippocampus*, **15**, 149-153.
- Burgess, N., Jackson, A., Hartley, T., & O'Keefe, J.** (2000). Predictions derived from modelling the hippocampal role in navigation. *Biol.Cybern.*, **83**, 301-312.
- Burgess, N. & O'Keefe, J.** (1996). Neuronal computations underlying the firing of place cells and their role in navigation. *Hippocampus*, **6**, 749-762.
- Burwell, R. D. & Amaral, D. G.** (1998b). Cortical afferents of the perirhinal, postrhinal, and entorhinal cortices of the rat. *J.Comp Neurol.*, **398**, 179-205.
- Burwell, R. D. & Amaral, D. G.** (1998a). Perirhinal and postrhinal cortices of the rat: interconnectivity and connections with the entorhinal cortex. *Journal of Comparative Neurology*, **391**, 293-321.
- Burwell, R. D., Witter, M. P., & Amaral, D. G.** (1995). Perirhinal and postrhinal cortices of the rat: a review of the neuroanatomical literature and comparison with findings from the monkey brain. *Hippocampus* **6**[3], 390-408.
- Buzsaki, G.** (2002). Theta oscillations in the hippocampus. *Neuron*, **33**, 325-340.
- Buzsaki, G.** (1989). Two-stage model of memory trace formation: a role for "noisy" brain states. *Neuroscience*, **31**, 551-570.
- Buzsaki, G., Grastyan, E., Tveritskaya, I. N., & Czopf, J.** (1979). Hippocampal evoked potentials and EEG changes during classical conditioning in the rat. *Electroencephalogr.Clin.Neurophysiol.*, **47**, 64-74.
- Buzsaki, G., Horvath, Z., Urioste, R., Hetke, J., & Wise, K.** (1992). High-frequency network oscillation in the hippocampus. *Science*, **256**, 1025-1027.
- Cacucci, F., Lever, C., Wills, T. J., Burgess, N., & O'Keefe, J.** (2004). Theta-modulated place-by-direction cells in the hippocampal formation in the rat. *J.Neurosci.*, **24**, 8265-8277.
- Canolty, R. T., Edwards, E., Dalal, S. S., Soltani, M., Nagarajan, S. S., Kirsch, H. E. et al.** (2006). High gamma power is phase-locked to theta oscillations in human neocortex. *Science*, **313**, 1626-1628.
- Carlton, P. L.** (1968). Brain acetylcholine and habituation. *Prog.Brain Res.*, **28**, 48-60.
- Chen, L. L., Lin, L. H., Barnes, C. A., & McNaughton, B. L.** (1994). Head-direction cells in the rat posterior cortex. II. Contributions of visual and ideothetic information to the directional firing. *Exp.Brain Res.*, **101**, 24-34.
- Chen, L. L., Lin, L. H., Green, E. J., Barnes, C. A., & McNaughton, B. L.** (1994). Head-direction cells in the rat posterior cortex. I. Anatomical distribution and behavioral modulation. *Exp.Brain Res.*, **101**, 8-23.

- Chicurel, M. E. & Harris, K. M.** (1992). Three-dimensional analysis of the structure and composition of CA3 branched dendritic spines and their synaptic relationship with mossy fiber boutons in the rat hippocampus. *J.Comp.Neurol.*, **325**, 169-182.
- Chrobak, J. J. & Buzsaki, G.** (1996). High-frequency oscillations in the output networks of the hippocampal- entorhinal axis of the freely behaving rat. *J.Neurosci.*, **16**, 3056-3066.
- Chrobak, J. J. & Buzsaki, G.** (1998). Gamma oscillations in the entorhinal cortex of the freely behaving rat. *J.Neurosci.*, **18**, 388-398.
- Cohen, N. J. & Eichenbaum, H.** (1993). *Memory, amnesia and the hippocampal system*. MIT Press, Cambridge Massachusettes.
- Cressant, A., Muller, R. U., & Poucet, B.** (1997). Failure of centrally placed objects to control the firing fields of hippocampal place cells. *J.Neurosci.*, **17**, 2531-2542.
- Csicsvari, J., Hirase, H., Czurko, A., Mamiya, A., & Buzsaki, G.** (1999). Oscillatory coupling of hippocampal pyramidal cells and interneurons in the behaving Rat. *J.Neurosci.*, **19**, 274-287.
- Csicsvari, J., Hirase, H., Mamiya, A., & Buzsaki, G.** (2000). Ensemble patterns of hippocampal CA3-CA1 neurons during sharp wave-associated population events. *Neuron*, **28**, 585-594.
- Dayan, P. & Abbott, L. F.** (2002). *Computational neuroscience*. Cambridge, MA: MIT Press.
- Deadwyler, S. A. & Hampson, R. E.** (2004). Differential but complementary mnemonic functions of the hippocampus and subiculum. *Neuron*, **42**, 465-476.
- Duzel, E., Neufang, M., & Heinze, H. J.** (2005). The oscillatory dynamics of recognition memory and its relationship to event-related responses. *Cereb.Cortex*, **15**, 1992-2002.
- Eichenbaum, H.** (2004). Hippocampus: cognitive processes and neural representations that underlie declarative memory. *Neuron*, **44**, 109-120.
- Ekstrom, A. D., Caplan, J. B., Ho, E., Shattuck, K., Fried, I., & Kahana, M. J.** (2005). Human hippocampal theta activity during virtual navigation. *Hippocampus*, **15**, 881-889.
- Ekstrom, A. D., Kahana, M. J., Caplan, J. B., Fields, T. A., Isham, E. A., Newman, E. L. et al.** (2003). Cellular networks underlying human spatial navigation. *Nature*, **425**, 184-188.
- Etienne, A. S. & Jeffery, K. J.** (2004). Path integration in mammals. *Hippocampus*, **14**, 180-192.
- Etienne, A. S., Maurer, R., & Seguinot, V.** (1996). Path integration in mammals and its interaction with visual landmarks. *J.Exp.Biol.*, **199**, 201-209.
- Fell, J., Dietl, T., Grunwald, T., Kurthen, M., Klaver, P., Trautner, P. et al.** (2004). Neural bases of cognitive ERPs: more than phase reset. *J Cogn Neurosci*, **16**, 1595-1604.
- Fenton, A. A., Csizmadia, G., & Muller, R. U.** (2000). Conjoint control of hippocampal place cell firing by two visual stimuli. I. The effects of moving the stimuli on firing field positions. *J.Gen.Physiol*, **116**, 191-209.
- Fenton, A. A. & Muller, R. U.** (1998). Place cell discharge is extremely variable during individual passes of the rat through the firing field. *Proc.Natl.Acad.Sci.U.S.A.*, **95**, 3182-3187.

- Fontani, G., Farabollini, F., & Carli, G. (1984). Hippocampal electrical activity and behavior in the presence of novel environmental stimuli in rabbits. *Behav. Brain Res.*, **13**, 231-240.
- Fox, S. E., Wolfson, S., & Ranck, J. B., Jr. (1986). Hippocampal theta rhythm and the firing of neurons in walking and urethane anesthetized rats. *Exp. Brain Res.*, **62**, 495-508.
- Frank, L. M., Brown, E. N., & Wilson, M. (2000). Trajectory encoding in the hippocampus and entorhinal cortex. *Neuron*, **27**, 169-178.
- Frank, L. M., Stanley, G. B., & Brown, E. N. (2004). Hippocampal plasticity across multiple days of exposure to novel environments. *J. Neurosci.*, **24**, 7681-7689.
- Fried, I., MacDonald, K. A., & Wilson, C. L. (1997). Single neuron activity in human hippocampus and amygdala during recognition of faces and objects. *Neuron*, **18**, 753-765.
- Fuhs, M. C. & Touretzky, D. S. (2006). A spin glass model of path integration in rat medial entorhinal cortex. *J. Neurosci.*, **26**, 4266-4276.
- Fyhn, M., Hafting, T., Treves, A., Moser, E. I., & Moser, M. B. (2006). Coherence in ensembles of entorhinal grid cells. *Soc. Neurosci. Abstr.*, **68.9/BB17**.
- Fyhn, M., Hafting, T., Treves, A., Moser, M. B., & Moser, E. I. (2007). Hippocampal remapping and grid realignment in entorhinal cortex. *Nature*, **446**, 190-194.
- Fyhn, M., Molden, S., Hollup, S., Moser, M. B., & Moser, E. (2002). Hippocampal neurons responding to first-time dislocation of a target object. *Neuron*, **35**, 555-566.
- Gabrieli, J. D., Brewer, J. B., Desmond, J. E., & Glover, G. H. (1997). Separate neural bases of two fundamental memory processes in the human medial temporal lobe. *Science*, **276**, 264-266.
- Germroth, P., Schwerdtfeger, W. K., & Buhl, E. H. (1989). Morphology of identified entorhinal neurons projecting to the hippocampus: A light microscopical study combining retrograde tracing and intracellular injection. *Neuroscience*, **30**, 683-691.
- Giocomo, L. M., Zilli, E. A., Fransen, E., & Hasselmo, M. E. (2007). Temporal frequency of subthreshold oscillations scales with entorhinal grid cell field spacing. *Science*, **315**, 1719-1722.
- Giovannini, M. G., Rakovska, A., Benton, R. S., Pazzagli, M., Bianchi, L., & Pepeu, G. (2001). Effects of novelty and habituation on acetylcholine, GABA, and glutamate release from the frontal cortex and hippocampus of freely moving rats. *Neuroscience*, **106**, 43-53.
- Givens, B. & Olton, D. S. (1995). Bidirectional modulation of scopolamine-induced working memory impairments by muscarinic activation of the medial septal area. *Neurobiol. Learn. Mem.*, **63**, 269-276.
- Gloor, P. (1997). The hippocampal system. In *The temporal lobe and limbic system* (pp. 325-589). Oxford: Oxford University Press.
- Gray, J. A. & McNaughton, N. (2000). *The neuropsychology of anxiety*. (2nd ed.) Oxford: O.U.P.
- Greene, J. R. & Mason, A. (1996). Neuronal diversity in the subiculum: correlations with the effects of somatostatin on intrinsic properties and on GABA-mediated IPSPs in vitro. *J. Neurophysiol.*, **76**, 1657-1666.

- Grunwald, T. & Kurthen, M. (2006). Novelty detection and encoding for declarative memory within the human hippocampus. *Clin.EEG.Neurosci.*, **37**, 309-314.
- Grunwald, T., Lehnertz, K., Heinze, H. J., Helmstaedter, C., & Elger, C. E. (1998). Verbal novelty detection within the human hippocampus proper. *Proc Natl Acad Sci U S A.*, **95**, 3193-3197.
- Guzowski, J. F., McNaughton, B. L., Barnes, C. A., & Worley, P. F. (1999). Environment-specific expression of the immediate-early gene Arc in hippocampal neuronal ensembles. *Nat.Neurosci.*, **2**, 1120-1124.
- Hafting, T., Fyhn, M., Molden, S., Moser, M. B., & Moser, E. I. (2005). Microstructure of a spatial map in the entorhinal cortex. *Nature*, **436**, 801-806.
- Hafting, T., Fyhn, M., Moser, M. B., & Moser, E. I. (2006). Phase precession and phase locking in entorhinal grid cells. *Soc.Neurosci.Abst.*, **68.8/BB16**.
- Halgren, E., Squires, N. K., Wilson, C. L., Rohrbaugh, J. W., Babb, T. L., & Crandall, P. H. (1980). Endogenous potentials generated in the human hippocampal formation and amygdala by infrequent events. *Science*, **210**, 803-805.
- Harris, K. D., Henze, D. A., Hirase, H., Leinekugel, X., Dragoi, G., Czurko, A. et al. (2002). Spike train dynamics predicts theta-related phase precession in hippocampal pyramidal cells. *Nature*, **417**, 738-741.
- Hartley, T., Burgess, N., Lever, C., Cacucci, F., & O'Keefe, J. (2000). Modeling place fields in terms of the cortical inputs to the hippocampus. *Hippocampus*, **10**, 369-379.
- Hasselmo, M. E. (2006). The role of acetylcholine in learning and memory. *Curr.Opin.Neurobiol.*, **16**, 710-715.
- Hasselmo, M. E., Bodelon, C., & Wyble, B. P. (2002). A proposed function for hippocampal theta rhythm: separate phases of encoding and retrieval enhance reversal of prior learning. *Neural Comput.*, **14**, 793-817.
- Hasselmo, M. E. & Eichenbaum, H. (2005). Hippocampal mechanisms for the context-dependent retrieval of episodes. *Neural Netw.*, **18**, 1172-1190.
- Hasselmo, M. E. & McClelland, J. L. (1999). Neural models of memory. *Curr Opin.Neurobiol.*, **9**, 184-188.
- Hasselmo, M. E., Schnell, E., & Barkai, E. (1995). Dynamics of learning and recall at excitatory recurrent synapses and cholinergic modulation in rat hippocampal region CA3. *J.Neurosci.*, **15**, 5249-5262.
- Hasselmo, M. E., Wyble, B. P., & Wallenstein, G. V. (1996). Encoding and retrieval of episodic memories: role of cholinergic and GABAergic modulation in the hippocampus. *Hippocampus*, **6**, 693-708.
- Hayman, R. M., Chakraborty, S., Anderson, M. I., & Jeffery, K. J. (2003). Context-specific acquisition of location discrimination by hippocampal place cells. *Eur.J.Neurosci.*, **18**, 2825-2834.
- Hetherington, P. A. & Shapiro, M. L. (1997). Hippocampal place fields are altered by the removal of single visual cues in a distance-dependent manner. *Behav.Neurosci.*, **111**, 20-34.

- Hirase, H., Czurko, H. H., Csicsvari, J., & Buzsaki, G.** (1999). Firing rate and theta-phase coding by hippocampal pyramidal neurons during 'space clamping'. *Eur.J.Neurosci.*, **11**, 4373-4380.
- Holscher, C., Anwyl, R., & Rowan, M. J.** (1997). Stimulation on the positive phase of hippocampal theta rhythm induces long-term potentiation that can be depotentiated by stimulation on the negative phase in area CA1 in vivo. *J.Neurosci.*, **17**, 6470-6477.
- Honey, R. C., Watt, A., & Good, M.** (1998). Hippocampal lesions disrupt an associative mismatch process. *J.Neurosci.*, **18**, 2226-2230.
- Hopfield, J. J.** (1982). Neural networks and physical systems with emergent collective computational abilities. *Proc.Natl.Acad.Sci.U.S.A.*, **79**, 2554-2558.
- Hori, E., Tabuchi, E., Matsumura, N., Tamura, R., Eifuku, S., Endo, S. et al.** (2003). Representation of place by monkey hippocampal neurons in real and virtual translocation. *Hippocampus*, **13**, 190-196.
- Huang, Y. Y. & Kandel, E. R.** (2005). Theta frequency stimulation induces a local form of late phase LTP in the CA1 region of the hippocampus. *Learn.Mem.*, **12**, 587-593.
- Huerta, P. T. & Lisman, J. E.** (1995). Bidirectional synaptic plasticity induced by a single burst during cholinergic theta oscillation in CA1 in vitro. *Neuron*, **15**, 1053-1063.
- Huxter, J., Burgess, N., & O'Keefe, J.** (2003). Independent rate and temporal coding in hippocampal pyramidal cells. *Nature*, **425**, 828-832.
- Insausti, R., Herrero, M. T., & Witter, M. P.** (1997). Entorhinal cortex of the rat: cytoarchitectonic subdivisions and the origin and distribution of cortical efferents. *Hippocampus*, **7**, 183.
- Ishizuka, N., Weber, J., & Amaral, D. G.** (1990). Organization of intrahippocampal projections originating from CA3 pyramidal cells in the rat. *J.Comp.Neurol.*, **295**, 580-623.
- Jacobs, J., Hwang, G., Curran, T., & Kahana, M. J.** (2006). EEG oscillations and recognition memory: theta correlates of memory retrieval and decision making. *Neuroimage.*, **32**, 978-987.
- Jarosiewicz, B., McNaughton, B. L., & Skaggs, W. E.** (2002). Hippocampal population activity during the small-amplitude irregular activity state in the rat. *J.Neurosci.*, **22**, 1373-1384.
- Jarsky, T., Mady, R., Kennedy, B., & Spruston, N.** (2008). Distribution of bursting neurons in the CA1 region and the subiculum of the rat hippocampus. *J.Comp.Neurol.*, **506**, 535-547.
- Jeewajee, A., Lever, C., Burton, S., O'Keefe, J., & Burgess, N.** (2008). Environmental novelty is signaled by reduction of the hippocampal theta frequency. *Hippocampus*, **18**, 340-348.
- Jeffery, K. J. & O'Keefe, J. M.** (1999). Learned interaction of visual and idiothetic cues in the control of place field orientation. *Exp.Brain Res.*, **127**, 151-161.
- Jensen, O. & Colgin, L. L.** (2007). Cross-frequency coupling between neuronal oscillations. *Trends Cogn.Sci.*

Jensen, O., Idiart, M. A., & Lisman, J. E. (1996). Physiologically realistic formation of autoassociative memory in networks with theta/gamma oscillations: role of fast NMDA channels. *Learn.Mem.*, **3**, 243-256.

Jensen, O. & Lisman, J. E. (2000). Position reconstruction from an ensemble of hippocampal place cells: contribution of theta phase coding. *J.Neurophysiol.*, **83**, 2602-2609.

Jensen, O. & Lisman, J. E. (1996a). Novel lists of 7 +/- 2 known items can be reliably stored in an oscillatory short-term memory network: interaction with long-term memory. *Learn.Mem.*, **3**, 257-263.

Jensen, O. & Lisman, J. E. (1996b). Theta/gamma networks with slow NMDA channels learn sequences and encode episodic memory: role of NMDA channels in recall. *Learn.Mem.*, **3**, 264-278.

Jones, M. W. & Wilson, M. A. (2005). Phase precession of medial prefrontal cortical activity relative to the hippocampal theta rhythm. *Hippocampus (Special issue on Theta, Eds: N Burgess & J O'Keefe)*, **15**, 867-873.

Jung, M. W. & McNaughton, B. L. (1993). Spatial selectivity of unit activity in the hippocampal granular layer. *Hippocampus*, **3**, 165-182.

Jung, M. W., Wiener, S. I., & McNaughton, B. L. (1994). Comparison of spatial firing characteristics of units in dorsal and ventral hippocampus of the rat. *J.Neurosci.*, **14**, 7347-7356.

Jung, R. & Kornmuller, A. (1938). Eine methodik der ableitung lokalisierter Potentialschwankungen aus subcorticalen Hirngebeiten. *Arch.Psychiatr.Nervenkr.*, **109**, 1-30.

Kali, S. & Dayan, P. (1999). Spatial representations in related environments in a recurrent model of area CA3 of the rat. *Proceedings of the Ninth International Conference on Artificial Neural Networks*. 138-139.

Kali, S. & Dayan, P. (2000). The involvement of recurrent connections in area CA3 in establishing the properties of place fields: a model. *J.Neurosci.*, **20**, 7463-7477.

Kamondi, A., Acsady, L., Wang, X. J., & Buzsaki, G. (1998). Theta oscillations in somata and dendrites of hippocampal pyramidal cells in vivo: activity-dependent phase-precession of action potentials. *Hippocampus*, **8**, 244-261.

Kee, N., Teixeira, C. M., Wang, A. H., & Frankland, P. W. (2007). Preferential incorporation of adult-generated granule cells into spatial memory networks in the dentate gyrus. *Nat.Neurosci.*, **10**, 355-362.

Kentros, C., Hargreaves, E., Hawkins, R. D., Kandel, E. R., Shapiro, M., & Muller, R. V. (1998). Abolition of long-term stability of new hippocampal place cell maps by NMDA receptor blockade. *Science*, **280**, 2121-2126.

Klink, R. & Alonso, A. (1997). Muscarinic modulation of the oscillatory and repetitive firing properties of entorhinal cortex layer II neurons. *J.Neurophysiol.*, **77**, 1813-1828.

Kloosterman, F., van Haeften, T., Witter, M. P., & Lopes da Silva, F. H. (2003). Electrophysiological characterization of interlaminar entorhinal connections: an essential link for re-entrance in the hippocampal-entorhinal system. *Eur.J.Neurosci.* **18**[11], 3037-3052.

- Knierim, J. J.** (2003). Hippocampal remapping: implications for spatial learning and navigation. In K.J. Jeffery (Ed.), (1st ed., pp. 226-239). Oxford: Oxford University Press.
- Knierim, J. J., Kudrimoti, H. S., & McNaughton, B. L.** (1998). Interactions between idiothetic cues and external landmarks in the control of place cells and head direction cells. *J. Neurophysiol.*, **80**, 425-446.
- Knierim, J. J. & Rao, G.** (2003). Distal landmarks and hippocampal place cells: effects of relative translation versus rotation. *Hippocampus*, **13**, 604-617.
- Knight, R.** (1996). Contribution of human hippocampal region to novelty detection. *Nature.*, **383**, 256-259.
- Kohler, C.** (1985). Intrinsic projections of the retrohippocampal region in the rat brain. I. The subicular complex. *Journal of Comparative Neurology*, **236**, 504-522.
- Kohler, C.** (1986). Intrinsic connections of the retrohippocampal region in the rat brain. II. The medial entorhinal area. *J. Comp. Neurol.* **246**, 149-169.
- Kohler, C.** (1988). Intrinsic connections of the retrohippocampal region in the rat brain. III. The lateral entorhinal area. *J. Comp. Neurol.*, **271**, 208-228.
- Kohler, S., Danckert, S., Gati, J. S., & Menon, R. S.** (2005). Novelty responses to relational and non-relational information in the hippocampus and the parahippocampal region: a comparison based on event-related fMRI. *Hippocampus.*, **15**, 763-774.
- Kramis, R., Vanderwolf, C. H., & Bland, B. H.** (1975). Two types of hippocampal rhythmical slow activity in both the rabbit and the rat: relations to behavior and effects of atropine, diethyl ether, urethane, and pentobarbital. *Exp. Neurol.*, **49**, 58-85.
- Kumar, S. S., Jin, X., Buckmaster, P. S., & Huguenard, J. R.** (2007). Recurrent circuits in layer II of medial entorhinal cortex in a model of temporal lobe epilepsy. *J. Neurosci.* **27**[6], 1239-1246.
- Kumaran, D. & Maguire, E. A.** (2006). An unexpected sequence of events: mismatch detection in the human hippocampus. *PLoS. Biol.*, **4**, e424.
- Laptev, D.** (2008). *Interaction of perception and motion in continuous attractor representations of position.*, Ph.D Thesis, University College London.
- Lawson, V. H. & Bland, B. H.** (1993). The role of the septohippocampal pathway in the regulation of hippocampal field activity and behavior: analysis by the intraseptal microinfusion of carbachol, atropine, and procaine. *Exp. Neurol.*, **120**, 132-144.
- Lee, I., Hunsaker, M. R., & Kesner, R. P.** (2005). The role of hippocampal subregions in detecting spatial novelty. *Behav. Neurosci.*, **119**, 145-153.
- Lee, I., Rao, G., & Knierim, J. J.** (2004). A double dissociation between hippocampal subfields: differential time course of CA3 and CA1 place cells for processing changed environments. *Neuron*, **42**, 803-815.
- Lenck-Santini, P. P., Rivard, B., Muller, R. U., & Poucet, B.** (2005). Study of CA1 place cell activity and exploratory behavior following spatial and nonspatial changes in the environment. *Hippocampus*, **15**, 356-369.
- Lengyel, M., Szatmary, Z., & Erdi, P.** (2003). Dynamically detuned oscillations account for the coupled rate and temporal code of place cell firing. *Hippocampus*, **13**, 700-714.

Leutgeb, J. K., Leutgeb, S., Moser, M. B., & Moser, E. I. (2007). Pattern separation in the dentate gyrus and CA3 of the hippocampus. *Science*, **315**, 961-966.

Leutgeb, J. K., Leutgeb, S., Treves, A., Meyer, R., Barnes, C. A., McNaughton, B. L. et al. (2005). Progressive transformation of hippocampal neuronal representations in "morphed" environments. *Neuron*, **48**, 345-358.

Leutgeb, S., Leutgeb, J. K., Treves, A., Moser, M. B., & Moser, E. I. (2004). Distinct ensemble codes in hippocampal areas CA3 and CA1. *Science*, **305**, 1295-1298.

Lever, C., Cacucci, F., Burgess, N., & O'Keefe, J. (1999). Squaring the circle: place cell firing patterns in environments which differ only geometrically are not unpredictable. *Soc.Neurosci.Abst.*, **24**, 556.2.

Lever, C., Wills, T., Cacucci, F., Burgess, N., & O'Keefe, J. (2002). Long-term plasticity in hippocampal place-cell representation of environmental geometry. *Nature*, **416**, 90-94.

Li, X. G., Somogyi, P., Ylinen, A., & Buzsaki, G. (1994). The hippocampal CA3 network: an in vivo intracellular labeling study. *J.Comp.Neurol.*, **339**, 181-208.

Lisman, J. E. & Idiart, M. A. (1995). Storage of 7 ± 2 short-term memories in oscillatory subcycles. *Science*, **267**, 1512-1515.

Lisman, J. E. & Otmakhova, N. A. (2001). Storage, recall, and novelty detection of sequences by the hippocampus: elaborating on the SOCRATIC model to account for normal and aberrant effects of dopamine. *Hippocampus*, **11**, 551-568.

Lorente de No, R. (1933). Studies on the structure of the cerebral cortex. *J.Psychol.Neurol.*, **45**, 381-438.

Ludvig, N., Tang, H. M., Gohil, B. C., & Botero, J. M. (2004). Detecting location-specific neuronal firing rate increases in the hippocampus of freely-moving monkeys. *Brain Res.*, **1014**, 97-109.

M'Harzi, M., Palacios, A., Monmaur, P., Willig, F., Houcine, O., & Delacour, J. (1987). Effects of selective lesions of fimbria-fornix on learning set in the rat. *Physiol.Behav.*, **40**, 181-188.

Makeig, S., Westerfield, M., Jung, T. P., Enghoff, S., Townsend, J., Courchesne, E. et al. (2002). Dynamic brain sources of visual evoked responses. *Science*, **295**, 690-694.

Mann, E. O. & Paulsen, O. (2007). Role of GABAergic inhibition in hippocampal network oscillations. *Trends Neurosci.*, **30**, 343-349.

Manns, J. R., Zilli, E. A., Ong, K. C., Hasselmo, M. E., & Eichenbaum, H. (2007). Hippocampal CA1 spiking during encoding and retrieval: relation to theta phase. *Neurobiol.Learn.Mem.*, **87**, 9-20.

Markus, E. J., Qin, Y. L., Leonard, B., Skaggs, W. E., McNaughton, B. L., & Barnes, C. A. (1995). Interactions between location and task affect the spatial and directional firing of hippocampal neurons. *J.Neurosci.*, **15**, 7079-7094.

Marr, D. (1971). Simple memory: a theory for archicortex. *Philos.Trans.R.Soc.Lond.B Biol.Sci.*, **262**, 23-81.

Maurer, A. P., Cowen, S. L., Burke, S. N., Barnes, C. A., & McNaughton, B. L. (2006). Organization of hippocampal cell assemblies based on theta phase precession. *Hippocampus* **16**, 785-794.

- Maurer, A. P., Van Rhoads, S. R., Sutherland, G. R., Lipa, P., & McNaughton, B. L.** (2005). Self-motion and the Origin of Differential Spatial Scaling Along the Septo-Temporal Axis of the Hippocampus. *Hippocampus*, **15**, 841-852.
- McCartney, H., Johnson, A. D., Weil, Z. M., & Givens, B.** (2004). Theta reset produces optimal conditions for long-term potentiation. *Hippocampus*, **14**, 684-687.
- McClelland, J. L., McNaughton, B. L., & O'Reilly, R. C.** (1995). Why there are complementary learning systems in the hippocampus and neocortex: insights from the successes and failures of connectionist models of learning and memory. *Psychol.Rev.*, **102**, 419-457.
- McHugh, T. J., Jones, M. W., Quinn, J. J., Balthasar, N., Coppari, R., Elmquist, J. K. et al.** (2007). Dentate gyrus NMDA receptors mediate rapid pattern separation in the hippocampal network. *Science*, **317**, 94-99.
- McNaughton, B. L. & Barnes, C. A.** (1977). Physiological identification and analysis of dentate granule cell responses to stimulation of the medial and lateral perforant pathways in the rat. *J.Comp.Neurol.*, **175**, 439-454.
- McNaughton, B. L., Barnes, C. A., & O'Keefe, J.** (1983). The contributions of position, direction, and velocity to single unit activity in the hippocampus of freely-moving rats. *Exp.Brain Res.*, **52**, 41-49.
- McNaughton, B. L., Battaglia, F. P., Jensen, O., Moser, E. I., & Moser, M. B.** (2006). Path integration and the neural basis of the 'cognitive map'. *Nat.Rev.Neurosci.*, **7**, 663-678.
- Meeter, M., Murre, J. M., & Talamini, L. M.** (2004). Mode shifting between storage and recall based on novelty detection in oscillating hippocampal circuits. *Hippocampus*, **14**, 722-741.
- Mehta, M. R., Lee, A. K., & Wilson, M. A.** (2002). Role of experience and oscillations in transforming a rate code into a temporal code. *Nature*, **417**, 741-746.
- Mitchell, S. J. & Ranck, J. B., Jr.** (1980). Generation of theta rhythm in medial entorhinal cortex of freely moving rats. *Brain Res.*, **189**, 49-66.
- Montgomery, S. M. & Buzsaki, G.** (2007). Gamma oscillations dynamically couple hippocampal CA3 and CA1 regions during memory task performance. *Proc.Natl.Acad.Sci.U.S.A.*, **104**, 14495-14500.
- Mormann, F., Fell, J., Axmacher, N., Weber, B., Lehnertz, K., Elger, C. E. et al.** (2005). Phase/amplitude reset and theta-gamma interaction in the human medial temporal lobe during a continuous word recognition memory task. *Hippocampus*, **15**, 890-900.
- Moser, E. I. & Paulsen, O.** (2001). New excitement in cognitive space: between place cells and spatial memory. *Curr.Opin.Neurobiol.*, **11**, 745-751.
- Muller, R. U.** (1996). A quarter of a century of place cells. *Neuron*, **17**, 813-822.
- Muller, R. U., Bostock, E., Taube, J. S., & Kubie, J. L.** (1994). On the directional firing properties of hippocampal place cells. *J.Neurosci.*, **14**, 7235-7251.
- Muller, R. U. & Kubie, J. L.** (1987). The effects of changes in the environment on the spatial firing of hippocampal complex-spike cells. *J.Neurosci.*, **7**, 1951-1968.
- Muller, R. U. & Kubie, J. L.** (1989). The firing of hippocampal place cells predicts the future position of freely moving rats. *J.Neurosci.*, **9**, 4101-4110.

- Muller, R. U., Kubie, J. L., & Ranck, J. B., Jr.** (1987). Spatial firing patterns of hippocampal complex-spike cells in a fixed environment. *J.Neurosci.*, **7**, 1935-1950.
- Murray, J. D.** (2003). *Mathematical Biology, II: Spatial Models and Biomedical Applications*. (3rd ed.) (vols. II) Berlin: Springer.
- Myers, C. E., Ermita, B. R., Harris, K., Hasselmo, M., Solomon, P., & Gluck, M. A.** (1996). A computational model of cholinergic disruption of septohippocampal activity in classical eyeblink conditioning. *Neurobiol.Learn.Mem.*, **66**, 51-66.
- Naber, P. A., Witter, M. P., & Lopes Silva, F. H.** (2000). Networks of the hippocampal memory system of the rat. The pivotal role of the subiculum. *Ann.N.Y.Acad.Sci.*, **911**, 392-403.
- Nakazawa, K., Quirk, M. C., Chitwood, R. A., Watanabe, M., Yeckel, M. F., Sun, L. D. et al.** (2002). Requirement for hippocampal CA3 NMDA receptors in associative memory recall. *Science*, **297**, 211-218.
- Nerad, L. & Bilkey, D. K.** (2005). Ten- to 12-Hz EEG oscillation in the rat hippocampus and rhinal cortex that is modulated by environmental familiarity. *J.Neurophysiol.*, **93**, 1246-1254.
- Nolan, M. F., Dudman, J. T., Dodson, P. D., & Santoro, B.** (2007). HCN1 channels control resting and active integrative properties of stellate cells from layer II of the entorhinal cortex. *J.Neurosci.*, **27**, 12440-12451.
- Numan, R.** (1978). Cortical-limbic mechanisms and response control: A theoretical review. *Physiol.Psychol.*, **6**, 445-470.
- O'Keefe, J.** (1991). The hippocampal cognitive map and navigational strategies. In J.Paillard (Ed.), (pp. 273-295). Oxford University Press.
- O'Keefe, J.** (1996). The spatial prepositions in English, vector grammar and the cognitive map theory. In P.Bloom, M. Peterson, L. Nadel, & M. Garrett (Eds.), (pp. 277-316). Cambridge, Mass.: MIT Press.
- O'Keefe, J.** (2007). Hippocampal Neurophysiology of the Behaving Animal. In P.Andersen, R. Morris, D. G. Amaral, T. V. Bliss, & J. O'Keefe (Eds.), (pp. 475-548). Oxford: Oxford University Press.
- O'Keefe, J.** (1976). Place units in the hippocampus of the freely moving rat. *Exp.Neurol.*, **51**, 78-109.
- O'Keefe, J.** (2006). Hippocampal neurophysiology in the behaving animal. In P.Andersen, R. G. M. Morris, D. G. Amaral, T. V. P. Bliss, & J. O'Keefe (Eds.), (pp. 475-548). Oxford: Oxford Neuroscience.
- O'Keefe, J. & Burgess, N.** (1996). Geometric determinants of the place fields of hippocampal neurons. *Nature*, **381**, 425-428.
- O'Keefe, J. & Burgess, N.** (2005). Dual phase and rate coding in hippocampal place cells: theoretical significance and relationship to entorhinal grid cells. *Hippocampus*, **15**, 853-866.
- O'Keefe, J. & Dostrovsky, J.** (1971). The hippocampus as a spatial map. Preliminary evidence from unit activity in the freely-moving rat. *Brain Res.*, **34**, 171-175.

- O'Keefe, J. & Nadel, L. (1978). *The hippocampus as a cognitive map*. (1st ed.) Oxford: Oxford University Press.
- O'Keefe, J. & Recce, M. L. (1993). Phase relationship between hippocampal place units and the EEG theta rhythm. *Hippocampus*, **3**, 317-330.
- O'Keefe, J. & Speakman, A. (1987). Single unit activity in the rat hippocampus during a spatial memory task. *Exp.Brain Res.*, **68**, 1-27.
- Ono, T., Nakamura, K., Fukuda, M., & Tamura, R. (1991). Place recognition responses of neurons in monkey hippocampus. *Neurosci.Lett.*, **121**, 194-198.
- Orr, G., Rao, G., Houston, F. P., McNaughton, B. L., & Barnes, C. A. (2001). Hippocampal synaptic plasticity is modulated by theta rhythm in the fascia dentata of adult and aged freely behaving rats. *Hippocampus*, **11**, 647-654.
- Osipova, D., Takashima, A., Oostenveld, R., Fernandez, G., Maris, E., & Jensen, O. (2006). Theta and gamma oscillations predict encoding and retrieval of declarative memory. *J.Neurosci.*, **26**, 7523-7531.
- Paulsen, O. & Moser, E. I. (1998). A model of hippocampal memory encoding and retrieval: GABAergic control of synaptic plasticity. *Trends Neurosci.*, **21**, 273-278.
- Paulsen, O. & Sejnowski, T. J. (2000). Natural patterns of activity and long-term synaptic plasticity. *Curr.Opin.Neurobiol.*, **10**, 172-179.
- Paulsen, O. & Sejnowski, T. J. (2006). From invertebrate olfaction to human cognition: emerging computational functions of synchronized oscillatory activity. *J.Neurosci.*, **26**, 1661-1662.
- Pavlides, C., Greenstein, Y. J., Grudman, M., & Winson, J. (1988). Long-term potentiation in the dentate gyrus is induced preferentially on the positive phase of theta-rhythm. *Brain Res.*, **439**, 383-387.
- Quirk, G. J., Muller, R. U., & Kubie, J. L. (1990). The firing of hippocampal place cells in the dark depends on the rat's recent experience. *J.Neurosci.*, **10**, 2008-2017.
- Quirk, G. J., Muller, R. U., Kubie, J. L., & Ranck, J. B., Jr. (1992). The positional firing properties of medial entorhinal neurons: description and comparison with hippocampal place cells. *J.Neurosci.*, **12**, 1945-1963.
- Ranck, J. B., Jr. (1984). Head-direction cells in the deep cell layers of the dorsal presubiculum in freely moving rats. *Soc.Neurosci.Abstr.* **10**, 599.
- Ranganath, C. & Rainer, G. (2003). Neural mechanisms for detecting and remembering novel events. *Nat.Rev.Neurosci.*, **4**, 193-202.
- Recce, M. & O'Keefe, J. (1989). The tetrode: a new technique for multiunit extracellular recording. *Soc.Neurosci.Abstr.* **15**, 1250.
- Redish, A. D. (1999). *Beyond the Cognitive Map: From Place Cells to Episodic Memory*. Cambridge MA: MIT Press.
- Rivard, B., Li, Y., Lenck-Santini, P. P., Poucet, B., & Muller, R. U. (2004). Representation of objects in space by two classes of hippocampal pyramidal cells. *J.Gen.Physiol.*, **124**, 9-25.

- Rivas, J., Gaztelu, J. M., & Garcia-Austt, E. (1996). Changes in hippocampal cell discharge patterns and theta rhythm spectral properties as a function of walking velocity in the guinea pig. *Exp.Brain Res.*, **108**, 113-118.
- Rizzuto, D. S., Madsen, J. R., Bromfield, E. B., Schulze-Bonhage, A., & Kahana, M. J. (2006). Human neocortical oscillations exhibit theta phase differences between encoding and retrieval. *Neuroimage.*, **31**, 1352-1358.
- Rizzuto, D. S., Madsen, J. R., Bromfield, E. B., Schulze-Bonhage, A., Seelig, D., Aschenbrenner-Scheibe, R. et al. (2003). Reset of human neocortical oscillations during a working memory task. *Proc.Natl.Acad.Sci.U.S.A.*, **100**, 7931-7936.
- Rolls, E. T., Miyashita, Y., Cahusac, P. M., Kesner, R. P., Niki, H., Feigenbaum, J. D. et al. (1989). Hippocampal neurons in the monkey with activity related to the place in which a stimulus is shown. *J.Neurosci.*, **9**, 1835-1845.
- Rolls, E. T. & Treves, A. (1997). *Neural Networks and Brain Function*. Oxford University Press.
- Rugg, M. D. & Coles, M. G. (1995). *Electrophysiology of Mind: Event-Related Potentials and Cognition*. Oxford: O.U.P.
- Rutishauser, U., Mamelak, A. N., & Schuman, E. M. (2006). Single-trial learning of novel stimuli by individual neurons of the human hippocampus-amygdala complex. *Neuron.*, **49**, 805-813.
- Sainsbury, R. S., Harris, J. L., & Rowland, G. L. (1987). Sensitization and hippocampal type 2 theta in the rat. *Physiol.Behav.*, **41**, 489-493.
- Sainsbury, R. S., Heynen, A., & Montoya, C. P. (1987). Behavioral correlates of hippocampal type 2 theta in the rat. *Physiol.Behav.*, **39**, 513-519.
- Samsonovich, A. & McNaughton, B. L. (1997). Path integration and cognitive mapping in a continuous attractor neural network model. *J.Neurosci.*, **17**, 5900-5920.
- Sargolini, F., Fyhn, M., Hafting, T., McNaughton, B. L., Witter, M. P., Moser, M. B. et al. (2006). Conjunctive representation of position, direction, and velocity in entorhinal cortex. *Science*, **312**, 758-762.
- Save, E., Buhot, M. C., Foreman, N., & Thinus-Blanc, C. (1992). Exploratory activity and response to a spatial change in rats with hippocampal or posterior parietal cortical lesions. *Behav.Brain Res.*, **47**, 113-127.
- Save, E., Cressant, A., Thinus-Blanc, C., & Poucet, B. (1998). Spatial firing of hippocampal place cells in blind rats. *J.Neurosci.*, **18**, 1818-1826.
- Save, E., Nerad, L., & Poucet, B. (2000). Contribution of multiple sensory information to place field stability in hippocampal place cells. *Hippocampus*, **10**, 64-76.
- Save, E., Poucet, B., Foreman, N., & Buhot, M. C. (1992). Object exploration and reactions to spatial and nonspatial changes in hooded rats following damage to parietal cortex or hippocampal formation. *Behav.Neurosci.*, **106**, 447-456.
- Scharfman, H. E., Witter, M. P., & Schwarcz, R. (2000). The parahippocampal region. Implications for neurological and psychiatric diseases. Introduction. *Ann.N.Y.Acad.Sci.*, **911**, ix-xiii.

Sederberg, P. B., Kahana, M. J., Howard, M. W., Donner, E. J., & Madsen, J. R. (2003). Theta and gamma oscillations during encoding predict subsequent recall. *J.Neurosci.*, **23**, 10809-10814.

Sejnowski, T. J. & Paulsen, O. (2006). Network oscillations: emerging computational principles. *J.Neurosci.*, **26**, 1673-1676.

Sharp, P. E. (1996). Multiple spatial/behavioral correlates for cells in the rat postsubiculum: multiple regression analysis and comparison to other hippocampal areas. *Cereb.Cortex*, **6**, 238-259.

Sharp, P. E. (1997). Subicular cells generate similar spatial firing patterns in two geometrically and visually distinctive environments: comparison with hippocampal place cells. *Behav.Brain Res.*, **85**, 71-92.

Sharp, P. E. (1999). Comparison of the timing of hippocampal and subicular spatial signals: implications for path integration. *Hippocampus*, **9**, 158-172.

Sharp, P. E. (1991). Computer simulation of hippocampal place cells. *Psychobiology*, **19**, 103-115.

Sharp, P. E., Blair, H. T., & Cho, J. (2001). The anatomical and computational basis of the rat head-direction cell signal. *Trends Neurosci.*, **24**, 289-294.

Sharp, P. E. & Green, C. (1994). Spatial correlates of firing patterns of single cells in the subiculum of the freely moving rat. *J.Neurosci.*, **14**, 2339-2356.

Sinnamon, H. M. (2000). Priming pattern determines the correlation between hippocampal theta activity and locomotor stepping elicited by stimulation in anesthetized rats. *Neuroscience*, **98**, 459-470.

Sinnamon, H. M., Jassen, A. K., & Ilch, C. (2000). Hippocampal theta activity and facilitated locomotor stepping produced by GABA injections in the midbrain raphe region. *Behav.Brain Res.*, **107**, 93-103.

Skaggs, W. E., Knierim, J. J., Kudrimoti, H. S., & McNaughton, B. L. (1995). A model of the neural basis of the rat's sense of direction. *Adv.Neural Inf.Process Syst.*, **7**, 173-180.

Skaggs, W. E. & McNaughton, B. L. (1998). Spatial firing properties of hippocampal CA1 populations in an environment containing two visually identical regions. *J.Neurosci.*, **18**, 8455-8466.

Skaggs, W. E., McNaughton, B. L., & Gothard, K. M. (1993). An information-theoretic approach to deciphering the hippocampal code. In S.J.Hanson, J. D. Cowan, & C. L. Giles (Eds.), (pp. 1030-1037). San Mateo, CA: Morgan Kaufmann.

Skaggs, W. E., McNaughton, B. L., Wilson, M. A., & Barnes, C. A. (1996). Theta phase precession in hippocampal neuronal populations and the compression of temporal sequences. *Hippocampus*, **6**, 149-172.

Slawinska, U. & Kasicki, S. (1998). The frequency of rat's hippocampal theta rhythm is related to the speed of locomotion. *Brain Res.*, **796**, 327-331.

Small, S. A., Nava, A. S., Perera, G. M., Delapaz, R., & Stern, Y. (2000). Evaluating the function of hippocampal subregions with high-resolution MRI in Alzheimer's disease and aging. *Microsc.Res.Tech.*, **51**, 101-108.

Sokolov, E. N. (1963). Higher nervous functions; the orienting reflex. *Annu.Rev.Physiol.*, **25**, 545-580.

Somogyi, P. & Klausberger, T. (2005). Defined types of cortical interneurone structure space and spike timing in the hippocampus. *J.Physiol.*, **562**, 9-26.

Squire, L. R. & Zola-Morgan, S. (1991). The medial temporal lobe memory system. *Science*, **253**, 1380-1386.

Staff, N. P., Jung, H. Y., Thiagarajan, T., Yao, M., & Spruston, N. (2000). Resting and active properties of pyramidal neurons in subiculum and CA1 of rat hippocampus. *J.Neurophysiol.*, **84**, 2398-2408.

Strange, B. A., Fletcher, P. C., Henson, R. N., Friston, K. J., & Dolan, R. J. (1999). Segregating the functions of human hippocampus. *Proc.Natl.Acad.Sci.U.S.A.*, **96**, 4034-4039.

Swanson, L. W. (1983). *The hippocampus and the concept of the limbic system*. Academic Press, New York.

Swanson, L. W., Kohler, C., & Bjorklund, A. (1987). The limbic region. I. The septohippocampal system. In *Handbook of chemical neuroanatomy. Vol 5. Integrated systems of the CNS. Part 1.* (pp. 125-227). Elsevier, Amsterdam.

Swanson, L. W., Sawchenko, P. E., & Cowan, W. M. (1980). Evidence that the commissural, associational and septal projections of the regio inferior of the hippocampus arise from the same neuron. *Brain Res.*, **197**, 207-212.

Taube, J. S. & Burton, H. L. (1995). Head direction cell activity monitored in a novel environment and during a cue conflict situation. *J.Neurophysiol.*, **74**, 1953-1971.

Taube, J. S. & Muller, R. U. (1998). Comparisons of head direction cell activity in the postsubiculum and anterior thalamus of freely moving rats. *Hippocampus*, **8**, 87-108.

Taube, J. S., Muller, R. U., & Ranck, J. B., Jr. (1990a). Head-direction cells recorded from the postsubiculum in freely moving rats. I. Description and quantitative analysis. *J.Neurosci.*, **10**, 420-435.

Taube, J. S., Muller, R. U., & Ranck, J. B., Jr. (1990b). Head-direction cells recorded from the postsubiculum in freely moving rats. II. Effects of environmental manipulations. *J.Neurosci.*, **10**, 436-447.

Thiel, C. M., Huston, J. P., & Schwarting, R. K. (1998). Hippocampal acetylcholine and habituation learning. *Neuroscience*, **85**, 1253-1262.

Thompson, L. T. & Best, P. J. (1989). Place cells and silent cells in the hippocampus of freely-behaving rats. *J.Neurosci.*, **9**, 2382-2390.

Tolman, E. C. (1948). Cognitive maps in rats and men. *Psychol.Rev.*, **55**, 189-208.

Tonegawa, S., Tsien, J. Z., McHugh, T. J., Huerta, P., Blum, K. I., & Wilson, M. A. (1996). Hippocampal CA1-region-restricted knockout of NMDAR1 gene disrupts synaptic plasticity, place fields, and spatial learning. *Cold Spring Harb.Symp.Quant.Biol.*, **61**, 225-238.

Touretzky, D. S. & Redish, A. D. (1996). Theory of rodent navigation based on interacting representations of space. *Hippocampus*, **6**, 247-270.

- Ulanovsky, N. & Moss, C. F.** (2007). Hippocampal cellular network activity in freely moving echolocating bats. *Nat.Neurosci.* **10**, 224-233.
- Vanderwolf, C. H.** (1969). Hippocampal electrical activity and voluntary movement in the rat. *Electroencephalogr.Clin.Neurophysiol.*, **26**, 407-418.
- Vanderwolf, C. H.** (2001). The hippocampus as an olfacto-motor mechanism: were the classical anatomists right after all? *Behav.Brain Res.*, **127**, 25-47.
- Vinogradova, O. S.** (2001). Hippocampus as comparator: role of the two input and two output systems of the hippocampus in selection and registration of information. *Hippocampus*, **11**, 578-598.
- Wallenstein, G. V. & Hasselmo, M. E.** (1997). GABAergic modulation of hippocampal population activity: sequence learning, place field development, and the phase precession effect. *J.Neurophysiol.*, **78**, 393-408.
- Wan, H. S., Touretzky, D. S., & Redish, A. D.** (1994). A rodent navigation model that combines place code, head direction, and path integration information. *Soc.Neurosci.Abstr.*, **20**.
- West, M. J., Slomianka, L., & Gundersen, H. J. G.** (1991). Unbiased stereological estimation of the total number of neurons in the subdivisions of the rat hippocampus using the optical fractionator. *Anat.Rec.*, **231**, 482-497.
- Whishaw, I. Q. & Tomie, J. A.** (1997). Perseveration on place reversals in spatial swimming pool tasks: further evidence for place learning in hippocampal rats. *Hippocampus*, **7**, 361-370.
- Whishaw, I. Q. & Vanderwolf, C. H.** (1971). Hippocampal EEG and behavior: effects of variation in body temperature and relation of EEG to vibrissae movement, swimming and shivering. *Physiol.Behav.*, **6**, 391-397.
- Whishaw, I. Q. & Vanderwolf, C. H.** (1973). Hippocampal EEG and behavior: changes in amplitude and frequency of RSA (theta rhythm) associated with spontaneous and learned movement patterns in rats and cats. *Behav.Biol.*, **8**, 461-484.
- Williams, J. M. & Givens, B.** (2003). Stimulation-induced reset of hippocampal theta in the freely performing rat. *Hippocampus*, **13**, 109-116.
- Wills T.J., Lever C., Cacucci F., Burgess N., & O'Keefe J.** (2004). Abrupt shift in hippocampal place cell representation from square-like to circle-like in a morph box. *Soc.Neurosci.Abstr.*
- Wills, T., Lever, C., Cacucci, F., Burgess, N., & O'Keefe, J.** (2005). Attractor Dynamics in the Hippocampal Representation of the Local Environment. *Science*, **308**, 873-876.
- Wilson, M. A. & McNaughton, B. L.** (1993). Dynamics of the hippocampal ensemble code for space. *Science*, **261**, 1055-1058.
- Winson, J.** (1978). Loss of hippocampal theta rhythm results in spatial memory deficit in the rat. *Science*, **201**, 160-163.
- Witter, M. P.** (2006). Connections of the subiculum of the rat: topography in relation to columnar and laminar organization. *Behav.Brain Res.*, **174**, 251-264.
- Witter, M. P. & Groenewegen, H. J.** (1990). The subiculum: cytoarchitectonically a simple structure, but hodologically complex. *Prog.Brain Res.*, **83**, 47-58.

Witter, M. P., Groenewegen, H. J., Lopes da Silva, F. H., & Lohman, A. H. M. (1989). Functional organization of the extrinsic and intrinsic circuitry of the parahippocampal region. *Prog.Neurobiol.*, **33**, 161-253.

Witter, M. P. & Moser, E. I. (2006). Spatial representation and the architecture of the entorhinal cortex. *Trends Neurosci.*, **29**, 671-678.

Yoganarasimha, D., Yu, X., & Knierim, J. J. (2006). Head direction cell representations maintain internal coherence during conflicting proximal and distal cue rotations: Comparison with hippocampal place cells. *J.Neurosci.* **26**[2], 622-631.

Yu, A. J. & Dayan, P. (2005). Uncertainty, neuromodulation, and attention. *Neuron*, **46**, 681-692.

Zeineh, M. M., Engel, S. A., Thompson, P. M., & Bookheimer, S. Y. (2003). Dynamics of the hippocampus during encoding and retrieval of face-name pairs. *Science*, **299**, 577-580.

Zhang, K. (1996). Representation of spatial orientation by the intrinsic dynamics of the head-direction cell ensemble: a theory. *J.Neurosci.*, **16**, 2112-2126.

Zipser, D. (1985). A computational model of hippocampal place fields. *Behav.Neurosci.*, **99**, 1006-1018.